論文 / 著書情報
Article / Book Information

題目(和文)	
Title(English)	Low-Temperature Solution-Processed Metal Oxide Transistor for Flexible Electronics
著者(和文)	宮川幹司
Author(English)	Masashi Miyakawa
出典(和文)	学位:博士(工学), 学位授与機関:東京工業大学, 報告番号:甲第11600号, 授与年月日:2020年9月25日, 学位の種別:課程博士, 審査員:飯野 裕明,間中 孝彰,菅原 聡,大見 俊一郎,神谷 利夫
Citation(English)	Degree:Doctor (Engineering), Conferring organization: Tokyo Institute of Technology, Report number:甲第11600号, Conferred date:2020/9/25, Degree Type:Course doctor, Examiner:,,,,
学位種別(和文)	博士論文
Type(English)	Doctoral Thesis

Tokyo institute of technology

School of Engineering

Department of Electrical and Electronic Engineering

Low-Temperature Solution-Processed Metal Oxide Transistor for Flexible Electronics

Masashi Miyakawa

June 2020

THESIS SAMMARY

Recent rapid growth of digital technology requires various human interactive electronics such as information displays and sensors in area of information society. One of the primary components is thin-film transistors (TFTs). Simple and facile solution-processed metal oxide TFTs are promising device and have various advantages such as low cost, large-area fabrication, and process simplicity. However, the current substandard performance limits its wide range of practical applications. In this thesis, the general methods to improve the low-temperature solution-processed metal oxide TFTs in terms of electrical performance and process simplification were presented to enhance the overall performance for the large demands of flexible electronics.

The processing approach by hydrogen injection and oxidation (HIO) methods are demonstrated for low-temperature solution-processed metal oxide semiconductors using zinc tin oxide (ZTO) by organic precursor and indium gallium zinc oxide (IGZO) by aqueous precursor. The HIO method enables an efficient elimination of a large amount of residual species as well as film densification upon sequential oxidation. By detailed chemical analyses including X-ray photoelectron spectroscopy (XPS), Fourier transform infrared spectroscopy (FT-IR), secondary ion mass spectrometry (SIMS), and thermal desorption spectroscopy (TDS), the mechanisms of HIO methods were carefully investigated. Furthermore, the improvement in the TFT characteristics was confirmed in terms of mobility and electrical stability. The aqueous IGZO TFT with HIO method exhibit very stable characteristics even at 250˚C processing temperature. Furthermore, the compatibility of HIO method for flexible electronics is also demonstrated by the TFT arrays, which exhibit almost same performance as the TFT on silicon substrate. Therefore, the effectiveness of HIO method were clearly confirmed by enhanced TFT characteristics. The importance of the reduction of residuals insides the films is also clarified.

The material approach by aqueous fluorine-doped IGZO (IGZO:F) precursors demonstrated a high-performance metal-oxide TFTs at a low-temperature processing of 300˚C. The fluorine doping for aqueous precursor was effective to suppress the total impurities from metal ligands. It also enhances the TFT characteristics fabricated with IGZO:F precursor, enhancing the overall TFT performance such as the mobility, better switching characteristics, and reliability. Combining with HIO method, the mobility over 7 cm^2/Vs was achieved for the IGZO:F.

The simple TFTs fabrication techniques using direct patterning were investigated. Simple and reliable direct patterning process for totally carbon-free aqueous precursor

was demonstrated with good electrical performance and uniformity by utilizing a photo-oxidation of water molecules and nitrate ligands. The mechanisms of direct patterning were carefully examined by chemical analyses. The TFT exhibited uniformed mobilities with an average value of 4.3 $cm^2/V \cdot s$ and small deviations and good reliability.

Through this thesis, the investigations for low-temperature solution processed metal oxide using the processing and materials approaches demonstrate the routes to improve the TFT performance for flexible electronics. The developed low-temperature technology such as HIO method, fluorine doped aqueous precursor, and direct patterning could show the great potentials to lead the practical applications in the field of various flexible electronics. Current performances by those low-temperature technologies are still needed to be improved its performance compared to the metal oxides by vacuum processing. However, the use of multiple technologies such as HIO with innovative precursors could be essential methods to boost the current performance of solution-processed metal oxide TFTs. Further investigations open the door for obtaining good and reliable performance for low-temperature solution-processed metal oxide TFTs, which leads solution-based electronics.

Table of contents

Chapter 1: Introduction

1.1 Motivation

Recent rapid growth of digital technology requires various human interactive electronics such as information displays and sensors in area of information society. In particular, display devices are indispensable as the interface to obtain all information. Since the development of cathode ray tube, various display technologies have been developed continuously as the technological progress for clearer image quality, more realistic, more space-saving, larger screen size, and lower power consumption. The demands for information displays are still increasing to enhance our experiences with the latest development of emerging flexible electronics. As technology evolved, our lifestyle has drastically changed because those are our daily use of electronics.

The invention of flat panel display (FPD) such as active-matrix liquid crystal displays (AM-LCDs) and active matrix organic light emitting diode displays (AM-OLEDs) makes display thinner and lighter. With information technology, rapid growth of smartphones and tablets was progressed. Nowadays various types of display devices such as TVs, smartphone, Tablets, and Notebook PC are ubiquitous in our digital lives. Furthermore, the style is changing towards lighter and more flexible owing to the rise of the flexible display, which employs a plastic film as a display substrate. The emerging flexible display has great potential to revolutionize current flat display design drastically due to unique features such as lightness, flexibility, bendability, and portability, which

could not have been considered previously. It enables a new class of display with its flexibility. Thus, the technological progress of display devices is still changing our lifestyle.

Figure1.1. Various future applications requiring the flexible display

As the evolution of the display devices, thin-film transistor (TFT) technology has been developed as the one of most important components. The evolution of the displays has been continuously achieved with the development of TFT technologies because TFTs are developed as switching devices for controlling each pixel to drive the displays. Thus, one of the required technologies for display innovation is developing the high-performance TFTs. Hydrogenated amorphous silicon TFTs (a-Si:H TFTs) and low-temperature polycrystalline silicon TFT (LTPS TFTs) are some of the examples of invented TFTs [1].

The a-Si:H TFTs grew rapidly in the 1990s through the adoption of the laptop PCs. It has been used for a display backplane mostly in LCDs because of the high productivity.

LCDs adopting the a-Si:H TFTs are still current main technology for driving LCDs including small to large-area LCDs. However, the display trends towards higher resolution, brighter, and less power consumption, require beyond the performance of a-Si TFTs. Because Low TFT performance with mobility of less than 1 cm^2/Vs and its instability under bias stress is not enough to drive the advanced display devices such as large-size and high-resolution displays and AM-OLEDs.

LTPS TFTs have been proposed and developed to meet the increasing requirement of the display trends. The performance of LTPS TFTs can be leach to the mobility over 100 cm^2/Vs with good reliability under bias stress. LTPS TFTs are currently regarded as the main TFT technology to drive the small to middle-sized high-resolution displays for high-performance smartphone, tablet, and AMOLEDs. However, low productivity of LTPS TFTs limit their applications. LTPS TFTs are relying on the Si crystallization process, which requires many costly apparatuses such as an Excimer Laser, ion doping, and high-temperature annealing units. Therefore, the complicated manufacturing process of LTPS brought difficulties to apply for various displays including large area and low-cost.

Another current main TFT technology is oxide TFTs based on amorphous metal oxide semiconductors using amorphous indium-gallium-zinc oxide (a-IGZO). Now oxide TFTs are considered as a promising technology to overcome traditional disadvantages due to their high mobility of over 10 cm^2/Vs, high on/off ratio, and large area scalability[2-4]. After Hosono group publication of a-IGZO in 2004, many researcher groups and companies started its researches as an innovative channel material. Besides, the advantages of low temperature processability meet the requirements of an emerging

flexible display. Thus, a wide variety of applications with integrated IGZO TFTs have been proposed, including rigid and flexible active-matrix organic light-emitting diode (AMOLED) displays[5, 6].

Furthermore, current momentum towards connect everything by various IoT (Internet of Things) lead to develop various TFT-based applications with flexible electronics including wearable electronics[7, 8], non-volatile memories[9], RF-ID tags[10], near-field communication (NFC) tags[11-13], biosensors[14, 15], and sensors [16, 17] are presented. Those are expected to grow rapidly as emerging flexible electronics in area of human interactive, health care, E-textiles, energy and storage, robotics, and security sensors [18, 19]. The outstanding electrical characteristics of oxide TFTs compared to other TFTs have great potential to cover the demands of various electronics.

TFTs are traditionally fabricated using vacuum processes such as plasma chemical vapor deposition (CVD) for a-Si and LFPS TFTs and magnetron sputtering deposition for metal oxides TFTs. Although these well-established processes produce high-quality TFTs, the complicated and time-consuming vacuum processing limit their extensive usage for its applications including large-area, low-cost wearable, and sensor-embedded displays.

Contrarily, facile solution processing is a promising approach for fabricating scalable and low-cost TFTs, owing to the simple printing method[4-6]. The innovation of fabrication process has a possibility of drastic reducing the cost of devices and widen future ubiquitous electronics. Therefore, oxide TFTs fabrications bad on a solution processing method is a promising alternative to conventional vacuum processing[13-20]. Besides, it also helps to accelerate the momentum of digital technology with advantages

of facile processing.

However, the implementation of solution processing remains challenging due to low quality films associated with, for example, low density and impurities. One major drawback is substandard TFT performance, such as low mobility, a large subthreshold swing (S.S.), and instability. TFTs processed below 400°C are typically inactive due to a lack of metal-oxide bond formation and the impurities of residual species that generate a large amount of defects, which leads to poor TFT performance[20].

In this thesis, the general methods to improve the solution-processed metal oxide TFTs in terms of electrical performance and process simplification were discussed to obtain overall performance for next-generation flexible electronics.

1.2 Innovation of information display

First CRT device was invented by Karl Ferdinand Braun in 1897. It was a fluorescent screen, known as Braun's electrometer, and also a cathode-ray oscillograph. The CRT is consisted of an electron gun and a phosphorescent screen. The CRT has been used as information display such as television sets, PC monitor for decades. However, the CRT display was gradually replaced by flat panel LCDs due to the advantages such as thin, light, and low power consumption, in late 1990s. The first concept of active-matrix LCD incorporating a thin-film transistor (TFT) and a storage capacitor in each pixel for LC display driving was proposed by Bernard J. Lechner at RCA Laboratories in 1968, then the first working sample was made by T. Peter Brody et. al. at Westinghouse in 1973[21].

The introduction of active matrix driving enables a high-speed refresh rate even for

a significantly large number of pixels without the need to wait, compared to the traditional passive-matrix driving. With active matrix driving, we can apply an arbitrary voltage to each pixel by selecting the pixel by applying the select voltage to the select line which is connecting to the gate of TFT. Therefore, ideally, other pixels can be completely isolated. Early LCD were suffered from low picture quality due to the narrow viewing angle, low motion picture quality, low contrast ratio, and poor color performance. However, after the intensive efforts to over these disadvantages from late 1990s to early 2000s, the LCDs became the todays main technology for information display. Nowadays OLED displays are now growing as the next generation of displays. While LCD require back light units, OLED is an electroluminescent device that is self-emissive. Therefore, OLED has many advantages over LCD such as high-contrast ratio, thinner, lighter, and faster response time. Besides, the simple structure of OLED is suitable for emerging flexible OLED. This flexibility of information display is now regarded as the next evolution of information display, which enables the brand-new concept with the function of bendable, foldable, and rollable features. Now OLED has been adapted in many mobile displays and large-size TV and is growing explosively.

1.3 Requirement of information display applications

As the technology progress, the display resolutions in large-size TV and mobile device has been continuously increasing to purse the better picture quality. Evolution of the resolution is from video graphics array (VGA, 640), full high definition (HD, 2K), ultra-high definition (UHD, 4K), and recent Ultra-high definition (8K UHD) [22] [23]. Accordingly, the requirement of TFTs is increasing as a driving capability because TFTs need to charge up the storage capacitor within the addressing time. The addressing time for each pixel is shortened with increasing the number of pixels. Figure 1.2. shows the required calculated mobility for each resolution and frame rate for OLED display. When the resolution or frame rates is increasing, the TFTs need to write the required bias in a short period. Accordingly to this, the mobility higher than 4 cm^2/Vs is required for the 4K AM-OLED display with 120 Hz frame rates[24, 25]. The required mobility of 8K OLED with 120 Hz frame rates is more than 8 cm^2/Vs. Therefore, high-performance TFTs is being developed to meet the requirement of OLEDs. Besides to this, the uniformity of the TFT performance over large area is also important factor to obtain uniform picture quality. Although the compensation circuit technology has been developed to get uniform display image, the mobility and threshold voltage are carefully needed to be controlled to obtain good uniformity of the displays[26]. According to the previous display reports, the σ of the Vth variation under ± 0.15 V is preferred for the level of mass production[27] [28]. Another important factor is the reliability of the each TFTs. It was typically evaluated by positive bias and negative bias stress tests, which evaluate V_{th} sift under the certain bias continuous stress. Therefore, those TFT characteristics are the target value to pursue a practical application by solution-processing.

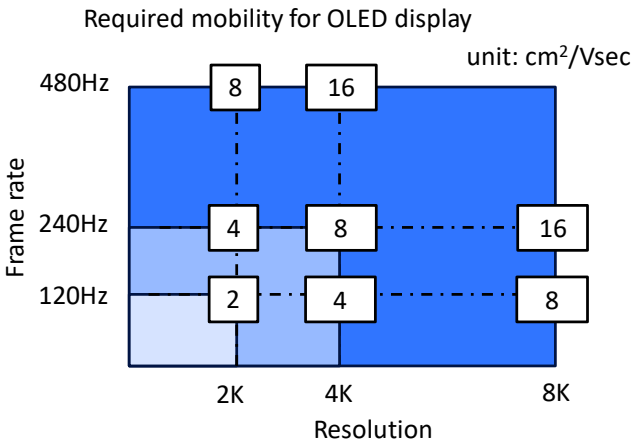

Figure1.2. Required mobility for each resolution and frame rate.
(Adapted from[26])

1.4 TFTs structure and electrical properties

TFT is fundamentally composed of three main parts: semiconductor layer, a dielectric layer, and terminals (gate, source, drain electrode). The source and drain electrode directly contact with semiconductor layer. The gate electrode is separated from the semiconductor by the insulating dielectric layer. Then, the current flow (I_{ds}) in the semiconductor between source and drain electrode can be controlled by turning on applied voltage to the gate electrode (V_{gs}) and drain electrode (V_{ds}). The operation principle is defined as enhancement mode (normally off) and depletion mode (normally on) when the threshold voltage (V_{th}) is positive or negative[29].

Figure 1.3. shows the typical conventional TFT structure. A TFT with gate opposite the substrate is referred to as top-gate structure, otherwise, it is bottom-gate structure. Additionally, a TFT is referred to as coplanar type when the source and drain electrodes is in the same plane of the semiconductor-dielectric interface[29]. The other side is called

staggered.

The bottom-gated top-contact structure is generally adopted in the fabrication of conventional a-Si TFTs and oxide TFTs for LCDs and AMOLED displays. This structure is classified into an etch stopper type and back channel etch type. Since the back channel of the TFT is exposed to the atmosphere for back channel etch type, the suitable passivation layer is employed to obtain stable operations.

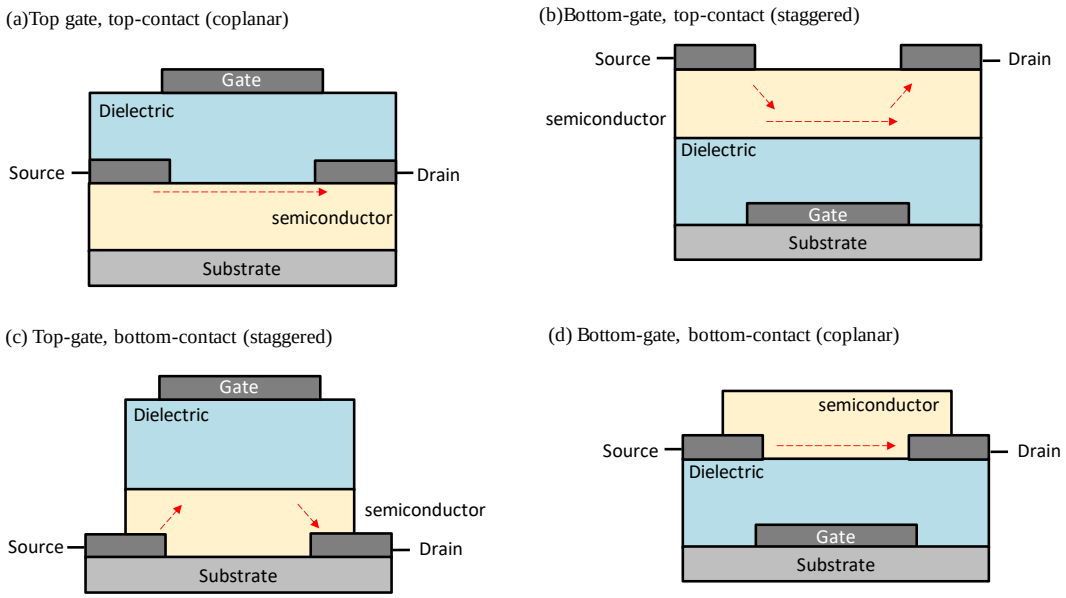

Figure1.3. Typical TFT configurations; (a) Top-gate top-contact, (b) Bottom-gate top-contact, (c) Top-gate, bottom-contact, (d) Bottom-gate bottom-contact

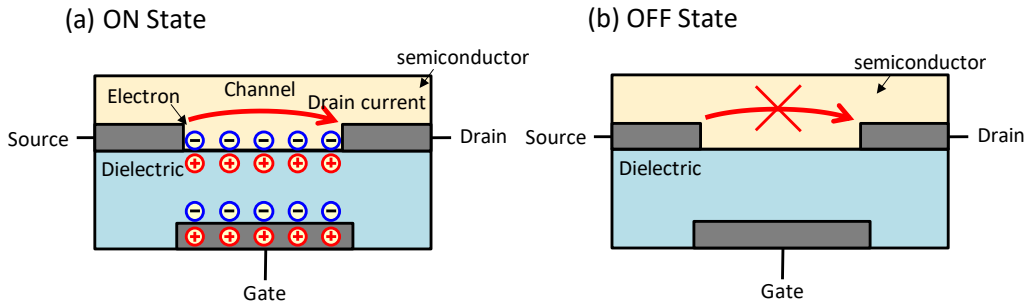

Figure1.4. Illustration of the operation of TFTs with n-type oxide for (a) On state and (b) Off state

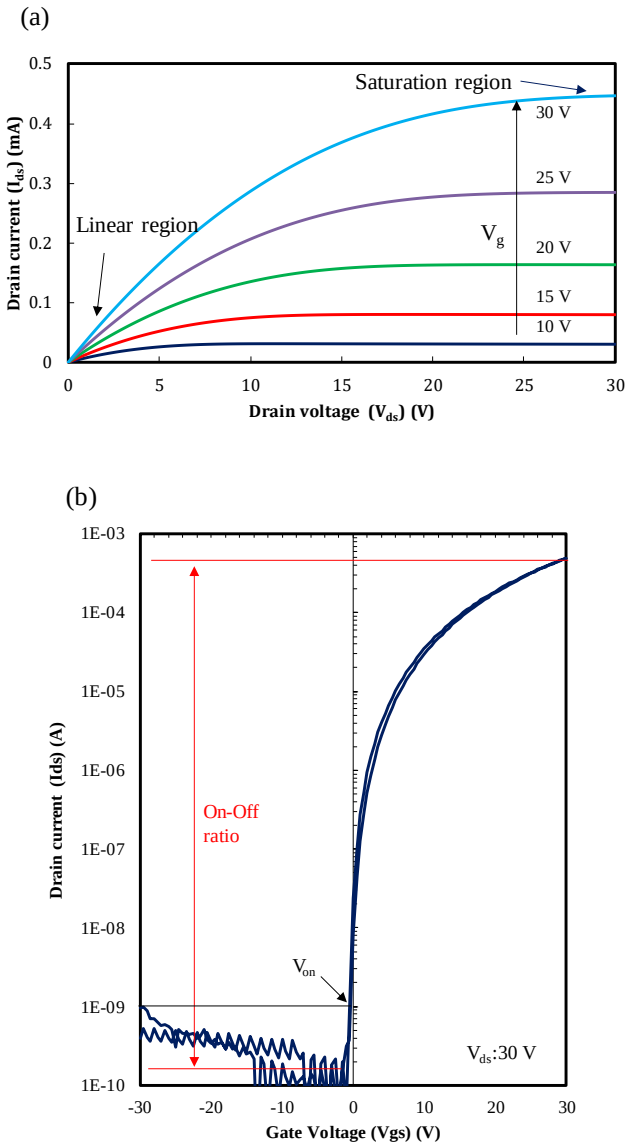

Figure1.5. Typical TFT characteristics for (a) Output plot and (b) Transfer plot with solution-processed oxide TFT

When the positive bias (V_{gs}) is applied to the gate electrode, a TFT with n-type semiconductor is “On” state. The electric field in dielectric layer generate the negative charge carrier (electrons) to accumulate in the semiconductor at the interface between semiconductor and dielectric layer. This accumulated layer forms a conducting channel

in the semiconductor, then allowing a current flow (I_{ds}) to be driven from the source to the drain by applied voltage to the gate electrode (V_{gs}). Contrary to this, there is no conducting channel in the semiconductor layer when the TFT is "OFF" state. This indicate that, there is no current flow (I_{ds}) between the source and drain electrode, even with an applied drain-source bias voltage (V_{ds}).

The performance of TFTs can be evaluated by measuring output plot (V_{ds} - I_{ds}) and transfer plot (V_{gs} - I_{ds}). The critical parameters such as the mobility (μ), current on/off ratio (I_{on}/I_{off}), threshold voltage (V_{on}), and subthreshold swing (S.S.) can be calculated.

At low drain voltages of V_{ds}, the I_{ds} follows Ohm's law. Therefore, I_{ds} is proportional to the V_{ds} and V_{gs}. This region is in the linear operation. The liner current of I_{ds} can be described by the following equation:

$$\mathrm{I_{ds,linear}} = \mu_{\mathrm{linear}}\, \mathrm{C}_i \frac{W}{L}\left(V_{gs} - V_{th} - \frac{V_{ds}}{2}\right) V_{ds}$$

As the V_{ds} increases to the V_{gs} , V_{dg} is zero bias and pintch-off of the channel occurs. At this point, the I_{ds} became saturated region, which is independent of the V_{ds}. This saturation current of I_{ds} is called as saturation operation. The saturation current can be described by the following equation:

$$\mathrm{I_{ds,saturaion}} = \mu_{\mathrm{saturation}} \frac{W}{2L} \mathrm{C}_i \left(V_{gs} - V_{th}\right)^2$$

μ is the mobility, C_i is the capacitance per unit area of the dielectric layer, L is the channel length, W is the channel width, V_{th} is the threshold voltage, V_{gs} is the gate voltage, and V_{ds} is the drain-source bias voltage.

1.5 Oxide semiconductors

Various kinds of oxide semiconductors have been researched widely and explored since the tin oxide TFT in 1964 [30]. Most early research is in field of single component oxide such as SnO_2, ZnO, and In_2O_3. Binary components tend to crystallize and have uncontrollable high carrier concentration, which cause unstable device characteristics [31, 32]. After Hosono's group reports of amorphous oxide semiconductor of In_2O_3-Ga_2O_3-ZnO system (a-IGZO) for the channel material with high mobility over 10 cm^2/Vs by in 2004 [2], oxide semiconductor is regarded as an excellent TFT materials and has been intensively researched and developed for the display application. Compatibility of simple deposition of IGZO by conventional DC-sputtering apparatus is also accelerate the intensive development to realize next generation displays. Multicomponent system is effective in amorphization due to the incorporation of aliovalent and different size cations. Thus, the stable amorphous phases are formed in IGZO. In addition to IGZO, other multicomponent amorphous oxide semiconductors have been developed, including In−Zn−O (IZO), Zn−Sn−O (ZTO), In−Sn−Zn−O (ITZO) etc [31].

Compared with other binary and ternary oxide semiconductors such as zinc oxide (ZnO), indium oxide (InO_x), zinc-tin oxide (ZTO), and indium-zinc oxide (IZO), IGZO is an electrically stable channel material due to the introduction of gallium as a carrier suppressor, which allows oxygen to be tightly bound, and prevent the generation of oxygen vacancies[31, 33, 34]. Considering the results of commercial AMOLED TV[6] products integrated with IGZO TFTs, IGZO is considered to be a novel composition for practical device applications.

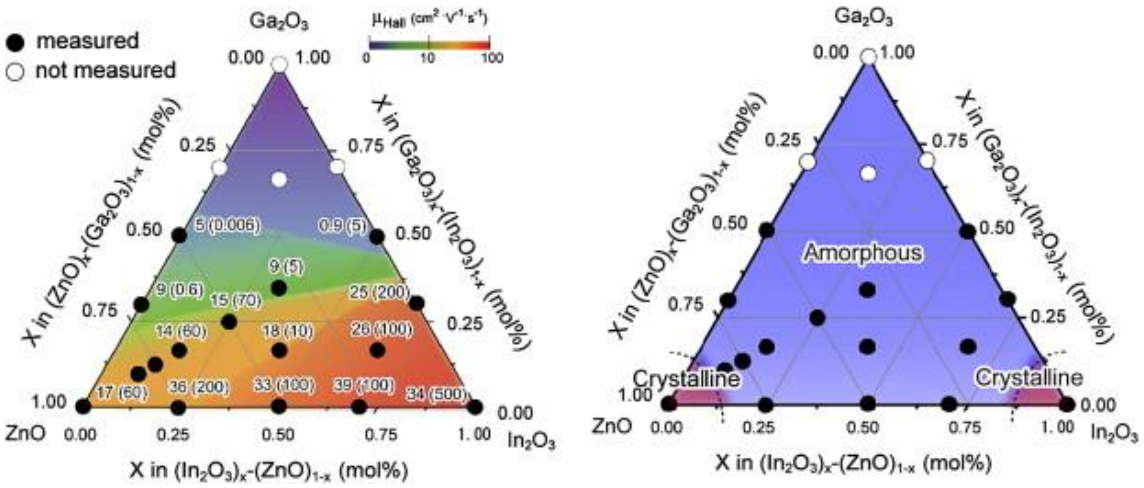

Figure1.6. The electron Hall mobilities and concentrations (left) and the amorphous formation region (right) in IGZO [35]

Figure 1.7. show the schematic orbital drawings for the carrier transport paths in crystalline and amorphous oxide semiconductors[2]. In silicon semiconductor, the bandgap for carrier conduction between the conduction band minimum (CBM) and the valence band maximum (VBM) is governed by covalent bonding, which is formed by the overlapping sp^3 orbitals. The magnitude of bond overlap is drastically affected by any fluctuations in the bond angle due to the strong directivity. This strong directivity of Si leads the large deterioration in amorphous Si, which is limited by hopping conduction. In oxide semiconductor, the bonding is ionic, which is formed by CBM of s orbital in metal and VBM of 2p orbital in oxygen atom. The spherical s orbital of heavy metal is spread widely and isotopically, which is less dependent on the directivity. Therefore, the overlap of the bonding is possible even in the amorphous oxide, which realize high mobility even in amorphous structure.

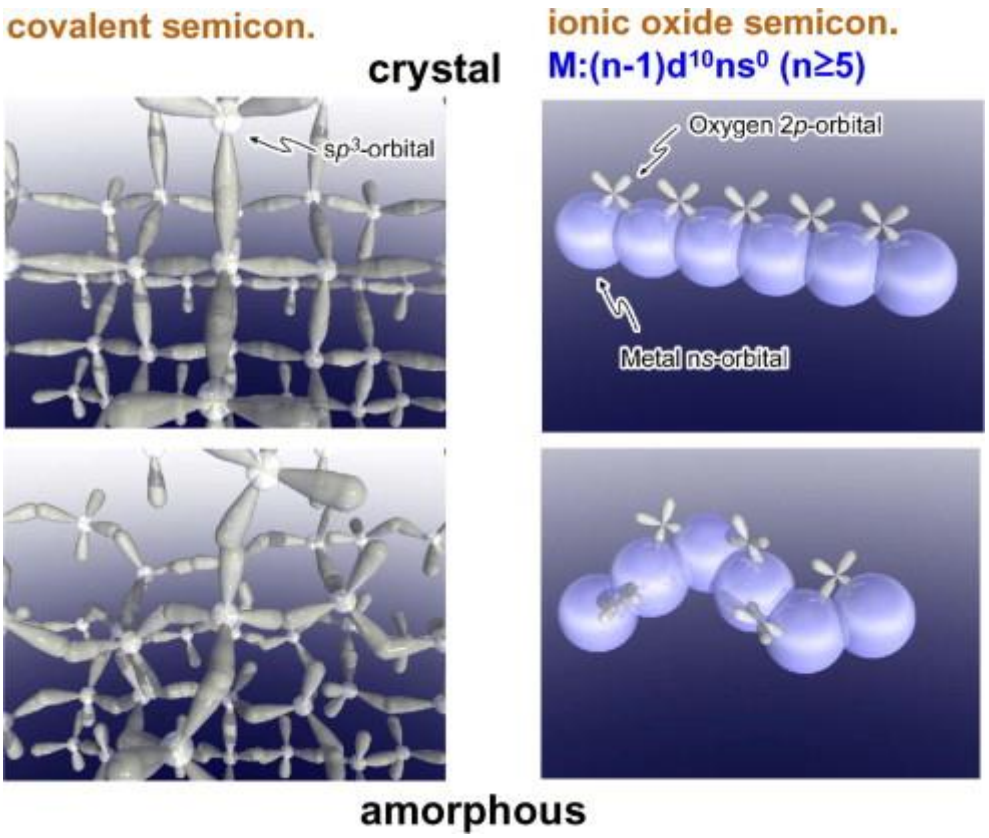

Figure 1.7. Schematic orbital drawing for the carrier transport in (a) silicon, (b) oxide semiconductor[2, 35]

Table 1.1. Comparisons of channel materials for TFTs

	Si		Oxide	Organic
	a-Si:H TFT	LTPS	Amorphous Oxide TFT (InGaZnO)	Organic TFT
Mobility [cm²/Vs]	< 1	50∼100	10	< 1∼10
Process temperature [°C]	-350	-500	RT-400	RT-150
Film deposition	CVD	CVD + ELA	Sputtering・Solution	Vacuum, Solution
Scalability	○	△	○	?
Uniformity	○	△	○	?
Long-term reliability	△	◎	○	?
Product application	LCD E-paper	High-resolution LCD Small-middle OLED	・LCD ・OLED	-

1.6 Solution processing for metal oxide

Solution processing is considered as a promising and desirable technology due to its advantages such as cost-effectiveness, simplicity, high throughput, its scalability to large area compared to the conventional vacuum-based deposition. Considering form the current momentum towards ubiquitous display and IoT society, the facile processing is required technology.

By for now, various kinds of technology have been explored to realize the high-quality metal oxide films by facile solution processing. The typical principal of solution-process of metal oxide is based on sol-gel process which is typically started from metal salts and alcohol solvents. The conventional chemical formulation of metal salt precursor is from metal salts in organic solvent such as 2-methoxyethanol with a small amount of ethanolamine for stability. The general reaction in chemical conversion process to form the Metal-Oxide-Metal (M-O-M) is by hydrolysis and condensation.

Hydrolysis

$M(OR)_x + H_2O \rightarrow M(OR)_{x-1}(OH) + ROH$

Condensation

$M(OR)_{x-1}(OH) + M(OR)_{x-1}(OH) \rightarrow (RO)_{x-1}M\text{-}O\text{-}M(OR)_{x-1} + H_2O$

$M(OR)_{x-1}(OH) + M(OR)_x \rightarrow (RO)_{x-1}M\text{-}O\text{-}M(OR)_{x-1} + ROH$

The process of forming metal oxide is typically by two step processes; 1. Soft annealing process at 100-150°C and 2. Thermal annealing at high-temperature over 300° C. 1st step of soft annealing process is mostly for the evaporation of the excess solvents. The film is oxidized via a 2nd step thermal annealing to form metal–oxide–metal (M-O-

M) bonds via condensation reaction[36]. Ideally, the ligands in metal salts and solvents are needed to be decomposed at that time to produce a high-quality oxide film. Any impurities that remain, such as organic contents, will suppress metal oxide condensation and degrade electrical performance[36, 37]. Therefore, 2nd step of thermal annealing is crucial process for the solution-processed metal oxide.

However, the implementation of solution processing remains challenging due to low quality films associated with, for example, low density and impurities. Usually, solution-processing methods require processing above 400^{o}C to facilitate conversion of the precursor to stable metal–oxide–metal bonds and decompose impurities from precursor[38, 39]. Figure 1.8. shows the model for the ideal metal oxide and low-temperature processed metal oxides. When the processing temperature is low, the films tend to contain unwanted residual species which is originated from the precursor compounds such as metal salt ligands and solvent.

Ideal oxide

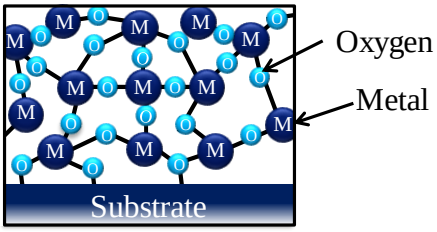

·Consisted from only metal & oxygen atoms
·Highly dense film

Low-temperature processed oxide

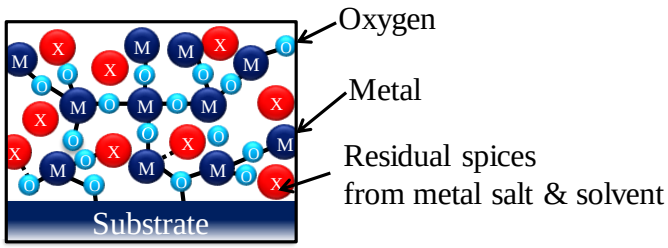

·Remaining residual spices
·Lack of Metal - Oxide - Metal bonds

Figure 1.8. Schematic model for ideal oxide films and low-temperature processed oxide film

Processing at temperatures as low as 350°C is desirable and even necessary for application in emerging flexible electronics on plastic substrates and lowering fabrication costs. To ensure innovation for future ubiquitous display and various flexible electronics applications, low-cost, yet high-performance TFT fabrication technology is necessary for producing ideal TFTs with high mobility and good stability to meet the requirement of practical applications.

1.7 Requirement of low-temperature process for flexible electronics

Considering the large demands of low-temperature processing, the processing temperature should be compatible with plastic substrates. Conventional polyimide (PI) films are resistant to high temperatures; the maximum processing temperature for this material is ca. 400°C. However, its deep-yellow color and poor optical transmittance are severe problems for optoelectronic applications. Therefore, the display integration in flexible substrate, colorless and transparent films is important to achieve high color accuracy and a wide color range, where the maximum processing temperature is less than 300°C generally [40, 41].

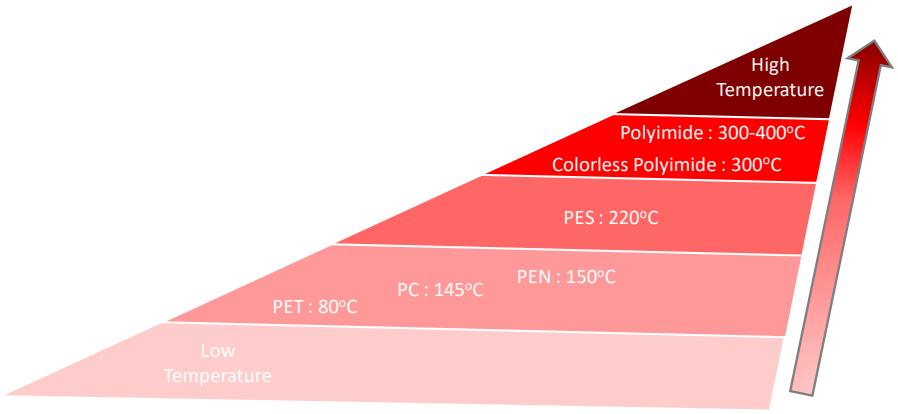

Figure 1.9. Available plastic flexible substrates and their glass transition temperatures.

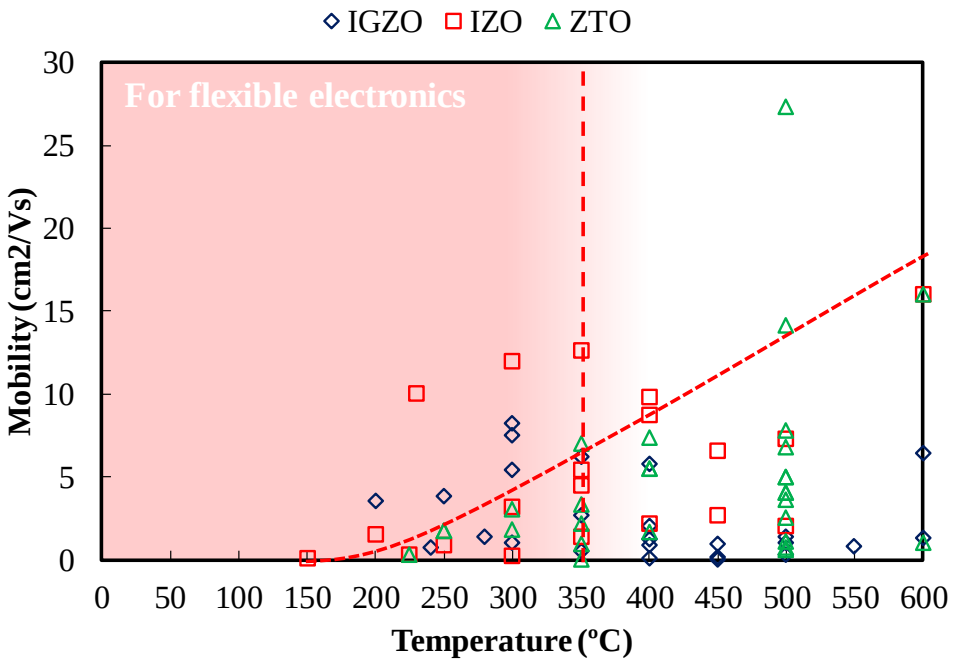

Figure 1.10. Typical trend of the mobility for the solution-processed multicomponent oxide TFTs from journals [42] [40] [31, 43, 44]

1.8 Low temperature technology for solution-processed oxide TFTs

Low temperature technology for solution-processed oxide TFTs has been intensively studied as figure 1.10. shows. To produce a high-performance solution-processed oxide semiconductor at low temperature, forming dense metal–oxygen–metal bonds within the metal oxide is crucial along with eliminating residual species from the precursor solution like metal ligands and the solvent. Many studies focused on developing the technology for obtaining better solution-processed metal oxides at low-temperature. The technology can be categorized into mainly two groups; material engineering and process engineering.

Associated with the material engineering, selections of metal salts and solvents are great impacts on the quality of metal oxides at low-temperature processing. Figure 1.11.

shows the weight loss of the various precursor for nitrate, acetate, and chloride, and fluorine ligands. As figure shows, the thermal decomposition of precursor is critically depending on its reagents. It is obvious that the reagents with easier decomposition is crucial to obtain better metal-oxide at low-temperature. By for now, various precursor systems were studied including metal salts dependence[37, 45], composition effects of precursors[38], alkoxide precursors[20], chemical energetic combustion precursors[46], and aqueous routes[36, 37, 47] for improving the performance of TFTs even at low temperature. Considering from the current results, promising strategies for low-temperature processing is based on the combustion precursor and aqueous route. Combustion precursor incorporating an oxidizer and fuel (acetylacetone etc.) can facilitate chemical conversion by a self-energy generation based on combustion chemistry[46, 48-51]. This combustion precursors were applied to the various metal oxide including semiconductor such as IGZO[49-51], ZTO[52], conductor, and dielectrics[48]. Another strategy is by the aqueous route with nitrate precursor[36, 37, 45, 47]. It enables elimination of unwanted carbon-impurities owing to its carbon-free systems. In general, a high temperature annealing over 500°C is needed to remove the carbon-related residual from organic solvent completely[40]. Therefore, aqueous system has advantageous to obtain a high-performance oxide TFT without concern of carbon impurities. Besides, water as solvent is very simple and cost-effective material. Furthermore, aqueous route is known to form aqua complexes, which enable low-temperature decomposition by the solvation of water molecules[37]. Thus, few residual impurities are possible even at low temperature. Recently, the applicability of printing process using aqueous precursor is also demonstrated to show the potential of aqueous precursor[53].

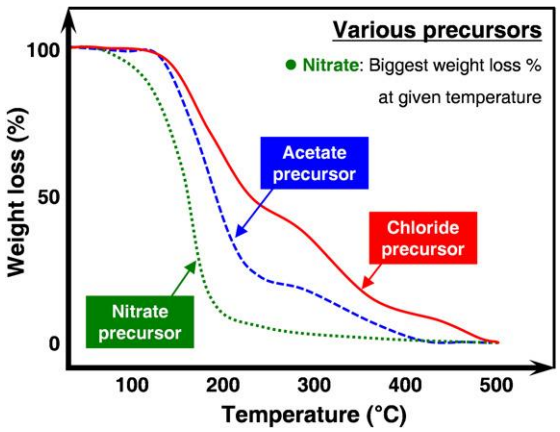

Figure 1.11. Comparison of weight loss with increasing temperature with respect to nitrate, acetate, and chloride precursors. [54]

Associated with the process engineering, various innovative methods including microwave annealing[55], high-pressure annealing[56], redox processes[57], O_2/O_3 annealing[58], laser irradiation processes[59, 60], and plasma treatment [61-63] are suggested to improve the film. Short-wavelength deep UV (DUV) irradiation of the precursor, assisted by oxidizing radicals from photochemical activation, is developed for an effective process in oxidation of the film and decomposition of the ligands in metal salts[64]. Besides, the combination techniques including UV irradiation and photo-annealing process[64-68] has also been reported.

By for now, various innovative low-temperature technologies were reported, however, the necessity of new technology including material and process is still needed for high-performance, yet simple solution-processing techniques for fabricating solution-processed oxide TFTs at low temperatures to meet the requirement of practical

applications such as high mobility, good uniformity with high reliability. In consideration of practical device applications, electrical stability is important issue.

1.9 Patterning process for solution processing

Fabricating TFT devices, multiple patterning process for the metal oxide films is inevitable for device integrations. Mostly solution processing techniques require conventional photolithography process used to pattern the semiconductor layer. However, it involves multiple steps of the process from coating to photoresist removal. Therefore, development of simple patterning technique is one of the crucial research interests to achieve high performance TFTs with facile solution processing. Direct patterning procedures is one of the great solutions to maximize the advantages of solution processing. As figure 1.12. shows, it has great advantage to reduce the process a lot. Photolithography requires multiple steps, involves a time-consuming baking and drying process, and produces a lot of waste, including toxic volatile organic compounds (VOCs) and other waste gases that are emitted into the environment[69]. In contrast, direct patterning is not only much simpler but cuts down on processing time, equipment cost, and chemical usage.

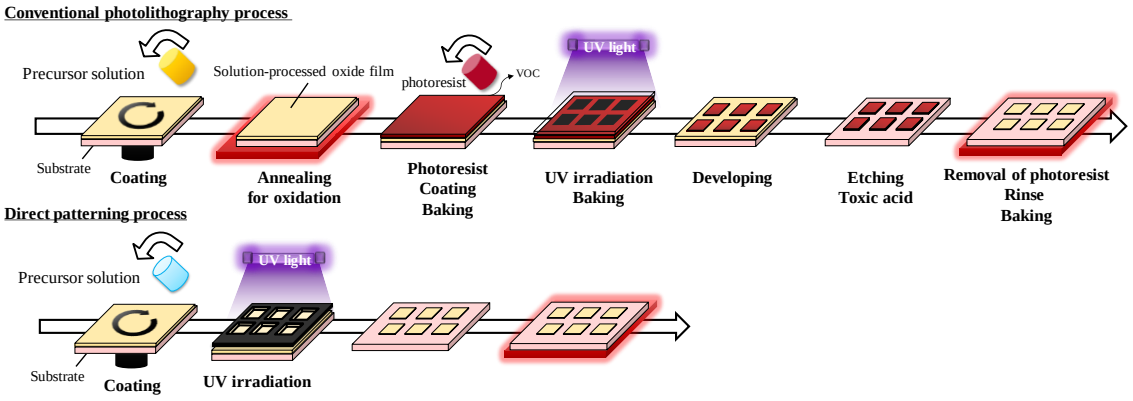

Figure 1.12. Comparison of process flow for metal oxide film fabrication using a conventional photolithography process vs. direct patterning process.

Although innovative researches by printing process for metal oxide has been researched including inkjet[70-72], flexography [73], and screen printing [74] has certain advantages in terms of material saving, const-effectiveness, and mask-less process. However, strict control of its conditions[44, 72] are very sensitive but necessary to obtain a good quality printed film of the right shape, size, uniformity, and thickness[75]. Besides, the controllability of those printing techniques has a difficulty especially for high resolution patterning.

Direct patterning has advantages to achieve uniform and fine patterning because the process is by optical means based on the photo-selective reaction. The coated films are selectively reacted and oxidized under UV irradiation via UV masks. The reacted films alter the film solubility in the subsequent etching process to achieve the patterning process. Therefore, optical based direct patterning has potential to apply for high resolution patterning.

Previous studies on direct patterning techniques used carbon-based photosensitive additives, such as β-diketonato ligand chelate complex (i.e., benzoylacetone and acetylacetone) for unique photosensitivity for UV reaction [75-78]. Besides, direct patterning of the precursor without the use of photosensitive additives by applying DUV irradiation was also reported[75, 79]. However, the direct-patterned oxide TFTs fabricated using these carbon-based additives exhibit substandard device performance due to the insufficient of oxidation of precursor. Those precursors were still prepared with carbon-based materials, such as organic solvents, additives, and ligands in metal salts.

In generally, after direct patterning process, patterned thin films were oxidized via a thermal annealing process to form metal–oxide–metal (M-O-M) bond via condensation reaction[36]. At the same time, ligands of metal salts and solvents must be completely decomposed to produce high-quality oxide films. Remaining impurities, such as organic contents, suppress the metal oxide condensation and degrade the electrical performance. Reducing the organic content in the precursor is critical to decrease carbon impurities in the fabricated oxide films and thus improve the electrical performance[36, 37]. Therefore, direct patterning method for carbon-free metal oxide precursors that do not contain any carbon-based species are highly required for reliable and better performance solution-processed metal oxide device applications.

1.10 Thesis organization

This thesis develops the processes and the materials for low-temperature solution-processed oxide TFTs. The objective of this work is to investigate the solution-processed oxide technology for achieving TFTs with high mobility and reliability by facile and simple processing, comparable to those fabricated by vacuum processing for flexible electronics. The patterning process for device integration is also investigated to enable efficient fabrication process.

Chapter 1 provided a motivation and background of metal oxide TFTs as, well as the advantages for solution-processing. **Chapter 2** provided experimental methods including the processes for the solution-processed oxide TFTs, evaluation of TFTs, and chemical analysis of oxide films.

Chapter 3 and 4 presents the process engineering for low-temperature solution-processed oxide TFTs, which is by the application of hydrogen injection and oxidation. **Chapter 3** focused on ZTO by organic precursor, while **chapter 4** focused on IGZO precursor by aqueous precursor. The TFT characteristics for ZTO and IGZO with HIO method were given with detailed chemical analysis.

Chapter 5 focused on the impact of material doping to the aqueous IGZO precursor. The characteristics of fluorine doped IGZO TFTs were addressed and discussed.

Chapter 6 addresses the direct patterning method for efficient device integration. Without conventional photolithography process, the uniform patterning for oxide films was achieved. The detailed mechanisms and TFT characteristics were discussed.

Chapter 7 summarizes the results obtained in this dissertation. The future outlook

of this study based on technology for the solution-processing oxide TFTs is addressed as well.

1.11 References

1. J.-H. Lee, D.N. Liu, and S.-T. Wu, *Introduction to flat panel displays*. Vol. 20. 2008: John Wiley & Sons.
2. K. Nomura, et al., *Room-temperature fabrication of transparent flexible thin-film transistors using amorphous oxide semiconductors.* Nature, 2004. **432**(7016): p. 488-92.
3. H. Yabuta, et al., *High-mobility thin-film transistor with amorphous InGaZnO4 channel fabricated by room temperature rf-magnetron sputtering.* Applied Physics Letters, 2006. **89**(11).
4. T. Kamiya, K. Nomura, and H. Hosono, *Present status of amorphous In-Ga-Zn-O thin-film transistors.* Sci Technol Adv Mater, 2010. **11**(4): p. 044305.
5. J.-S. Park, et al., *Flexible full color organic light-emitting diode display on polyimide plastic substrate driven by amorphous indium gallium zinc oxide thin-film transistors.* Applied Physics Letters, 2009. **95**(1).
6. C.-H. Oh, et al., *21.1:Invited Paper: Technological Progress and Commercialization of OLED TV.* SID Symposium Digest of Technical Papers, 2013. **44**(1): p. 239-242.
7. J.S. Heo, J. Eom, Y.H. Kim, and S.K. Park, *Recent Progress of Textile-Based Wearable Electronics: A Comprehensive Review of Materials, Devices, and Applications.* Small, 2017.
8. K.J. Yu, Z. Yan, M. Han, and J.A. Rogers, *Inorganic semiconducting materials for flexible and stretchable electronics.* npj Flexible Electronics, 2017. **1**(1).
9. M.-J. Lee, et al., *Low-Temperature-Grown Transition Metal Oxide Based Storage Materials and Oxide Transistors for High-Density Non-volatile Memory.* Advanced Functional Materials, 2009. **19**(10): p. 1587-1593.
10. P. Heremans, et al. *Flexible metal-oxide thin film transistor circuits for RFID and health patches*. in *Electron Devices Meeting (IEDM), 2016 IEEE International*. 2016. IEEE.
11. H. Ozaki, T. Kawamura, H. Wakana, T. Yamazoe, and H. Uchiyama, *Wireless operations for 13.56-MHz band RFID tag using amorphous oxide TFTs.* IEICE Electronics Express, 2011. **8**(4): p. 225-231.
12. B.-D. Yang, *A Transparent Logic Circuit for RFID Tag in a-IGZO TFT Technology.* ETRI Journal, 2013. **35**(4): p. 610-616.
13. K. Myny, A.K. Tripathi, J.-L. van der Steen, and B. Cobb, *Flexible thin-film NFC tags.* IEEE Communications Magazine, 2015. **53**(10): p. 182-189.

14. J.M. Rothberg, et al., *An integrated semiconductor device enabling non-optical genome sequencing.* Nature, 2011. **475**(7356): p. 348-52.
15. Y.S. Rim, et al., *Interface Engineering of Metal Oxide Semiconductors for Biosensing Applications.* Advanced Materials Interfaces, 2017. **4**(10).
16. D.J. Yang, et al., *Amorphous InGaZnO4 films: Gas sensor response and stability.* Sensors and Actuators B: Chemical, 2012. **171-172**: p. 1166-1171.
17. J.T. Smith, S.S. Shah, M. Goryll, J.R. Stowell, and D.R. Allee, *Flexible ISFET Biosensor Using IGZO Metal Oxide TFTs and an ITO Sensing Layer.* IEEE Sensors Journal, 2014. **14**(4): p. 937-938.
18. T. Sugahara, et al., *Fabrication with Semiconductor Packaging Technologies and Characterization of a Large -Scale Flexible Thermoelectric Module.* Advanced Materials Technologies, 2018.
19. A. Nathan, et al., *Flexible Electronics: The Next Ubiquitous Platform.* Proceedings of the IEEE, 2012. **100**(Special Centennial Issue): p. 1486-1517.
20. K.K. Banger, et al., *Low-temperature, high-performance solution-processed metal oxide thin-film transistors formed by a 'sol–gel on chip' process.* Nature Materials, 2011. **10**(1): p. 45-50.
21. T. Hase, T. Kano, E. Nakazawa, and H. Yamamoto, *Phosphor Materials for Cathode-Ray Tubes*, in *Advances in Electronics and Electron Physics*, P.W. Hawkes, Editor. 1990, Academic Press. p. 271-373.
22. Y.-H. Park, J. Kim, M. Kim, W. Lee, and S. Lee, *Programmable multimedia platform based on reconfigurable processor for 8K UHD TV.* IEEE Transactions on Consumer Electronics, 2015. **61**(4): p. 516-523.
23. E. Nakasu, *Super Hi-Vision on the Horizon: A Future TV System That Conveys an Enhanced Sense of Reality and Presence.* IEEE Consumer Electronics Magazine, 2012. **1**(2): p. 36-42.
24. T. Arai, *Oxide-TFT technologies for next-generation AMOLED displays.* Journal of the Society for Information Display, 2012. **20**(3).
25. T. Kamiya, K. Nomura, and H. Hosono, *Present status of amorphous In–Ga–Zn–O thin-film transistors.* Science and Technology of Advanced Materials, 2010. **11**(4): p. 044305.
26. T. Arai and T. Sasaoka, *49.1: Invited Paper: Emergent Oxide TFT Technologies for Next-Generation AM-OLED Displays.* SID Symposium Digest of Technical Papers, 2011. **42**(1): p. 710-713.
27. Y.-M. Ha, et al., *69-1:Invited Paper: Oxide TFT Development for AMLCDs and*

AMOLEDs. SID Symposium Digest of Technical Papers, 2016. **47**(1): p. 940-943.
28. Y. Takeda, et al., *37-2: Development of high mobility top gate IGZO-TFT for OLED display.* SID Symposium Digest of Technical Papers, 2019. **50**(1): p. 516-519.
29. C.R. Kagan and P. Andry, *Thin-Film Transistors*. 2003: CRC Press.
30. H.A. Klasens and H. Koelmans, *A tin oxide field-effect transistor.* Solid-State Electronics, 1964. **7**(9): p. 701-702.
31. E. Fortunato, P. Barquinha, and R. Martins, *Oxide semiconductor thin-film transistors: a review of recent advances.* Adv Mater, 2012. **24**(22): p. 2945-86.
32. K. Nomura, et al., *Amorphous Oxide Semiconductors for High-Performance Flexible Thin-Film Transistors.* Japanese Journal of Applied Physics, 2006. **45**(5B): p. 4303-4308.
33. Y. Sun and J.A. Rogers, *Inorganic Semiconductors for Flexible Electronics.* Advanced Materials, 2007. **19**(15): p. 1897-1916.
34. J. Yeon Kwon and J. Kyeong Jeong, *Recent progress in high performance and reliable n-type transition metal oxide-based thin film transistors.* Semiconductor Science and Technology, 2015. **30**(2).
35. H. Hosono, *Ionic amorphous oxide semiconductors: Material design, carrier transport, and device application.* Journal of Non-Crystalline Solids, 2006. **352**(9-20): p. 851-858.
36. Y. Hwan Hwang, et al., *An 'aqueous route' for the fabrication of low-temperature-processable oxide flexible transparent thin-film transistors on plastic substrates.* NPG Asia Materials, 2013. **5**(4).
37. Y.S. Rim, H. Chen, T.-B. Song, S.-H. Bae, and Y. Yang, *Hexaaqua Metal Complexes for Low-Temperature Formation of Fully Metal Oxide Thin-Film Transistors.* Chemistry of Materials, 2015. **27**(16): p. 5808-5812.
38. S. Jeong, Y.G. Ha, J. Moon, A. Facchetti, and T.J. Marks, *Role of gallium doping in dramatically lowering amorphous-oxide processing temperatures for solution-derived indium zinc oxide thin-film transistors.* Adv Mater, 2010. **22**(12): p. 1346-50.
39. A. Liu, H. Zhu, H. Sun, Y. Xu, and Y.Y. Noh, *Solution Processed Metal Oxide High-kappa Dielectrics for Emerging Transistors and Circuits.* Adv Mater, 2018: p. e1706364.
40. J.W. Park, B.H. Kang, and H.J. Kim, *A Review of Low-Temperature Solution-Processed Metal Oxide Thin-Film Transistors for Flexible Electronics.* Advanced Functional Materials, 2019.
41. H. Zhu, et al., *Printable Semiconductors for Backplane TFTs of Flexible OLED*

Displays. Advanced Functional Materials, 2019. **0**(0): p. 1904588.
42. W. Xu, H. Li, J.B. Xu, and L. Wang, *Recent Advances of Solution-Processed Metal Oxide Thin-Film Transistors.* ACS Appl Mater Interfaces, 2018. **10**(31): p. 25878-25901.
43. S.R. Thomas, P. Pattanasattayavong, and T.D. Anthopoulos, *Solution-processable metal oxide semiconductors for thin-film transistor applications.* Chem Soc Rev, 2013. **42**(16): p. 6910-23.
44. S.J. Kim, S. Yoon, and H.J. Kim, *Review of solution-processed oxide thin-film transistors.* Japanese Journal of Applied Physics, 2014. **53**(2S).
45. W.H. Jeong, J.H. Bae, and H.J. Kim, *High-Performance Oxide Thin-Film Transistors Using a Volatile Nitrate Precursor for Low-Temperature Solution Process.* IEEE Electron Device Letters, 2012. **33**(1): p. 68-70.
46. M.G. Kim, M.G. Kanatzidis, A. Facchetti, and T.J. Marks, *Low-temperature fabrication of high-performance metal oxide thin-film electronics via combustion processing.* Nat Mater, 2011. **10**(5): p. 382-8.
47. J.S. Seo, et al., *Solution-processed flexible fluorine-doped indium zinc oxide thin-film transistors fabricated on plastic film at low temperature.* Sci Rep, 2013. **3**: p. 2085.
48. M.-G. Kim, M.G. Kanatzidis, A. Facchetti, and T.J. Marks, *Low-temperature fabrication of high-performance metal oxide thin-film electronics via combustion processing.* Nature Materials, 2011. **10**(5): p. 382-388.
49. Y. Chen, et al., *Nitroacetylacetone as a Cofuel for the Combustion Synthesis of High-Performance Indium–Gallium–Zinc Oxide Transistors.* Chemistry of Materials, 2018. **30**(10): p. 3323-3329.
50. J.W. Hennek, et al., *Oxygen "getter" effects on microstructure and carrier transport in low temperature combustion-processed a-InXZnO (X = Ga, Sc, Y, La) transistors.* J Am Chem Soc, 2013. **135**(29): p. 10729-41.
51. X. Yu, et al., *Spray-combustion synthesis: Efficient solution route to high-performance oxide transistors.* Proceedings of the National Academy of Sciences, 2015. **112**(11): p. 3217-3222.
52. S.J. Kim, et al., *Independent chemical/physical role of combustive exothermic heat in solution-processed metal oxide semiconductors for thin-film transistors.* Journal of Materials Chemistry C, 2015. **3**(7): p. 1457-1462.
53. W.J. Scheideler, R. Kumar, A.R. Zeumault, and V. Subramanian, *Low-Temperature-Processed Printed Metal Oxide Transistors Based on Pure Aqueous Inks.*

Advanced Functional Materials, 2017. **27**(14).
54. S.J. Heo, D.H. Yoon, T.S. Jung, and H.J. Kim, *Recent advances in low-temperature solution-processed oxide backplanes.* Journal of Information Display, 2013. **14**(2): p. 79-87.
55. T. Jun, et al., *High-performance low-temperature solution-processable ZnO thin film transistors by microwave-assisted annealing.* Journal of Materials Chemistry, 2011. **21**(4): p. 1102-1108.
56. Y.S. Rim, et al., *Simultaneous modification of pyrolysis and densification for low-temperature solution-processed flexible oxide thin-film transistors.* Journal of Materials Chemistry, 2012. **22**(25): p. 12491-12497.
57. Y.J. Tak, et al., *Modified Stoichiometry in Homogeneous Indium-Zinc Oxide System as Vertically Graded Oxygen Deficiencies by Controlling Redox Reactions.* Advanced Materials Interfaces, 2016. **3**(4).
58. S.-Y. Han, G.S. Herman, and C.-h. Chang, *Low-Temperature, High-Performance, Solution-Processed Indium Oxide Thin-Film Transistors.* Journal of the American Chemical Society, 2011. **133**(14): p. 5166-5169.
59. S. Dellis, et al., *Rapid laser-induced photochemical conversion of sol–gel precursors to In2O3 layers and their application in thin-film transistors.* Journal of Materials Chemistry C, 2017. **5**(15): p. 3673-3677.
60. C.-N. Chen and J.-J. Huang, *Effects of excimer laser annealing on low-temperature solution based indium-zinc-oxide thin film transistor fabrication.* Journal of Applied Research and Technology, 2015. **13**(2): p. 170-176.
61. P.K. Nayak, M.N. Hedhili, D. Cha, and H.N. Alshareef, *High performance solution-deposited amorphous indium gallium zinc oxide thin film transistors by oxygen plasma treatment.* Applied Physics Letters, 2012. **100**(20).
62. K.-S. Kim, Y.-H. Hwang, I. Hwang, and W.-J. Cho, *Improved performance of solution-processed a-InGaZnO thin-film transistors due to Ar/O2 mixed-plasma treatment.* Journal of the Korean Physical Society, 2014. **65**(3): p. 399-403.
63. Y.-H. Hwang, K.-S. Kim, and W.-J. Cho, *Effects of combined Ar/O2plasma and microwave irradiation on electrical performance and stability in solution-deposited amorphous InGaZnO thin-film transistors.* Japanese Journal of Applied Physics, 2014. **53**(4S).
64. Y.H. Kim, et al., *Flexible metal-oxide devices made by room-temperature photochemical activation of sol-gel films.* Nature, 2012. **489**(7414): p. 128-32.
65. J. Leppäniemi, et al., *Rapid low-temperature processing of metal-oxide thin film*

transistors with combined far ultraviolet and thermal annealing. Applied Physics Letters, 2014. **105**(11).

66. S. Park, et al., *In-Depth Studies on Rapid Photochemical Activation of Various Sol-Gel Metal Oxide Films for Flexible Transparent Electronics.* Advanced Functional Materials, 2015. **25**(19): p. 2807-2815.

67. R.A. John, et al., *Low-Temperature Chemical Transformations for High-Performance Solution-Processed Oxide Transistors.* Chemistry of Materials, 2016. **28**(22): p. 8305-8313.

68. H. Jae-Sang, et al., *Photochemically Activated Flexible Metal-Oxide Transistors and Circuits Using Low Impurity Aqueous System.* IEEE Electron Device Letters, 2015. **36**(2): p. 162-164.

69. H. Chein and T.M. Chen, *Emission Characteristics of Volatile Organic Compounds from Semiconductor Manufacturing.* Journal of the Air & Waste Management Association, 2012. **53**(8): p. 1029-1036.

70. D.H. Lee, Y.J. Chang, G.S. Herman, and C.H. Chang, *A General Route to Printable High-Mobility Transparent Amorphous Oxide Semiconductors.* Advanced Materials, 2007. **19**(6): p. 843-847.

71. G.H. Kim, et al., *Inkjet-printed InGaZnO thin film transistor.* Thin Solid Films, 2009. **517**(14): p. 4007-4010.

72. Y. Wang, X.W. Sun, G.K.L. Goh, H.V. Demir, and H.Y. Yu, *Influence of Channel Layer Thickness on the Electrical Performances of Inkjet-Printed In-Ga-Zn Oxide Thin-Film Transistors.* IEEE Transactions on Electron Devices, 2011. **58**(2): p. 480-485.

73. J. Leppaniemi, O.H. Huttunen, H. Majumdar, and A. Alastalo, *Flexography-Printed In2 O3 Semiconductor Layers for High-Mobility Thin-Film Transistors on Flexible Plastic Substrate.* Adv Mater, 2015. **27**(44): p. 7168-75.

74. Y. Choi, et al., *Characteristics of gravure printed InGaZnO thin films as an active channel layer in thin film transistors.* Thin Solid Films, 2010. **518**(22): p. 6249-6252.

75. Y.S. Rim, et al., *Direct light pattern integration of low-temperature solution-processed all-oxide flexible electronics.* ACS Nano, 2014. **8**(9): p. 9680-6.

76. K. Shinmou, N. Tohge, and T. Minami, *Fine-Patterning of $¥bf ZrO_{2}$ Thin Films by the Photolysis of Chemically Modified Gel Films.* Japanese Journal of Applied Physics, 1994. **33**(Part 2, No. 8B): p. L1181-L1184.

77. H.S. Lim, Y.S. Rim, and H.J. Kim, *Photoresist-free fully self-patterned transparent amorphous oxide thin-film transistors obtained by sol-gel process.* Sci Rep,

2014. **4**: p. 4544.
78. H.J. Kim, et al., *Self-Pattern Process of InZnO Thin-Film Transistors using Photosensitive Precursors.* SID Symposium Digest of Technical Papers, 2017. **48**(1): p. 180-182.
79. K.-H. Wang, H.-W. Zan, and O. Soppera, *The zinc-loss effect and mobility enhancement of DUV-patterned sol–gel IGZO thin-film transistors.* Semiconductor Science and Technology, 2018. **33**(3).

Chapter 2: Experimental methods

This chapter present the general method to fabricate solution-processed oxide TFTs. Characterization techniques including evaluation and chemical analysis are also addressed to understand the quality of the fabricated films.

2.1 Precursor synthesis

Precursor synthesis was prepared by the following manner.

ZTO precursor with organic solvent

A precursor solution was prepared by dissolving zinc acetate dihydrate ($Zn(CH_3COO)_2 \cdot 2H_2O$) and tin chloride ($SnCl_2$) in 2-methoxyethanol at a specified Zn:Sn molar ratio. The precursor was stirred vigorously to completely dissolve the precursors in solution with a clear solution.

ZTO precursor with aqueous solvent

A precursor solution was prepared by dissolving zinc acetate dihydrate and tin chloride in deionized water at a specified Zn:Sn molar ratio. To increase the solubility in water, dilute hydrogen chroride solution (0.1%) was used. The precursor was stirred vigorously to completely dissolve the precursors in solution for more than 6 hours with a

clear solution.

IGZO precursor with aqueous solvent

A IGZO precursor solution was prepared by dissolving indium nitrate hydrate ($In(NO_3)_3 \cdot xH_2O$), gallium nitrate hydrate ($Ga(NO_3)_3 \cdot xH_2O$), and zinc nitrate hydrate ($Zn(NO_3)_2 \cdot xH_2O$) in deionized water at a specified molar ratio of In:Ga:Zn. The precursor was stirred vigorously to completely dissolve the precursors in solution.

Fluorine doped IGZO precursor with aqueous solvent

IGZO precursor solution was prepared by dissolving indium nitrate hydrate, gallium nitrate hydrate, and zinc nitrate hydrate in deionized water at a specified molar ratio of In:Ga:Zn. As a fluorine doping, dilute hydrogen fluoride solution was used to the precursor to produce F doped IGZO precursor. The precursor was stirred vigorously for complete dissolution.

Figure 2.1. Image for the IGZO precursor

2.2 Oxide Film fabrication

Spin-coating process

Solution-processed oxide thin films were deposited by spin-coating method on substrates. Spin coating is traditional and simple film fabrication method by using centrifugal force. After dispensing the precursor solution on to a substrate, then the substrate is spun at high speed between 1000 – 6000rpm. Rapid rotation results in the fabrication of uniform thin films. Soft annealing process at 100-150°C is preformed after spin-coating process to evaporate the excess solvents, followed by thermal annealing at high temperature over 300°C for forming M-O-M bonding.

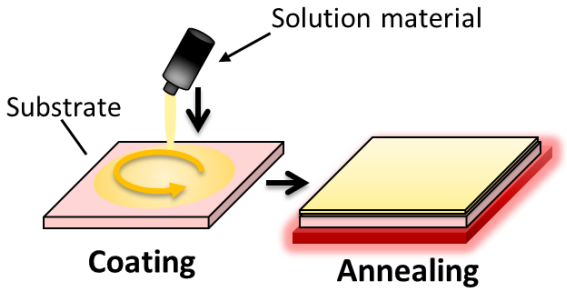

Figure 2.2. schematic of the standard spin-coating process.

Magnetron sputtering

Metal electrode using molybdenum (Mo) were deposited by magnetron sputtering method. Magnetron sputtering is a traditional vacuum deposition method for various types of materials including oxides, metal, alloys. The oxides materials such as IGZO and other metal are typically deposited by this method. Basic mechanisms of sputtering coating process are illustrated in figure 2.3. Firstly, a target material, which is deposited, is bombarded with energetic ions such as argon gases. The collision between the ions and

the surface ejects target materials as sputtered particles, followed by deposition on the substrate forming a thin film[1, 2]. The cathode is typically with the target materials, while the substrates are placed on the anode. In magnetron sputtering, magnets are employed to increase the sputtering efficiency due to improvement of plasma density compared to the sputtering method without magnet. The advantages of sputtering method are controllability and reproducibility of film by adjusting sputtering parameter such as pressure, the flow rate of gases, discharging power, and sputtering time.

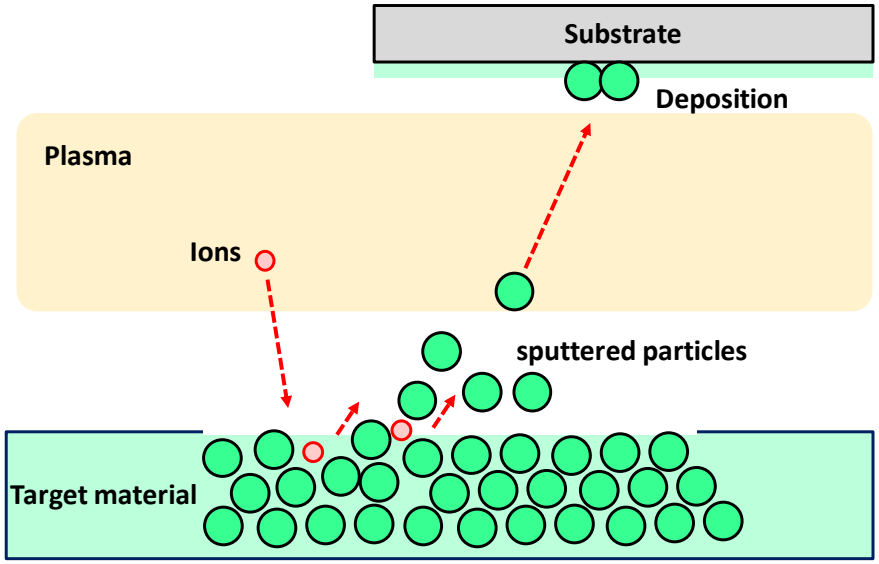

Figure 2.3. Schematic illustration of sputtering deposition for metal electrodes.

2.3 TFTs fabrication and evaluation

TFT fabrication

Figure 2.4. show the fabricated bottom-gated top-contact TFT structure. Considering the typical device structure of display backplane, the TFT characteristics were evaluated using this typical device structure. Firstly, synthesized precursors were spin-coated on n^+-Si substrates. The precursor solutions were passed through a polytetrafluoroethylene (PTFE) filter. Spin coating of the precursor solution was performed, followed by soft annealing at 150 °C for 10 min and subsequent annealing at a specific temperature (200 - 300°C) for 1 h in air to yield the solution-processed oxide thin film deposited on the substrate.

After fabrication of the solution processed IGZO thin film, the active area of the film was patterned as an island shape using a conventional photolithography method followed by wet chemical etching. Then, the molybdenum for source and drain electrodes were formed on the oxide films via a shadow mask by magnetron sputtering. Finally, thermal annealing was performed at 150°C for 1 h. The fabricated device was a bottom-gate, top-contact TFT with 1000 μm channel widths (W) and 100 μm channel lengths (L). The n^+-Si substrates were used as the gate electrode. To evaluate bias stability, the TFTs were encapsulated with a coating-type passivation layer (ZEOCOAT, cycloolefin resin, Zeon Corporation) to prevent interaction with the atmosphere at the back channel of the semiconductor layer.

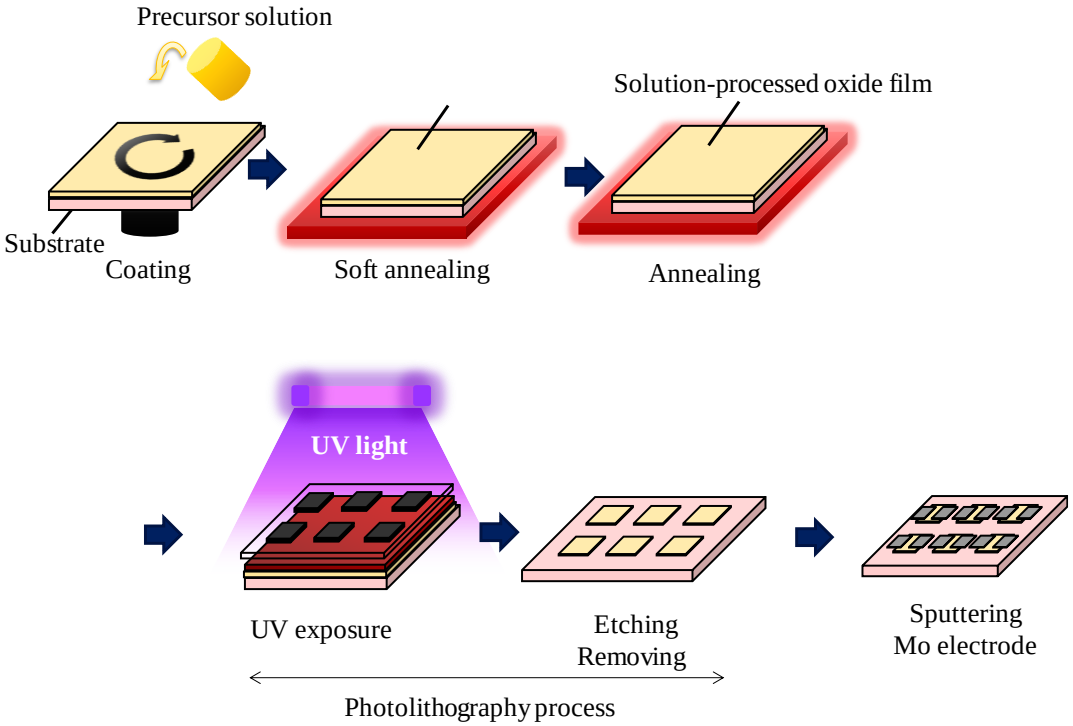

Figure 2.4. Fabricated flow for bottom-gate top-contact TFT with solution-processed oxide

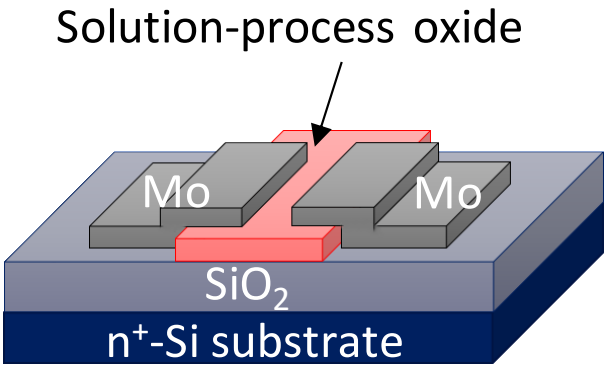

Figure 2.5. Schematic illustration of fabricated bottom-gate top-contact TFT structure with solution-processed oxide

TFT fabrication on flexible substrate

The IGZO TFTs on a flexible polyimide substrate were fabricated using polyimide varnish. A polyimide film was spin-coated on a glass substrate, followed by forming a barrier layer of SiO_2 by DC sputtering method. After formation of the gate electrode of molybdenum by DC sputtering, a SiO_2 gate insulator film was deposited by sputtering deposition. Then, the substrate was treated with oxygen plasma for 30 s to enhance hydrophilicity. Spin-coating of the oxide precursor was performed. then, the fabrication processes were followed with the same method as mentioned earlier. After fabrication of the TFTs on film with glass substrate, the polyimide film was mechanically peeled from the glass substrate.

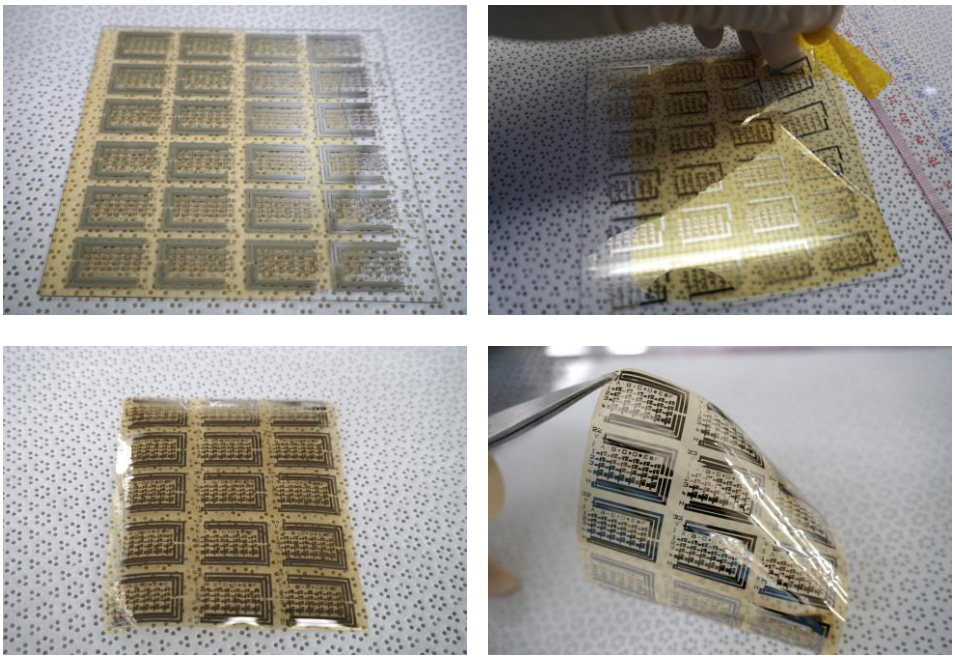

Figure 2.6. Images for the fabrication process for the oxide TFTs with flexible substrate

TFT evaluation

Evaluation of the TFTs was performed using an electrical measurement system with a probe station and a semiconductor analyzer (Keithley HP4156C) at 25°C.

The saturation mobility (μ) was calculated by the following equation:

$$\mu = \frac{2L}{WC_i}\left(\frac{\partial\sqrt{I_d}}{\partial V_g}\right)^2,$$

where W is the channel width, L is the channel length, V_g is the source-gate voltage, Id is the saturation current, and C_i is the capacitance of the gate dielectric per unit area.

The S.S. is the inverse of the maximum slope of the transfer characteristics, which indicate the applied gate voltage V_g to obtain 10 times larger I_{ds}. This value means the The S.S was calculated by the following equation:

$$\mathrm{S.S} = \left(\frac{\partial(\log_{10} I_{ds})}{\partial V_{gs}}\right)^{-1}$$

On/off current ratio (I_{on}/I_{off}) of TFTs indicate the ratio of the saturation current of I_{ds} to the noise signal of I_{ds} with off state.

2.4 Thin film characterization

Thermal Desorption Spectrometry (TDS)

TDS analyze the amount of desorption of the emitted gas by heating the temperature. The gases from the oxide film were continuously analyzed by a mass spectrometer as a function of the temperature. The desorbed impurities such as organic and inorganic residuals from the films were assessed by tracking the mass fragments.

Fourier Transform Infrared Spectroscopy (FT-IR)

FT-IR is the analytical method to identify the chemical structure by measuring the absorption of infrared light, which is based on the functional groups in the materials. Solution-processed oxides were also analyzed by FT-IR to analyze the chemical structure of the film. The thin film samples were prepared onto silicon-wafer as a substrate.

Secondary ion mass spectrometry (SIMS)

SIMS is the surface analysis to determine the elemental depth profile. The solution-processed oxide films were analyzed to evaluate the concentration of element inside films with depth analysis. When a primary ion such as oxygen or cesium are irradiated on the surface, the ions of atoms are ejected into the vacuum as sputtering. The ejected secondary ions were analyzed by mass-spectrometry.

X-ray Photoelectron Spectroscopy (XPS)

XPS is the surface analytical method to determine the atomic composition and chemical state of thin films. Irradiating a sample with X-ray results in emissions of photoelectrons, which represent the chemical state of elements. XPS analysis was performed for the oxide films to evaluate the chemical bonding within the films. M-O-M bonding of oxide films were analyzed by the curve fitting of the O1s peak. The O1s peak was deconvoluted into 3 components peaks including oxygen lattice, O_M (lattice oxygen), O_V (oxygen vacancy) and O_{OH} (hydroxyl) peaks at 530.4, 531.4, and 532.2 eV, respectively[3].

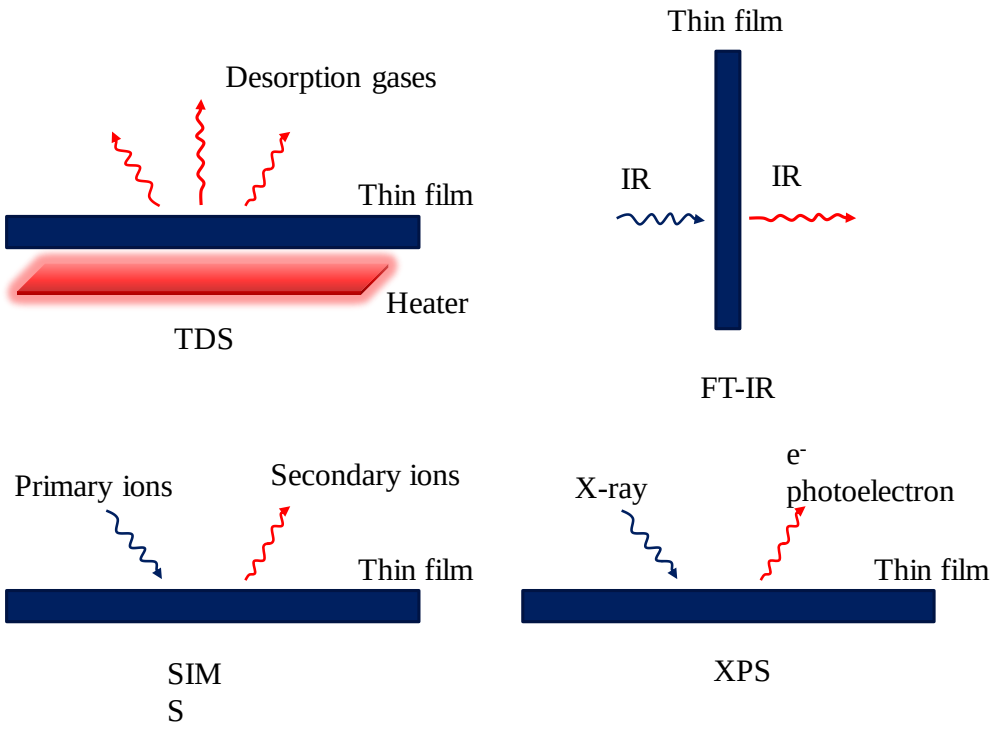

Figure 2.7. Schematic for film characterization

2.5 References

1. K. Wasa, M. Kitabatake, and H. Adachi, *Thin film materials technology: sputtering of control compound materials*. 2004: Springer Science & Business Media.
2. K. Wasa, *2 - Sputtering Phenomena*, in *Handbook of Sputtering Technology (Second Edition)*, K. Wasa, I. Kanno, and H. Kotera, Editors. 2012, William Andrew Publishing: Oxford. p. 41-75.
3. S. Jeong, Y.G. Ha, J. Moon, A. Facchetti, and T.J. Marks, *Role of gallium doping in dramatically lowering amorphous-oxide processing temperatures for solution-derived indium zinc oxide thin-film transistors.* Adv Mater, 2010. **22**(12): p. 1346-50.

Chapter 3: Application of hydrogen injection and oxidation to organic based solution-processed zinc tin oxide semiconductors

3.1 Introduction

To ensure the effective decomposition of residual species for low-temperature solution-processed metal oxide, new methodology initiates a reduction reaction by introducing a hydrogen injection process. One of the greatest impediments to achieve high device performance following low temperature processing is the efficient decomposition of residual species. This chapter focus on Zinc Tin Oxide (ZTO) by organic precursor as conventional precursor system[1-8].

According to previous research regarding hydrogen plasma and oxide materials, hydrogen plasma is effective at reducing the resistivity of oxide films by acting as a reducing agent. The hydrogen generates oxygen vacancies due to the generation of O-H and H_2O condensation [9]. In previous annealing processes related to hydrogen, hydrogen increases the carrier concentration via the formation of donor states and oxygen vacancies by a reduction reaction with weak chemical bonds [10]. We considered that the reduction reaction of hydrogen is effective at decomposing residual species even in low-temperature solution-processed oxide films.

In this chapter, hydrogen injection and oxidation process (HIO) by the combination process of hydrogen plasma and subsequent oxidation. The hydrogen plasma treatment was applied directly as an effective reducing agent for residual species. In addition, subsequent oxidation was applied to achieve film densification after removal of the impurities. The maximum temperature that is applied over the entire fabrication process can be as low as 300 °C.

3.2 Experimental

Precursor synthesis

A 0.3 M precursor solution was prepared by dissolving zinc acetate dihydrate ($Zn(CH_3COO)_2 \cdot 2H_2O$, Aldrich) and tin chloride ($SnCl_2$, Aldrich) in 2-methoxyethanol at a Zn:Sn molar ratio of 2:1. The precursor was stirred vigorously to completely dissolve the precursors in solution. All reagents were obtained from Aldrich and were used as received without further purification.

Film fabrication

Solution-processed ZTO films were fabricated by spin-coating onto 200-nm-thick, thermally oxidized SiO_2/n^+-Si substrates. The SiO_2 substrates were treated by O_2 plasma for 30 s to obtain a hydrophilic surface and a good interface with the semiconductor layer. These n^+-Si substrates also served as the gate electrode, with a resistivity of 1 mΩcm. Spin coating of the precursor solution was performed at 3000 rpm for 30 sec at room temperature, followed by and subsequent annealing at a specific temperature (200 - 300°C) for 1 h in air. In this manner, about 10-nm-thick ZTO films were deposited on the

substrates. The precursor solution was passed through a 0.22 μm polytetrafluoroethylene (PTFE) filter.

Hydrogen injection and oxidation process

The Hydrogen injection and oxidation process (HIO) process was applied to some of the solution-processed thin films. Figure 3.1. shows a schematic illustration of the HIO process used for the solution-processed thin film. Hydrogen injection was conducted by hydrogen plasma treatment using plasma etching apparatus, after which an additional annealing process was immediately performed, which represents the oxidation process. The plasma treatment condition for the hydrogen injection process was pure H_2 at a flow rate of 50 sccm with a source power of 200 W. Following the plasma treatment, the oxidation process by thermal annealing was immediately applied at the same temperature as that for the first anneal for 1 h in air. The thin films not subjected to the HIO process were also prepared using only the latter oxidation process to achieve the same annealing time.

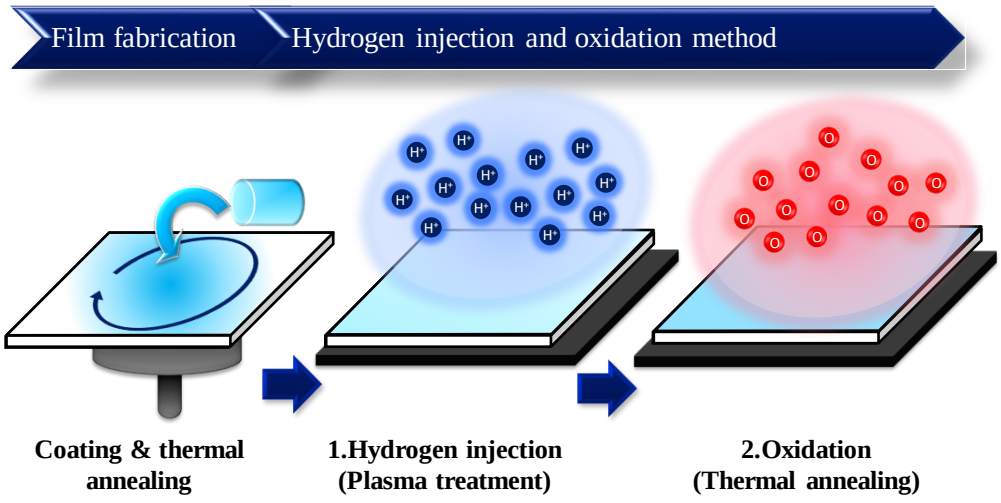

Figure 3.1. Schematic illustration of experimental process for a solution processed ZTO film with HIO method. Solution processed films were prepared using spin-coating and thermal annealing. HIO method is consisted from 2 separate process by hydrogen injection process and oxidation process.

3.3 TFT fabrication and characterization

After fabrication of the solution processed thin film, the active area of the film was patterned as an island shape using a conventional photolithography method followed by wet chemical etching using ITO-07N (Kanto Chemical Co. Inc.). Patterned source/drain (S/D) electrodes (Mo) were formed on the thin films via a shadow mask by DC sputtering. The thickness of the electrodes was ca. 50 nm. The fabricated device was a bottom-gate, top-contact TFT with 1000 μm channel widths (W) and 100 μm channel lengths (L). The n^+-Si substrates were used as the gate electrode. Evaluation of the TFTs was performed using an electrical measurement system with a probe station and a semiconductor analyzer (Keithley HP4156C). The fabricated films were characterized using secondary ion mass spectrometry (SIMS; PHI Corporation ADEP11010), thermal desorption spectroscopy (TDS; ESCO EMD-WA1000S), and X-ray photoelectron spectroscopy (XPS; ULVAC-PHI PHI Quantera II).

3.4 Chemical and structural analysis for ZTO film

To verify the effects of the HIO process, the concentrations of residual species were determined by secondary ion mass spectrometry (SIMS) and thermal desorption spectroscopy (TDS) analyses of ZTO films made with and without HIO processing. Figure 3.2. shows the C, Cl and H atom depth profiles of each sample, as obtained by SIMS measurements, while Figure 3.3. presents the TDS data. The desorption of chloride and carbon atoms was assessed by tracking the mass fragments at m/z values of 35 and 44, corresponding to Cl^+ and CO_2^+. The amounts of carbon and chloride atoms were analyzed because the ZTO TFT precursor solution contained chloride and acetate salts. In addition, the concentration of hydrogen was assessed so as to verify the effectiveness of the hydrogen injection process. Interestingly, as shown in Figures 3.2. and 3.3., the HIO processed ZTO film contained lower concentrations of carbon and chloride atoms.

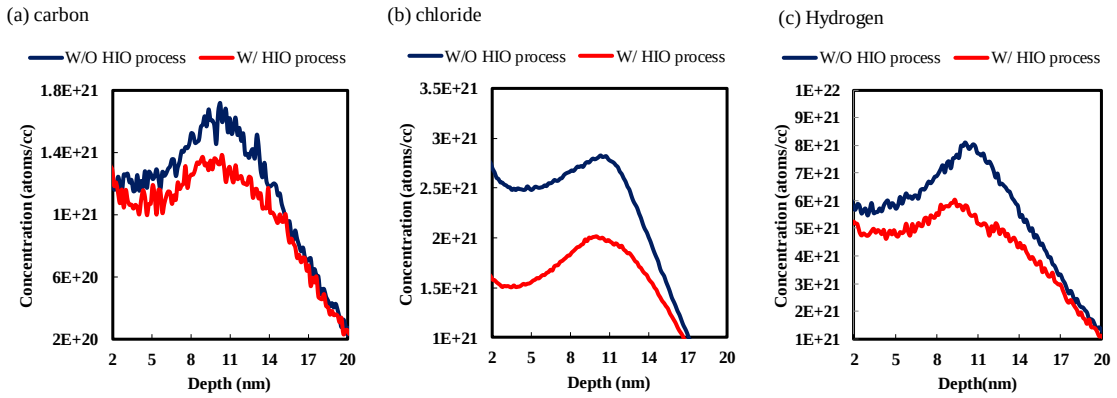

Figure 3.2. SIMS spectra showing (a) carbon, (b) chloride and (c) hydrogen concentrations in ZTO films fabricated at a low temperature with and without the HIO process

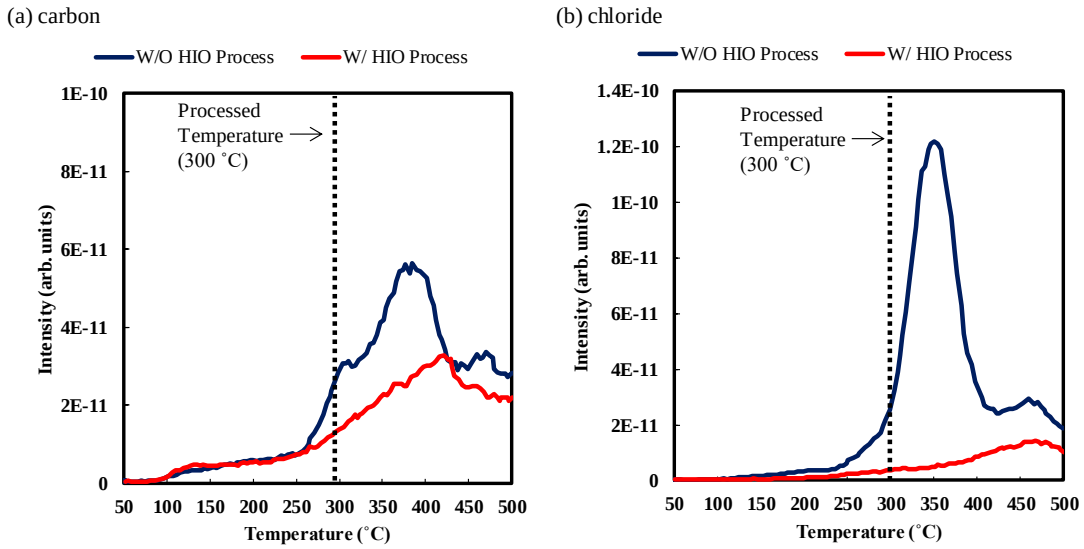

Figure 3.3. TDS spectra for (a) carbon (m/z of 35) and (b) chloride (m/z of 35) obtained from ZTO films fabricated at a low temperature with and without the HIO process.

It is therefore evident that the HIO process is effective at eliminating these residual species. The chloride concentration was especially decreased following the HIO process. A reduction in the hydrogen concentration was also observed, despite the hydrogen injection step. The SIMS depth profiles indicate that there is some variation in these decreases with film depth, although decreases are observed even in the middle of the films. The TDS results demonstrate that the conventional process generated rapid increases in the concentrations of Cl and C fragments above 350 °C, and so it is apparent that the ZTO film requires much high annealing temperatures. In contrast, the extent of desorption from the ZTO film treated with the HIO process was significantly decreased. To further analyze the ZTO film made with the HIO process, the densities of these films were determined by X-ray reflectivity (XRR). Table 3.1. presents the densities of ZTO films fabricated with and without the HIO process, from which it can be seen that the HIO processed ZTO film was denser.

Table 3.1. Densities of ZTO films made without and with the HIO process.

	Without HIO process	With HIO process
Film density	4.81 g/cm^3	4.96 g/cm^3

The chemical states of ZTO films prepared with and without the HIO process were examined by X-ray photoelectron spectroscopy (XPS), and Figure 3.4. summarizes the O 1s results. The O 1s peaks were analyzed by curve-fitting the O1 (lattice oxygen), O2 (oxygen deficient) and O3 (hydroxyl) peaks. For this purpose, three peaks were assessed, at 530.4, 531.4 and 532.2 eV [11]. The 530.4 eV was assigned to oxygen bonded to metallic atoms, the 531.4 eV peak to oxygen vacancies and the peak at 532.2 eV to impurity-related oxygen species, such as hydroxyl groups. Table 3.2. presents the resulting data. Figure 3.4. confirms increased metal oxide-to-metal bond formation (associated with O1 oxygen bonds) following the application of the HIO method. In addition, a reduction of the O2 peak is observed in the case of the ZTO fabricated with the HIO method.

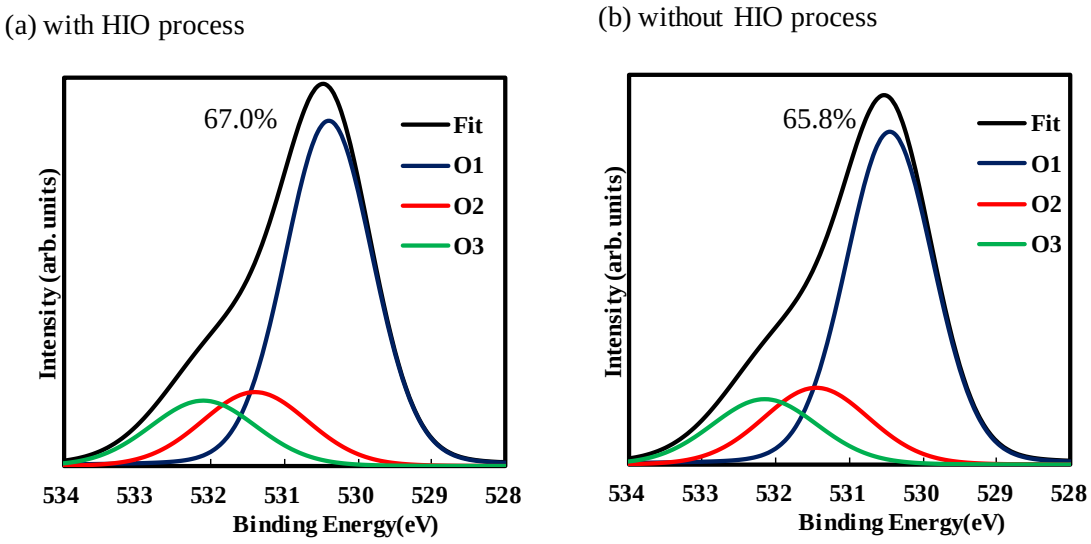

Figure 3.4. O 1s XPS spectra obtained from ZTO films fabricated (a) with and (b) without the HIO process.

Table 3.2. XPS O 1s peak data for ZTO films made without and with the HIO process.

	O 1s peak area		
	O1 (lattice oxygen)	O2 (oxygen deficient)	O3 (hydroxyl)
Without HIO process	65.8	18.4	15.8
With HIO process	67.0	17.5	15.5

The data obtained for the low temperature processed ZTO show that it contains numerous residual species, such as chloride and carbon atoms. Because the annealing temperature was not sufficiently high, unreacted precursors remained. According to previous studies regarding the hydrogen plasma treatment of aluminum doped ZTO films[9], hydrogen can act as an effective reducing agent, increasing the quantity of free electrons and improving the film conductivity due to the generation of oxygen vacancies.

In a study of IGZO TFTs, hydrogen added at an adequate concentration was found to function as an electron donor in interstitial locations or at oxygen sites as the result of passivation of oxygen vacancies and total traps[12, 13]. The decrease in the trap concentration can be explained by asserting the role of OH groups. Thus, the improvements observed in device performance following HIO processing are not only due to greater conductivity. It indicates that this HIO process is different from other plasma treatment processes based on the ion bombardment effect[14-17].

The HIO process is based on a combination of a hydrogen injection process and an oxidation process, and Figure 3.5. provides an illustration describing the HIO mechanism. We assumed that the following three steps are included in the current HIO process: hydrogen injection, a reduction reaction, and oxidation.

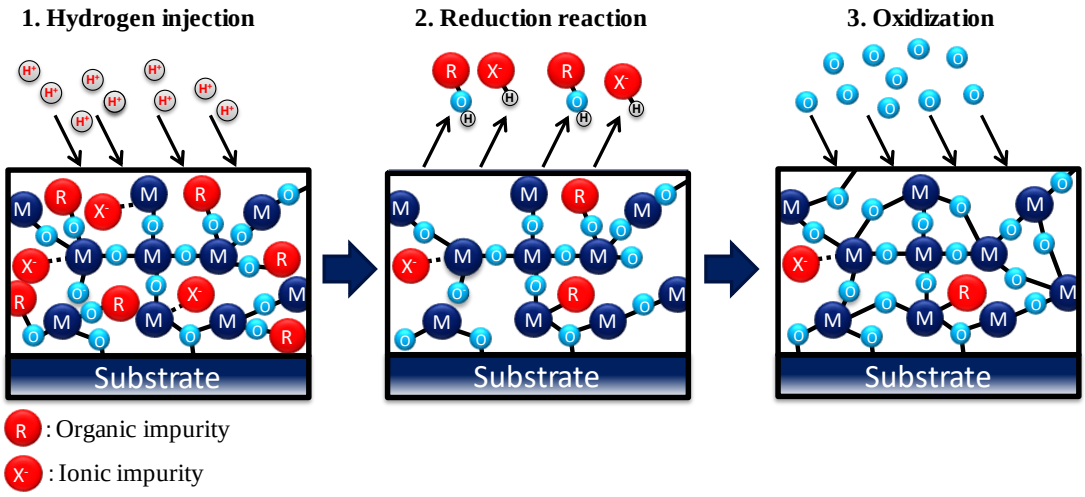

Figure 3.5. Schematic summarizing the HIO process as applied to a low temperature solution-processed oxide semiconductor film. The dark blue and light blue circles represent metal and oxygen atoms, respectively. Residual organic and ionic impurities are indicated by red circles. The HIO process is shown to consist of a reduction reaction induced by hydrogen injection, leading to desorption of the residual species.

Based on the large decreases in the concentrations of residual species, the effect of

the hydrogen is evidently critical to eliminating these residual compounds. The decreased hydrogen concentration following the HIO process may imply that the injected hydrogen acted as an effective reducing agent and thus promoted reduction reactions. During the hydrogen injection process, the efficient reduction of organic and ionic impurities takes place, as the H^+ in the hydrogen plasma readily reacts with oxygen and chloride atoms in the ZTO films. The following are the general chemical reactions involved.

$$M\text{-}OR + H^+ \rightarrow M^+ + R\text{-}OH$$

$$M^+\text{-}\ Cl^- + H^+ \rightarrow M^+ + H\text{-}Cl$$

Here -OR represents the carbon impurities originating from the acetate base in the ZTO precursor, while Cl^- is the chloride impurity. The resulting decrease in the hydrogen concentration is consistent with the release of the reaction products into the gas phase during this process. Thus, we believe that the efficient reduction of organic and ionic impurities takes place based on the above chemical reduction reactions, as shown in Figure 3.5. During the reduction reactions initiated by the hydrogen injection process, oxygen bonds to the metal are also degraded. However, sequential oxidation during the subsequent annealing reforms oxygen bonds among the pore sites at which the impurities were located. Based on the evident film densification generated by the HIO process, this is attributed to efficient oxidation.

3.5 TFT characteristics for ZTO thin film by applying HIO

Finally, to analyze the feasibility of the proposed HIO process, ZTO TFTs were fabricated using the HIO process at a relatively low temperature of 300°C. After deposition of the oxide films, the active areas were defined by a conventional photolithography method to eliminate any parasitic currents. Following this, the HIO process was applied to the defined oxide films, using the same conditions in each trial. Finally, patterned source/drain (S/D) electrodes (Mo) were formed via a shadow mask technique. In this manner, bottom-gate, top-contact ZTO TFTs were obtained with 1000 μm channel widths (W) and 100 μm channel lengths (L). Figure 3.6(a) provides an illustration of the cross-section of these devices and a photographic image of a finished TFT.

Figure 3.6(b) summarizes the transfer characteristics of ZTO TFTs fabricated with and without the HIO process. The transfer characteristics of these ZTO TFTs at gate voltages (V_g) ranging from –30 to 30 V were assessed at a fixed drain voltage (V_d) of 30 V. The calculated electrical characteristics are also summarized in Table 3. As the Figure 3.6. clearly shows, the TFT performance was improved by applying the HIO process. In previous studies regarding the effects of annealing temperature, the device performance obtained from ZTO TFTs was found to vary significantly with the annealing temperature[6]. Specifically, lower temperature processing (below 400°C) resulted in a significant reduction of the device performance. By employing the HIO process, a drastic improvement in the field-effect mobility was achieved, obtaining a value over 3.0 cm^2/Vs at a low temperature of 300°C. In addition, the suppression of hysteresis in the V_{hyst} data at a drain current of 10^{-9} A was confirmed for the ZTO TFT made by applying the HIO

method. This non-equilibrium hysteresis characteristic is considered as electron trapping within or near the channel electron accumulation layer between ZTO and its gate dielectric induced by the gate voltage. Considering the amount of existing impurities insides ZTO, residual species such as carbon and chloride impurities act as either carrier traps or defect sites. We propose that the suppression of the hysteresis by applying the HIO is consistent with a reduction of residual species. Although the suppression of hysteresis was achieved. ZTO film with HIO still has the 1.9V hysteresis. This indicates that the film still has large amount of the electron trapping. Therefore, further improvement process is needed to obtain better TFT characteristics.

(a)

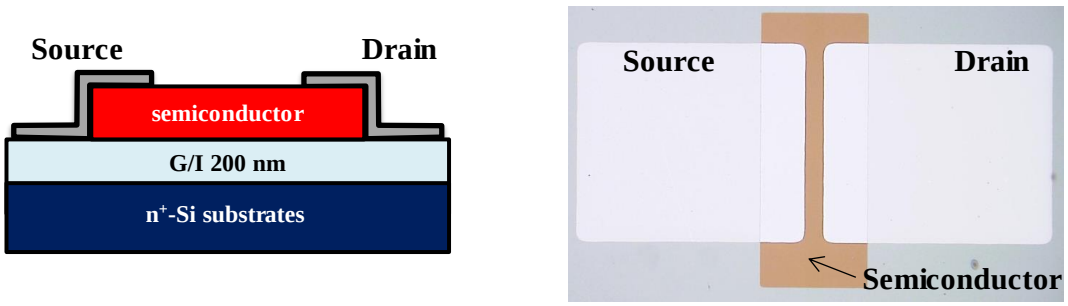

(b)

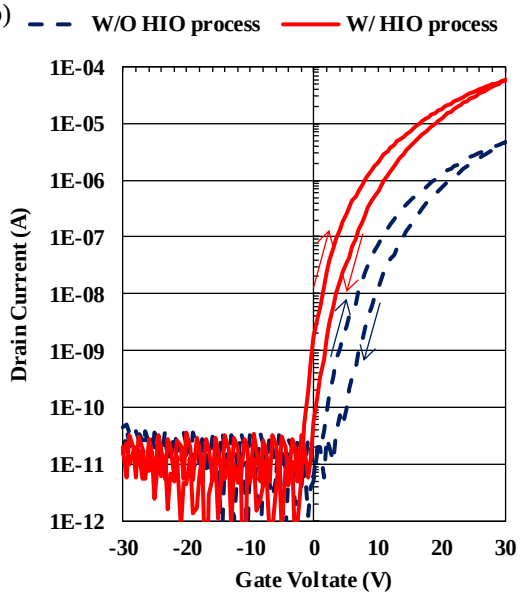

Figure 3.6. (a) Schematic diagram of a bottom-gate, top-contact TFT and a photographic image of a fabricated TFT, and transfer characteristics of (b) ZTO TFTs for which W/L = 1000 μm/100 μm, fabricated with and without the HIO process.

In addition, compared with previous plasma treatment processes that generate higher off currents due to the ion bombardment effect[13], these results do not show any such deterioration. Therefore, based on the above analyses, we attribute the improved performance of the ZTO TFTs to a significant decrease in the concentrations of residual species as well as to increased film densification. The removal of residual species is important because these tend to act as carrier traps that interfere with efficient carrier conductivity.

Table 3.3. The electrical characteristics of ZTO TFTs made without and with the HIO process.

	Mobility (cm^2/Vs)	I_{on}/I_{off}	S.S. (V/decade)	V_{on} (V)	V_{hyst} (V)
Without HIO process	0.3	-10^5	1.4	7.1	3.1
With HIO process	3.1	-10^6	1.0	1.7	1.9

3.6 Conclusions

This work demonstrated a general method employing the HIO process for the fabrication of low temperature solution-processed oxide semiconductors using ZTO with organic precursor. The HIO method is able to efficiently eliminate a large amount of residual species as well as to promote film densification upon sequential oxidation. Moreover, improvements in the TFT characteristics were seen upon applying the HIO process to ZTO TFTs.

3.7 References

1. C.-G. Lee and A. Dodabalapur, *Solution-processed zinc–tin oxide thin-film transistors with low interfacial trap density and improved performance.* Applied Physics Letters, 2010. **96**(24).
2. C.G. Choi, S.-J. Seo, and B.-S. Bae, *Solution-Processed Indium-Zinc Oxide Transparent Thin-Film Transistors.* Electrochemical and Solid-State Letters, 2008. **11**(1).
3. H.S. Kim, P.D. Byrne, A. Facchetti, and T.J. Marks, *High performance solution-processed indium oxide thin-film transistors.* J Am Chem Soc, 2008. **130**(38): p. 12580-1.
4. D.H. Lee, Y.J. Chang, G.S. Herman, and C.H. Chang, *A General Route to Printable High-Mobility Transparent Amorphous Oxide Semiconductors.* Advanced Materials, 2007. **19**(6): p. 843-847.
5. B.S. Ong, C. Li, Y. Li, Y. Wu, and R. Loutfy, *Stable, Solution-Processed, High-Mobility ZnO Thin-Film Transistors.* Journal of the American Chemical Society, 2007. **129**(10): p. 2750-2751.
6. S.-J. Seo, C.G. Choi, Y.H. Hwang, and B.-S. Bae, *High performance solution-processed amorphous zinc tin oxide thin film transistor.* Journal of Physics D: Applied Physics, 2009. **42**(3).
7. Y.-H. Kim, J.-I. Han, and S.K. Park, *Effect of Zinc/Tin Composition Ratio on the Operational Stability of Solution-Processed Zinc–Tin–Oxide Thin-Film Transistors.* IEEE Electron Device Letters, 2012. **33**(1): p. 50-52.
8. J.S. Lee, Y.-J. Kwack, and W.-S. Choi, *Low-temperature Solution-processed Zinc-tin-oxide Thin-film Transistor and Its Stability.* Journal of the Korean Physical Society, 2011. **59**(5): p. 3055-3059.
9. M. Morales-Masis, et al., *Hydrogen plasma treatment for improved conductivity in amorphous aluminum doped zinc tin oxide thin films.* APL Materials, 2014. **2**(9).
10. Y.J. Tak, et al., *Modified Stoichiometry in Homogeneous Indium-Zinc Oxide System as Vertically Graded Oxygen Deficiencies by Controlling Redox Reactions.* Advanced Materials Interfaces, 2016. **3**(4).
11. Y.J. Kim, et al., *Impact of the cation composition on the electrical performance of solution-processed zinc tin oxide thin-film transistors.* ACS Appl Mater Interfaces, 2014. **6**(16): p. 14026-36.
12. J. Kim, et al., *A study on H2 plasma treatment effect on a-IGZO thin film transistor.* Journal of Materials Research, 2012. **27**(17): p. 2318-2325.

13. T. Kamiya, K. Nomura, and H. Hosono, *Origins of High Mobility and Low Operation Voltage of Amorphous Oxide TFTs: Electronic Structure, Electron Transport, Defects and Doping.* Journal of Display Technology, 2009. **5**(7): p. 273-288.
14. P.K. Nayak, M.N. Hedhili, D. Cha, and H.N. Alshareef, *High performance solution-deposited amorphous indium gallium zinc oxide thin film transistors by oxygen plasma treatment.* Applied Physics Letters, 2012. **100**(20).
15. K.-S. Kim, Y.-H. Hwang, I. Hwang, and W.-J. Cho, *Improved performance of solution-processed a-InGaZnO thin-film transistors due to Ar/O2 mixed-plasma treatment.* Journal of the Korean Physical Society, 2014. **65**(3): p. 399-403.
16. Y.-H. Hwang, K.-S. Kim, and W.-J. Cho, *Effects of combined Ar/O2plasma and microwave irradiation on electrical performance and stability in solution-deposited amorphous InGaZnO thin-film transistors.* Japanese Journal of Applied Physics, 2014. **53**(4S).
17. J.-S. Kim, et al., *Plasma treatment effect on charge carrier concentrations and surface traps in a-InGaZnO thin-film transistors.* Journal of Applied Physics, 2014. **115**(11).

Chapter 4: Application of hydrogen injection and oxidation to aqueous based solution-processed indium gallium zinc oxide semiconductors

4.1 Introduction

In this chapter, to obtain high-performance low-temperature solution-processed oxide TFTs, a simple aqueous IGZO precursor was synthesized with nitrate metal salts and without any organic solvents, which is expected to result in less residual species. Furthermore, HIO method which is by hydrogen injection process and subsequent oxidation was applied to achieve high device performance following low temperature processing by the efficient decomposition of residual species and film densification. Solution-processed IGZO TFTs were fabricated at low temperature to evaluate the electrical stability of the IGZO TFTs.

4.2 Experimental

Precursor synthesis

A 0.3 M IGZO precursor solution was prepared by dissolving indium nitrate hydrate ($In(NO_3)_3 \cdot xH_2O$), gallium nitrate hydrate ($Ga(NO_3)_3 \cdot xH_2O$), and zinc nitrate hydrate ($Zn(NO_3)_2 \cdot xH_2O$) in deionized water. The molar concentration of 0.3 M was achieved by setting the molar ratio of In:Ga:Zn to 4:1:1. The precursor was stirred vigorously to completely dissolve the precursors in solution. All reagents were obtained from Aldrich and were used as received without further purification.

Film fabrication

Solution-processed IGZO thin films were fabricated by spin-coating onto 200 nm thick thermally oxidized SiO_2/n^+-Si substrates. The SiO_2 substrates were treated by O_2 plasma for 30 s to obtain a hydrophilic surface and a good interface with the semiconductor layer. The precursor solution was passed through a 0.22 μm polytetrafluoroethylene (PTFE) filter. The n^+-Si substrate was used as the gate electrode, while the SiO_2 layer was used as the gate insulator. Spin-coating of the precursor was performed at 3000 rpm for 30 s at room temperature, followed by pre-annealing at 150 °C for 10 min and subsequent annealing at a specific temperature (200 - 300°C) for 1 h in air to yield the IGZO thin film deposited on the substrate. The thickness of the films was about 10 nm.

Hydrogen injection and oxidation process

The HIO process was applied to some of the solution-processed thin films. Hydrogen injection was conducted by hydrogen plasma treatment, after which an additional

annealing process was immediately performed, which represents the oxidation process. The plasma treatment condition for the hydrogen injection process was H_2 at a flow rate of 50 sccm with a source power of 200 W using plasma etching unit. Following the plasma treatment, the oxidation process by thermal annealing was immediately applied at the same temperature as that for the first anneal for 1 h in air. The thin films not subjected to the HIO process were also prepared using only the latter oxidation process to achieve the same annealing time.

TFT fabrication and characterization

After fabrication of the solution processed IGZO thin film, the active area of the film was patterned as an island shape using a conventional photolithography method followed by wet chemical etching using diluted 0.7% hydrochloric acid (Kanto Chemical Co. Inc.). Patterned source/drain (S/D) electrodes (Mo) were formed on the thin films via a shadow mask by DC sputtering. The thickness of the electrodes was ca. 50 nm. The fabricated device was a bottom-gate, top-contact TFT with 1000 μm channel widths (W) and 100 μm channel lengths (L). The n^+-Si substrates were used as the gate electrode. Evaluation of the TFTs was performed using an electrical measurement system with a probe station and a semiconductor analyzer (Keithley HP4156C).

The IGZO TFTs on a flexible polyimide substrate were fabricated using polyimide varnish. A polyimide film was spin-coated on a glass substrate and a barrier layer was formed. After formation of the gate electrode of molybdenum (50 nm), a 200-nm-thick SiO_2 gate insulator film was deposited by sputtering deposition. Then, the substrate was treated with oxygen plasma for 30 s to enhance hydrophilicity. Spin-coating of the IGZO film was performed. The direct-patterning process was performed by the same

aforementioned method. After patterning, the films were annealed at 300 °C for 1 h in air. Then, the source and drain (S/D) electrodes were formed. Shadow masks were used to pattern all the layers of the TFTs. After fabrication of the TFTs, the polyimide film was mechanically peeled from the glass substrate.

The fabricated films were characterized using secondary ion mass spectrometry (SIMS; PHI Corporation ADEP11010), thermal desorption spectroscopy (TDS; ESCO EMD-WA1000S), and X-ray photoelectron spectroscopy (XPS; ULVAC-PHI PHI Quantera II).

4.3 Chemical and structural analysis for aqueous based IGZO film

To analyze the HIO method for low-temperature solution-processed IGZO films, thermal desorption spectroscopy (TDS) and Fourier transform infrared (FT-IR) spectroscopy were conducted to determine the concentrations of residual species originating from the IGZO precursor. In the TDS analysis, the desorption of nitrogen compounds was assessed by tracking the mass fragments at m/z values of 28 and 30, which correspond to N_2 and NO from the precursor compounds. Sample films with and without the HIO method were prepared by annealing at 250 °C for 1 h after the spin-coating process. Hydrogen plasma was done with 40 sec. Figure 4.1. shows the TDS spectra related to m/z of 28 (N_2) and 30 (NO). A large number of desorption signals with a peak at around 250 °C was observed for the IGZO film produced without the HIO method. This indicated that the process temperature at 250 °C is insufficient for thermal oxidation, even with an aqueous precursor. However, considerable decreases in desorption were confirmed for the IGZO film produced with the HIO method. Therefore, it is considered that the HIO method is effective at reducing residual species, even for low-temperature processed IGZO films.

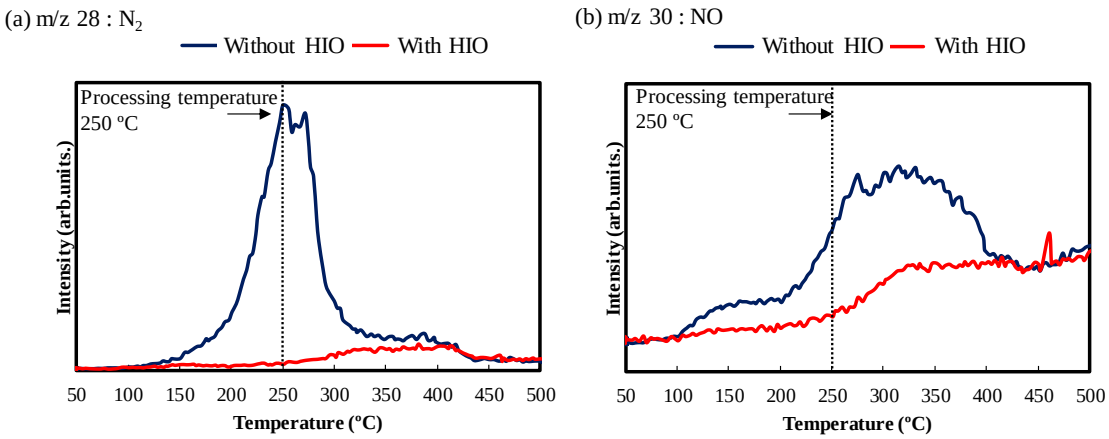

Figure 4.1. TDS spectrums relating to (a) m/z: 28 (N_2) and (b) m/z: 30 (NO) for the solution processed IGZO film processed at 250 ºC with and without HIO method.

Figure 4.2. shows FT-IR spectra for the IGZO films subjected to the various processes. All the IGZO sample films were prepared at 250 °C for 1 h. Peaks related to metal salts were confirmed for the non-HIO treated IGZO film in the region from 1250 to 1500 cm^{-1}. The absorption bands centered at 1400 and 1340 cm^{-1} are ascribed to N-O stretching modes in the nitrate ligand. However, a change in these metal salt peaks was confirmed after the hydrogen injection process with 40 sec; the peaks related to nitrate salts were significantly decreased. The hydrogen injection process is thus effective at decomposing residual metal salts, which is consistent with the previous TDS results. Broad absorption peaks from 2700 to 3700 cm^{-1}, which are related to the OH stretching vibration, were also observed. The peak centered at 1650 cm^{-1} is related to H-O-H bending. In previous reports related to OH groups of IGZO films, these OH peaks are considered to originate from a partial metal-hydroxide (M-OH), a residual organic chemical species, and the remaining H_2O molecules from the films[1, 2]. In the region of the OH peaks, a high wavenumber is considered as a free state of M-OH bonding without hydrogen

bonding, and a low wavenumber is considered to represent M-OH bonding with hydrogen bonding. Figure 4.2(c) shows that the intensities of the OH group peaks increased after the hydrogen injection process and decreased after the HIO method. In addition, OH peak shifts were observed after the hydrogen injection process. The intensity of the M-O-H peaks also changed during the HIO method. Considering the decrease in the metal salt peaks and the increase in OH group peaks, the injected hydrogen atoms play an important role in reacting with oxygen bonded to nitrate and metal atoms, which generates an OH state. The peak shifts can be understood by taking the generation of hydrogen bonding into consideration. Thus, the residual species related to metal salts and the partial parts of M-O were converted to an OH state. It is thus considered that hydrogen reacted with residual NO and OH as a reduction reaction. In contrast, there were large decreases in intensity of the OH peak after the HIO method, which suggests condensation of the OH state, which may generate a M-O-M state. In previous reports, the consumption of M-OH was found to accelerate a sol-gel reaction by the introduction of catalysts[3] . The increase of M-OH is another key point for the acceleration of M-O-M state generation by the consumption of M-OH as condensation in the IGZO films.

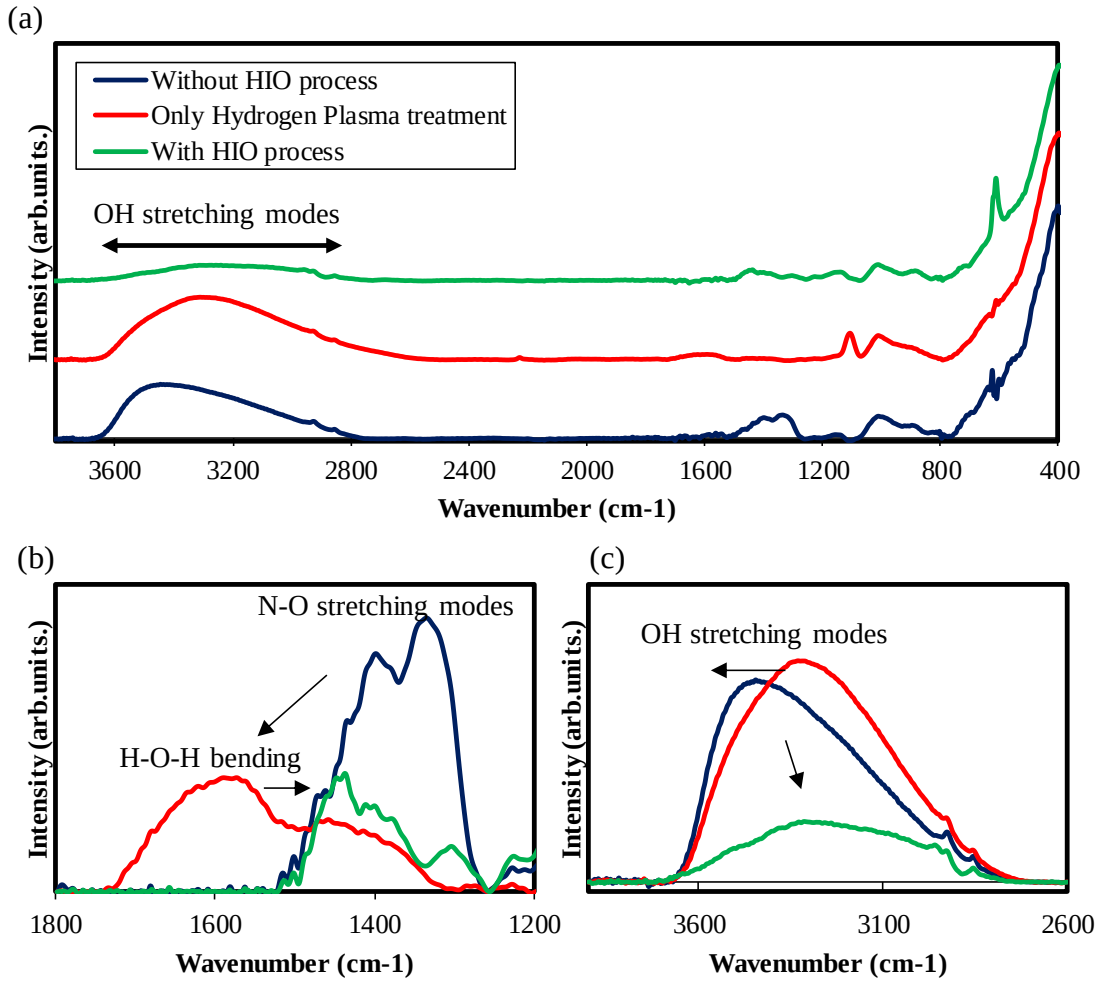

Figure 4.2. FT-IR spectra as a function of process dependence for the IGZO films processed at 250 ºC. (a) all regions, (b) extracted FT-IR results in the 1200-1800 cm^{-1}, (c) extracted FT-IR results in the 2600-3900 cm^{-1}.

To consider the chemical bonding state, the binding energy of O 1s measured using X-ray photoelectron spectroscopy (XPS). Figure 4.3. shows XPS O 1s spectra for the IGZO films prepared at 250 °C. The XPS spectra were measured after etching the film surface by Ar sputtering. The O 1s peaks were analyzed by curve fitting the O1 (lattice oxygen), O2 (oxygen vacancy) and O3 (hydroxyl) peaks at 530.4, 531.4 and 532.2 eV,

respectively [4]. The XPS data indicate that the IGZO films treated with the HIO method changed from the M-OH to the M-O state, according to the increases of the O1 and O3 peaks. The O2 peaks indicated a decrease in the oxygen vacancy states. These XPS results suggest that the condensation of M-O was achieved by application of the HIO method, which is consistent with the chemical analysis results.

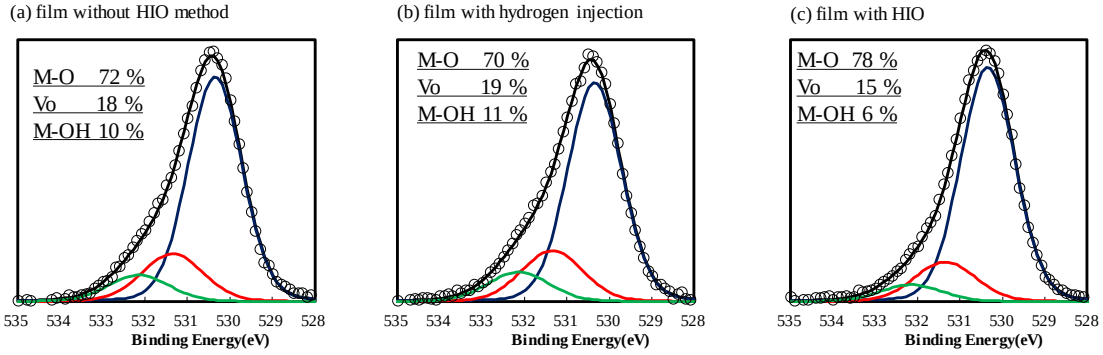

Figure 4.3. Binding energy of O1s measured by XPS for (a) film without HIO method, (b) film with hydrogen injection, (c) film with HIO method. All films are fabricated at 250 ºC. The XPS spectrums were analyzed by curve-fitting the O1 (lattice oxygen), O2 (oxygen deficient) and O3 (hydroxyl) peaks.

4.4 TFT characteristics for IGZO thin film by applying HIO

Figure 4.4 shows the schematic of the TFT structure and image of fabricated IGZO TFT. Figures 4.5(a-c) show the transfer characteristics of IGZO TFTs fabricated with and without the HIO method as a function of the process temperature (200, 250, 300 °C), and a comparison of the mobility, S.S, and switch-on voltage (V_{on}) @ Ids = 10^{-9} A for these processes. The transfer characteristics of the IGZO TFTs at applied gate voltages ranging from -30 V to 30 V were assessed. The applied drain voltage was 30 V. The output characteristics of the TFTs fabricated with and without the HIO method at 250 °C are

shown in Figures 4.6(a) and (b). The transfer characteristics of an IGZO TFT with HIO at 250 °C as a function of drain voltage (1, 10, 20, 30 V) is shown in Figure 4.6(c).

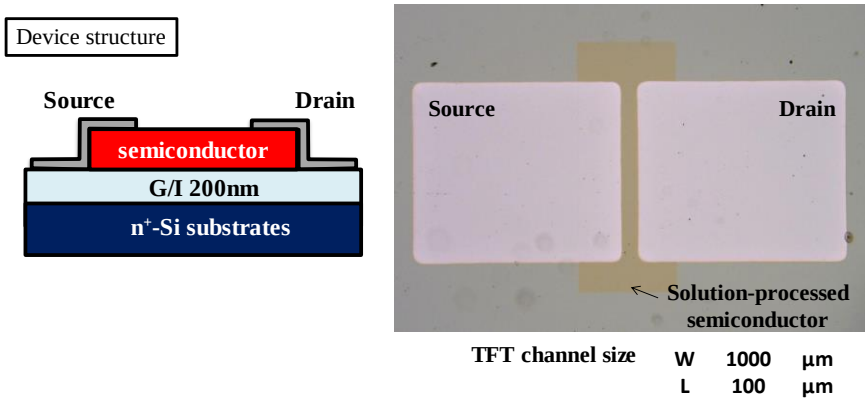

Figure 4.4. Illustration of device structure and photographic image of fabricated IGZO-TFT.

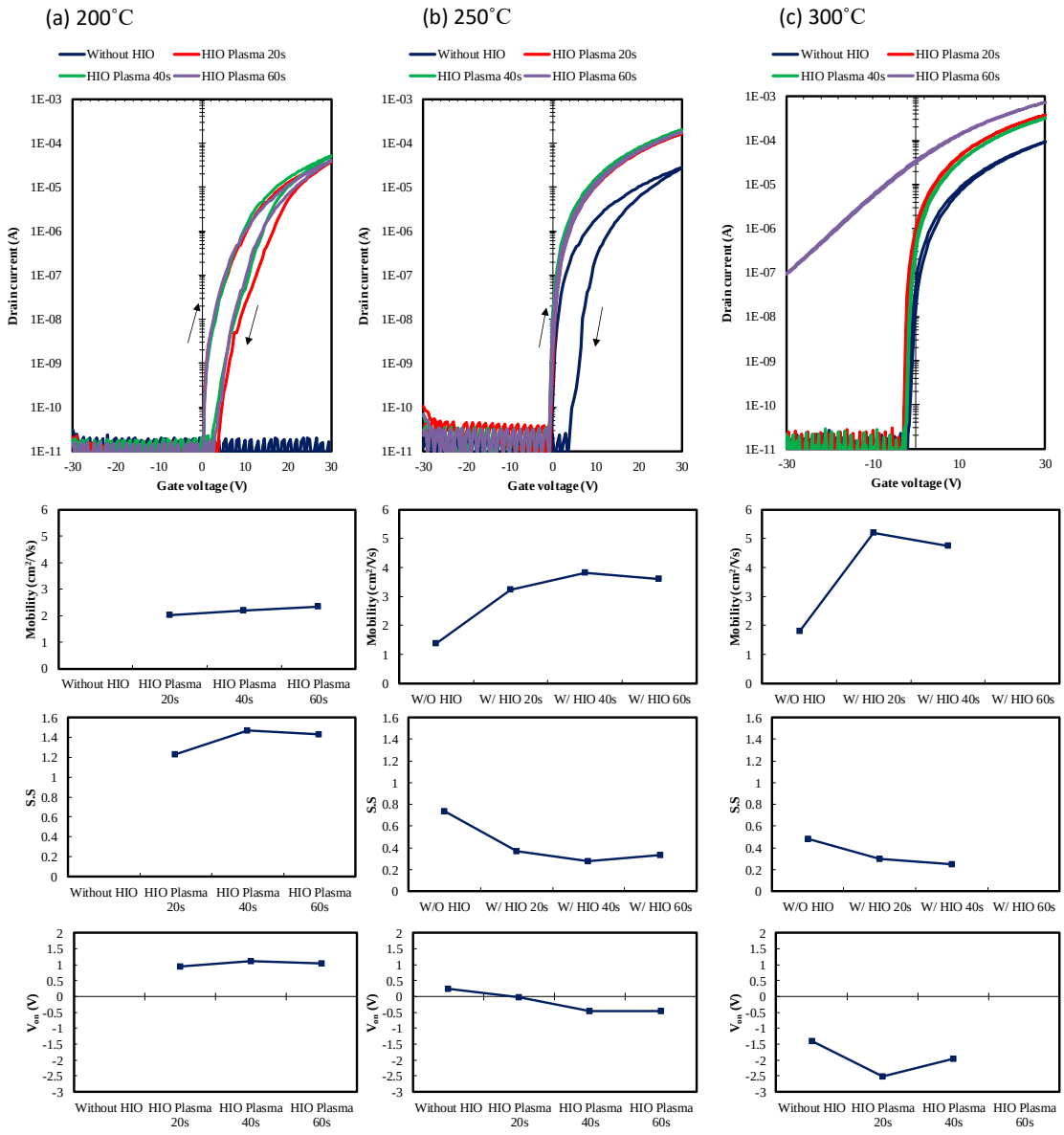

Figure 4.5. Transfer characteristics of solution-processed IGZO TFTs with W/L = 1000 µm / 100 µm, fabricated with and without the HIO method at (a) 200, (b) 250. The applied drain voltage was 30 V. (c) comparison of the mobility for solution-processed IGZO TFTs. Output characteristics of solution-processed IGZO, fabricated (d) without and (e) with the HIO method at 250 ˚C.

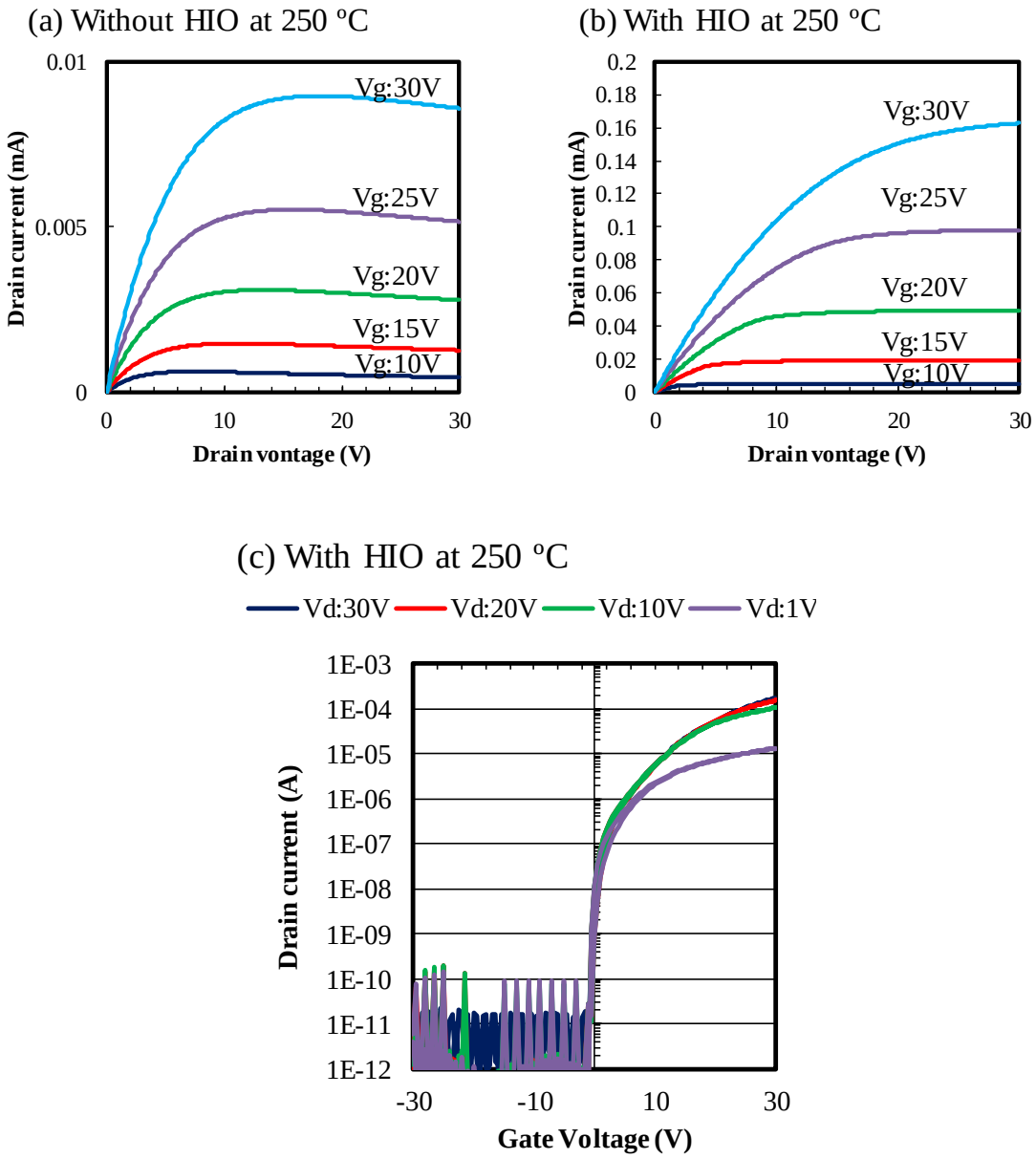

Figure 4.6. Output characteristics of solution processed IGZO, fabricated (a) without and (b) with the HIO method at 250 ˚C.

As shown in Figure 4.5 (a-c), the IGZO TFTs fabricated by the lower temperature process exhibited lower TFT performance. This is due to insufficient metal-oxide bond formation and the presence of impurities. Thus, the oxidation process for bond formation by the chemical conversion process is a critical process to determine the electrical

performance. As the TFT characteristics show, the presence of residual species due to the insufficient decomposition of anions in the precursor critically interrupts the efficient transport of carriers. The precursor solution needs to chemical conversion from metal salt complexes to oxide. In addition, anions decomposition of nitrate is considered as critical important point. While decomposition of the aqueous precursor is easier than other organic precursor, those temperature is not enough to get metal-oxygen-metal bonding.

In contrast, considerable improvement of the TFT performance was obtained for all TFTs with the HIO method. Even with a very low processing temperature of 200 °C, TFT switching behavior was successfully observed. The dependence of hydrogen plasma time shows that the injection time is needed to be optimized. The HIO method is thus effective at enhancing the TFT characteristics. The TFT performance with a processing temperature of 250 °C showed a reasonable mobility of 3.8 cm^2/Vs, a high I_{on}/I_{off} ratio of 10^6, small S.S. of less than 0.3 V/decade, as well as a small hysteresis. At a processing temperature of 300 °C, the mobility over 5 cm^2/Vs was obtained.

In addition, the transfer characteristics of the 6 fabricated TFTs shown in Figure 4.6, indicate that solution-processing with the HIO method results in good device uniformity. The deviation using sigma in each TFT characteristic also show uniform characteristics within 0.2 $cm^2/Vs$for mobility, 0.1 V/decade for S.S. and 0.1 V for V_{on}.

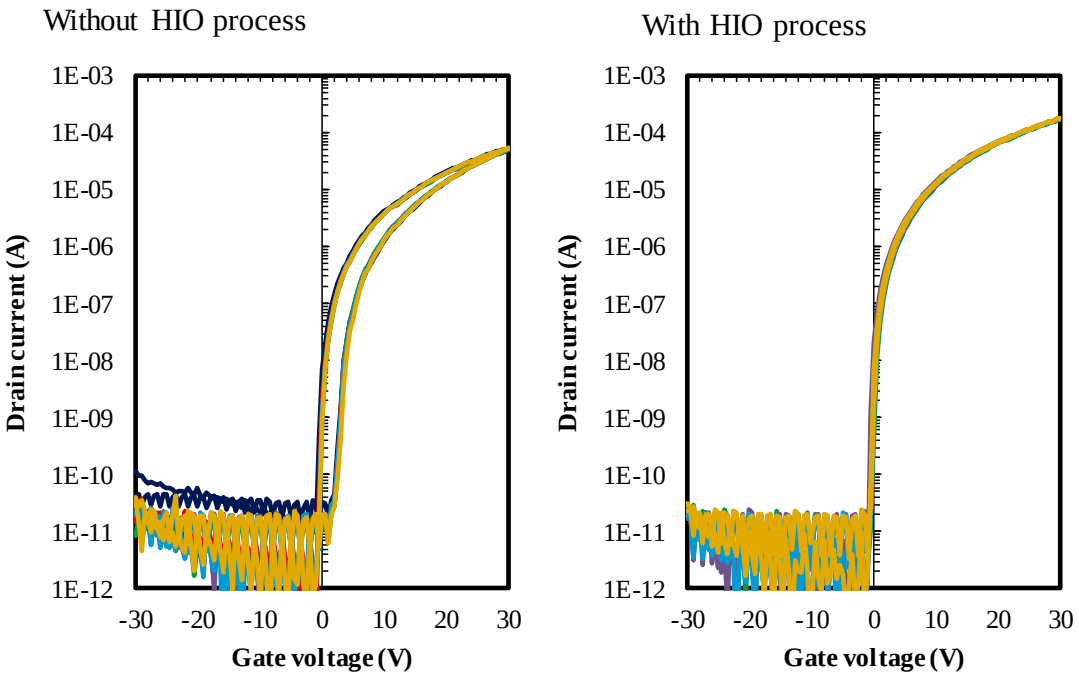

Figure 4.6. Transfer characteristics of solution processed IGZO TFTs with W/L = 1000 µm / 100 µm, fabricated with and without the HIO method for 6 IGZO TFTs at 250 °C.

Table 4.1. Calculated electrical parameters of solution-processed 6 IGZO TFTs fabricated with and without the HIO method at different processing temperatures.

	Mobility (cm^2/Vs)	I_{on} / I_{off} ratio	S.S. (V/decade)	V_{on} (V)
250 ºC without HIO	1.4±0.1	-10^5	0.5±0.1	0.4±0.1
250 ºC with HIO	3.8±0.2	-10^6	0.4±0.1	-0.3±0.1

PBS and NBS evaluations were performed to verify the electrical stability and reliability of the IGZO TFTs. Figures 4.7(a)-(f) show the transfer characteristics of the IGZO TFTs produced with and without the HIO method at 250 °C under PBS and NBS. The transfer characteristics of these IGZO TFTs at V_g ranging from -15 V to 15 V were assessed. The applied drain voltage was 10 V. The stress voltages for PBS and NBS were 20 V and -20 V, respectively. The maximum stress time was set to 1 h. In this evaluation, the passivation layer was fabricated with polymer insulating material. Therefore, the field-induced adsorption/desorption from atmosphere is suppressed. Figures 4.7(e) and (f) show the change in the switch-on voltage, ΔV_{on} (changes of V_{on} shifts after 3600 s) as a function of the cumulative stress time for PBS and NBS, respectively. The switch-on voltage shift for PBS with the TFT subjected to the HIO method was significantly improved by more than 10 V, whereas that for the TFT prepared without the HIO method was larger than 15 V. Suppression of the NBS shifts was also confirmed. Even though the process temperature was 250 °C, both PBS and NBS results showed significantly stable performance. Figure 4.7 shows the results for the change in the V_{on} shift after 3,600 s for PBS and NBS as a function of the hydrogen injection time in the HIO method. The dependence of V_{on} on the hydrogen injection time was assessed from 0 to 60 s. For the PBS evaluation, the suppression of ΔV_{on} was confirmed, even with a very short injection time of 20 s. The characteristics with NBS indicated the 40 s hydrogen injection time resulted in the best characteristics. The shift is comparable to that for IGZO TFTs for vacuum processed devices. Considering the operation mode of the display device, the great improvement of PBS characteristics is considerably important aspect of this HIO method.

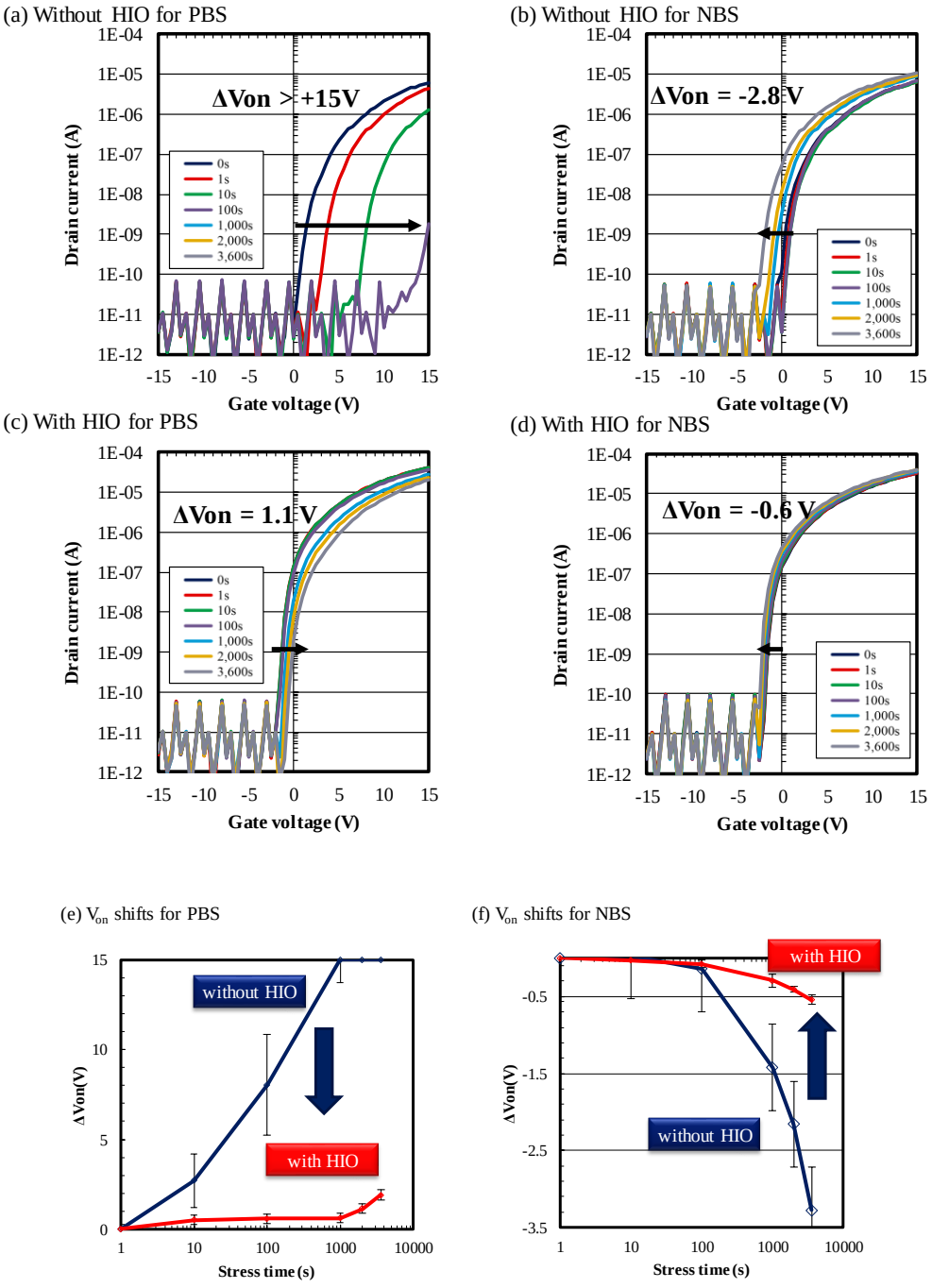

Figure 4.7(a)-(d). Transfer characteristics of IGZO TFTs processed at 250 ºC under a positive gate bias stress (PBS) and a negative gate bias stress (NBS), fabricated with and without the HIO method. The applied drain voltage was 10 V.

Change of switch-on voltage as a function of the cumulative stress time for (e) PBS and (f) NBS.

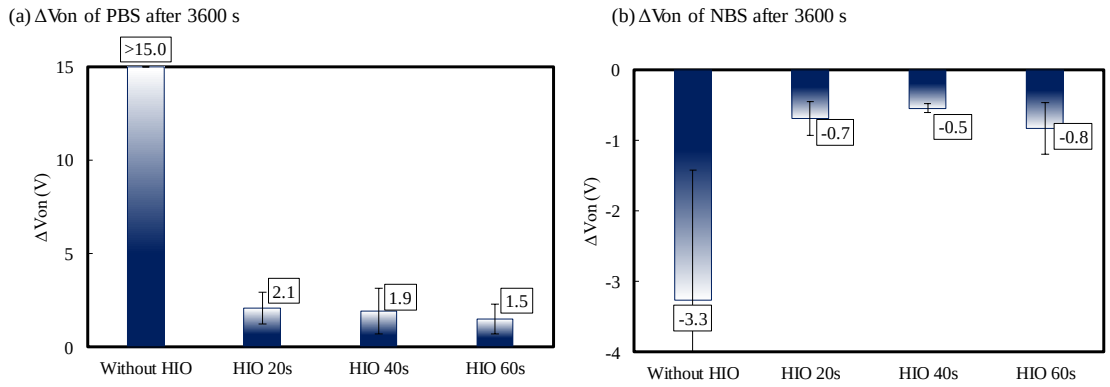

Figure 4.8. Changes of Von shifts after 3,600 s for (a) PBS and (b) NBS as a function of hydrogen injection processing time of HIO method. The processing time of hydrogen injection of HIO method was changed from 0s to 60s.

In previous reports related to the shifts in V_{on} under PBS, electron trapping such as electrically charged oxygen or molecular migration at the semiconductor-insulator interface has been addressed[4]. It is suggested that that negatively charged residual species such as NO_3^- have a critical influence on the large shifts for the IGZO TFTs without HIO. Therefore, elimination of these species is the main factor for this improvement. The suppression of oxygen vacancies by the passivation effect of hydrogen is also considered. In a previous study on IGZO TFTs, the addition of hydrogen at an adequate concentration resulted in the passivation of oxygen vacancies and total traps[5, 6]. In the NBS characteristics, hole trapping sites due to an increase of hydroxide groups (M-OH) were reported in solution-processed IZO films[7]. Changes in the amount of hydroxide groups should be addressed in order to analyze the suppression of the V_{on} shift. Hole trapping states such as hydroxide groups result in a large V_{on} shift by PBS. Metal hydroxide in an aqueous precursor was previously reported to convert to metal oxide through condensation reaction or oxidation[8]. Thus, the oxidation process by HIO

occurred via the condensation of OH states after generation of the metal hydroxide by the hydrogen injection process. However, remaining hydroxide groups behave as hole trapping sites, which causes the V_{on} shift in the NBS characteristics. Therefore, the results of the V_{on} shifts under NBS as a function of hydrogen injection time indicated the amount of hydroxide groups. The hydrogen injection process generated hydroxide groups and oxidation during thermal annealing consumes these groups. The NBS characteristics suggest that 40 s of hydrogen injection was the optimum processing time to balance the generation and consumption of M-OH. It is likely that the total amount of M-OH groups was adjusted, and hole trapping sites were also decreased by application of the HIO method for 40 s.

Figure 4.9 shows proposed reaction models for the HIO method. The low-temperature solution-processed IGZO film contains a large amount of impurities, such as NO_3 and OH groups. In addition, the formation of M-O-M bonding is insufficient. These defects act as charge trapping sites, which lead to a large V_{th} shift under the PBS and NBS conditions. Therefore, unstable IGZO TFTs exhibited large shifts of more than 15 V under PBS. During the hydrogen injection process, hydrogen reacts with residual NO_3 and OH in a reduction reaction and removes these impurities in the form of HNO_3 or H_2O gas, which results in an increase in the M-OH state. The hydroxide sites were oxidized and generated the M-O-M state. After elimination of the residual species, the vacant sites were oxidized more easily. The passivation effect of the hydrogen is also another factor and an advantage of the HIO method. Therefore, sufficient M-O-M bonding were generated to obtain stable TFT characteristics under bias stress, even with a low temperature process such as 250 °C. Considering from the effect of the HIO process for ZTO fabricated with

a conventional organic related precursor, which suggested that the HIO method is widely applicable to various precursors. However, comparison of the effect of the HIO process to a conventional organic related precursor suggests that the HIO method with an aqueous precursor is more effective because the oxidation process of HIO generally occurs via condensation of the OH state in the aqueous precursor. The hydrogen injection process with an aqueous precursor can thus generate OH groups, which are then converted to metal oxides through condensation reactions or oxidation.

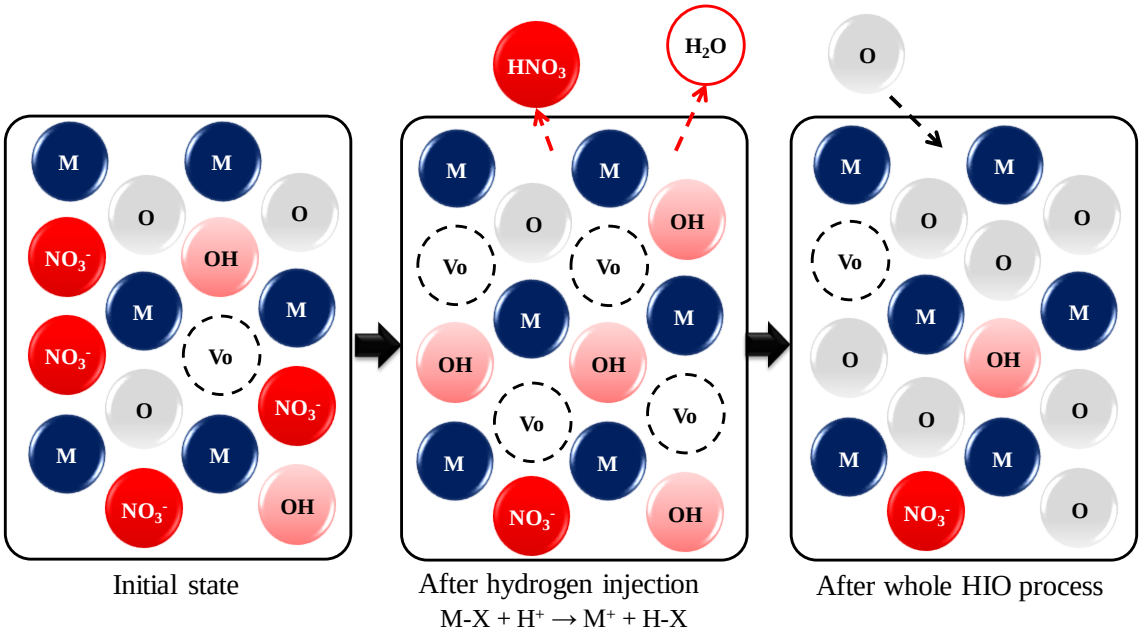

Figure 4.9. A reaction models for HIO method with low-temperature solution-processed IGZO film. At initial state without HIO process, the residual species such as NO_3 and OH groups remained. During hydrogen injection process, hydrogen reacted to decompose and generate hydroxide state. After HIO method, efficient decreases of residual species enhanced generation of M-O-M bonding state.

Compared with TFTs fabricated by the conventional sputtering process, the mobility is still low. However, we consider further improvement of the mobility will be possible by optimization of the HIO method, such as the conditions of hydrogen plasma, oxidation, and the timing and process flows of the HIO method. Better performance is also expected by investigation of the compositional effect of the oxide semiconductor. The significant improvements of TFT electrical performance by this simple HIO method was shown to be beneficial for low-cost oxide device fabrication.

Finally, the comparisons of TFT characteristics by low-temperature processing was discussed. Table 4.2 shows the summary of recent researches relating to the solution processed IGZO TFTs at low temperature. As the table shows, the reports for stability characteristics are limited. The HIO method is considered as very effective method to achieve reliable TFT performances as well as reasonable mobility compared with previous researches. Considering the resent researches, photo-activation process is considered as another promising technology to achieve oxide at very low-temperature. HIO process with photo-activation such as deep UV and laser must be promising to improve the low mobility of solution-processed IGZO.

Table 4.2. Comparison of low-temperature solution-processed IGZO TFTs

Approaches	Channel material	Deposition method	Processing temp.	Mobility	On/off ratio	Stability PBS, NBS	GI/ substrate	Bias Vg, Vd	Ref
This work	IGZO	Spin-coating	250	3.8V±0.2	-10^6	PBS: 1.1V NBS: -0.5V 1MV/cm 3600sec	SiO_2/Si	-30-30V 30V	
	IGZO	Spin-coating	300	5.1V±0.2	-10^6	PBS: 1.1V NBS: -0.5V 1MV/cm 3600sec	SiO_2/Si	-30-30V 30V	
Combustion	IGZO	Spin-coating	240	0.74	-10^3	-	Al2O3/Si	-3 - 3V	[9]
Combustion	IGZO	Spin-coating	260	2.26	-10^3	-	Al2O3/Si	-3 - 3V	[9]
Combustion	IGZO	Spin-coating	300	7.5	-10^7	PBS:0.9V 1200sec	SiO2/Si	-40-80V	[10]
Combustion	IGZO	Spin-coating	250	1.28	-10^7		SiO2/Si	-40-80V	[11]
Combustion	IGZO	Spin-coating	300	5.43	-10^8	PBS:1.3V 1200sec	SiO2/Si	-40-80V	[11]
Combustion PVP doped	IGZO	Inkjet	300	3.3	-10^7		SiO2/Si	-40-40V 1V	[12]
Lamp—DUV (185 and 254 nm)	IGZO	Spin-coating	150	6.94	-10^8	PBS: 2.4V 10ksec	Al2O3/Si	-10-10V 10V	[13]
Pulse deep UV	IGZO	Spin-coating	250	1	-10^6	-	SiO_2/Si	-30-30V 30V	[14]
Laser	IGZO	Inkjet	200	1.5	-10^6		SiO_2/Si	-40-40V 10V	[15]
High pressure annealing	IGZO	Spin-coating	280	1.38	-10^5	PBS: 6.4V 1000sec	SiO_2/Si	-30-30V 30V	[16]
Flash White Light Deep UV	IGZO	Spin-coating	RT	7.7	-10^6	-	SiO_2/Si	-30-30V 30V	[17]
Aqueous humid UV	IGZO	Spin-coating	300	5.1	-	-	SiO_2/Si	-40-40V 40V	[18]

4.5 Application for the flexible substrate

To confirm the compatibility of HIO method for flexible electronics, we fabricated a flexible IGZO TFTs. As Figure 4.11 shows, a bottom-gate, top-contact IGZO TFT was successfully fabricated on top a flexible polyimide substrate. The calculated mobility of the TFT was 5.1 $cm^2/V \cdot s$, which is almost similar value with the TFTs using silicon wafer. We confirmed that the HIO method was applicable for flexible electronics.

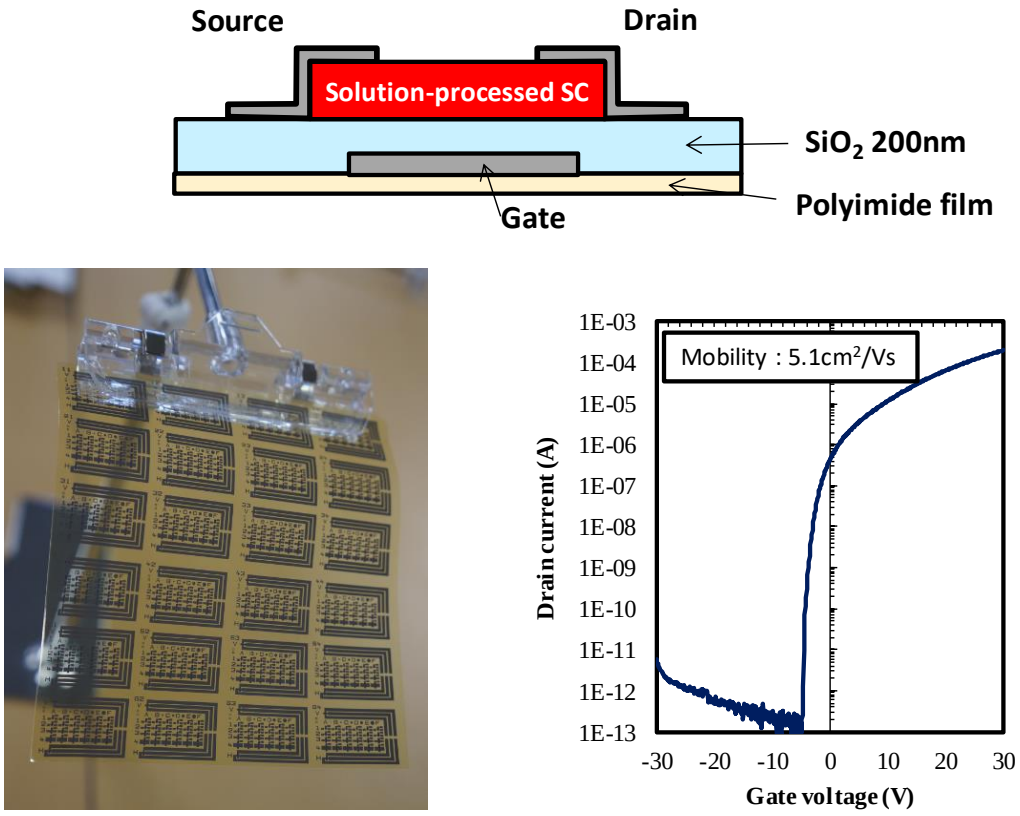

Figure 4.10. (a) Schematic diagram of a bottom-gate, top-contact TFT and a photographic image of a fabricated TFT, and transfer characteristics of solution processed IGZO TFT on flexible substrate.

4.6 Conclusion

The high stability of low-temperature solution-processed IGZO TFTs was demonstrated by application of the HIO method. Improvement in the TFT characteristics was confirmed in terms of the mobility and electrical stability. To achieve low-temperature solution-processed oxide materials, the decomposition of residual species is of primary importance. This HIO method is a simple process to enhance the quality of solution-processed oxide films by the decomposition of residual species using a reduction reaction. The HIO method has been demonstrated to be an inexpensive and effective means for realizing solution-processed oxide semiconductors for device applications.

4.7 References

1. K. Umeda, et al., *Impact of UV/O3 treatment on solution-processed amorphous InGaZnO4 thin-film transistors.* Journal of Applied Physics, 2013. **113**(18).
2. M. Morales-Masis, et al., *Hydrogen plasma treatment for improved conductivity in amorphous aluminum doped zinc tin oxide thin films.* APL Materials, 2014. **2**(9).
3. S. Jeong, et al., *Chemically improved high performance printed indium gallium zinc oxide thin-film transistors.* Journal of Materials Chemistry, 2011. **21**(43): p. 17066-17070.
4. L.-C. Liu, J.-S. Chen, and J.-S. Jeng, *Role of oxygen vacancies on the bias illumination stress stability of solution-processed zinc tin oxide thin film transistors.* Applied Physics Letters, 2014. **105**(2).
5. T. Kamiya, K. Nomura, and H. Hosono, *Origins of High Mobility and Low Operation Voltage of Amorphous Oxide TFTs: Electronic Structure, Electron Transport, Defects and Doping.* Journal of Display Technology, 2009. **5**(7): p. 273-288.
6. J. Kim, et al., *A study on H2 plasma treatment effect on a-IGZO thin film transistor.* Journal of Materials Research, 2012. **27**(17): p. 2318-2325.
7. J.S. Seo and B.S. Bae, *Improved electrical performance and bias stability of solution-processed active bilayer structure of indium zinc oxide based TFT.* ACS Appl Mater Interfaces, 2014. **6**(17): p. 15335-43.
8. Y. Hwan Hwang, et al., *An 'aqueous route' for the fabrication of low-temperature-processable oxide flexible transparent thin-film transistors on plastic substrates.* NPG Asia Materials, 2013. **5**(4).
9. H. Wang, et al., *Low-temperature facile solution-processed gate dielectric for combustion derived oxide thin film transistors.* RSC Adv., 2014. **4**(97): p. 54729-54739.
10. Y. Chen, et al., *Nitroacetylacetone as a Cofuel for the Combustion Synthesis of High-Performance Indium–Gallium–Zinc Oxide Transistors.* Chemistry of Materials, 2018. **30**(10): p. 3323-3329.
11. J.W. Hennek, et al., *Oxygen "getter" effects on microstructure and carrier transport in low temperature combustion-processed a-InXZnO (X = Ga, Sc, Y, La) transistors.* J Am Chem Soc, 2013. **135**(29): p. 10729-41.
12. S. Wu, et al., *Inkjet printing of oxide thin film transistor arrays with small spacing with polymer-doped metal nitrate aqueous ink.* Journal of Materials Chemistry C, 2017. **5**(30): p. 7495-7503.
13. J.S. Heo, et al., *Water-Mediated Photochemical Treatments for Low-Temperature*

Passivation of Metal-Oxide Thin-Film Transistors. ACS Appl Mater Interfaces, 2016. **8**(16): p. 10403-12.

14. M. Benwadih, R. Coppard, K. Bonrad, A. Klyszcz, and D. Vuillaume, *High Mobility Flexible Amorphous IGZO Thin-Film Transistors with a Low Thermal Budget Ultra-Violet Pulsed Light Process.* ACS Appl Mater Interfaces, 2016. **8**(50): p. 34513-34519.

15. H. Huang, H. Hu, J. Zhu, and T. Guo, *Inkjet-Printed In-Ga-Zn Oxide Thin-Film Transistors with Laser Spike Annealing. Journal of Electronic Materials,* 2017. **46**(7): p. 4497-4502.

16. S. Yoon, S.J. Kim, Y.J. Tak, and H.J. Kim, *A solution-processed quaternary oxide system obtained at low-temperature using a vertical diffusion technique.* Sci Rep, 2017. 7: p. 43216.

17. C.-J. Moon and H.-S. Kim, *Intense Pulsed Light Annealing Process of Indium–Gallium–Zinc–Oxide Semiconductors via Flash White Light Combined with Deep-UV and Near-Infrared Drying for High-Performance Thin-Film Transistors.* ACS Applied Materials & Interfaces, 2019. **11**(14): p. 13380-13388.

18. S. Ogura, H. Cheong, S. Uemura, H. Ushijima, and N. Fukuda, *Flexible InGaZnO TFT devices obtained via humid-UV irradiation with an aqueous-fluoroalcoholic precursor.* Flexible and Printed Electronics, 2016. **1**(4).

Chapter 5: Impact of fluorine doping on solution-processed In–Ga–Zn–O thin-film transistors using an efficient aqueous route

5.1 Introduction

In this chapter, fluorine doping of a solution-processed metal-oxide semiconductor was evaluated by efficient hexaaqua metal complexation, for obtaining a high-performance solution-processed metal oxide at low-temperature. TFTs fabricated using conventional IGZO and a fluorine-doped IGZO (IGZO:F) precursor are compared. An aqueous route with nitrate ligands produces high-quality oxide films, due to aqua complexes formation. These represent easily decomposable precursors for metal-oxide conversion at low temperature[5]. Furthermore, in previous studies on the compositional effects of oxide materials, anion doping by fluorination is known for enhancing electrical characteristics through mobility and stability[1-4]. Fluorine doping increases the carrier concentration due to the generation of free carriers[2]. Moreover, the stability improvement by the passivation effect for defects like oxygen deficiency and weakly bonded oxygen is also reported[2]. Therefore, impact of fluorine doping on this efficient aqueous route was investigated.

5.2 Experimental

Precursor synthesis

A 0.3 M IGZO precursor solution was prepared by dissolving indium nitrate hydrate ($In(NO_3)_3 \cdot xH_2O$), gallium nitrate hydrate ($Ga(NO_3)_3 \cdot xH_2O$), and zinc nitrate hydrate ($Zn(NO_3)_2 \cdot xH_2O$) in deionized water. The molar concentration of 0.3 M was achieved by setting the molar ratio of In:Ga:Zn to 4:1:1. To characterize the effects of fluorine doping, dilute hydrogen fluoride solution was used to the precursor to produce In:F molar ratios of 4:1 (Low:0.1% HF) and 1:1 (High: 0.4%HF). Thus, the compositions of In, Ga, Zn, and F was 4:1:1:1 for Low IGZO:F and 4:1:1:4 for High IGZO:F, respectively. The precursor was stirred vigorously for 6 h, for complete dissolution and to form aqua complexes in the solution. The precursor was stirred vigorously to completely dissolve the precursors in solution. All reagents were obtained from Aldrich and were used as received without further purification.

Film fabrication

The solution-processed IGZO and IGZO:F thin films were fabricated by spin-coating with onto a 200-nm thick thermally oxidized SiO_2/n^+-Si substrate at room temperature. The n^+-Si substrate served as the gate electrode, with the SiO_2 layer as the dielectric. The substrate was treated with 150 W oxygen plasma for 30 s before spin-coating to enhance hydrophilicity. The precursor solution was then passed through a 0.22-μm polytetrafluoroethylene filter, followed by spin-coating at 4,000 rpm for 30 s. Then, pre-annealing was conducted at 150°C for 10 min, and post-annealing was performed at 300°C in air for 1 h, yielding a solution-processed oxide thin film on the substrates. Thus, the maximum temperature was set at 300°C, while the resulting film thickness was

approximately 7 nm.

Hydrogen injection and oxidation process

The HIO process was applied to some of the solution-processed thin films. Hydrogen injection was conducted by hydrogen plasma treatment, after which an additional annealing process was immediately performed, which represents the oxidation process. The plasma treatment condition for the hydrogen injection process was pure H_2 at a flow rate of 50 sccm with a source power of 200 W. Following the plasma treatment, the oxidation process by thermal annealing was immediately applied at the same temperature as that for the first anneal for 1 h in air. The thin films not subjected to the HIO process were also prepared using only the latter oxidation process to achieve the same annealing time.

TFT fabrication and characterization

After fabrication of the films, photolithography was used to produce a pattern on the semiconductor layer, avoiding overestimating the TFT's performance. Finally, patterned molybdenum source/drain electrodes (50 nm) formed using a shadow mask, produced bottom-gate, top-contact TFTs with 1,000-μm channel widths and 100-μm channel lengths. To evaluate bias stability, the TFTs were encapsulated with a coating-type insulation layer (ZEOCOAT, cycloolefin resin, Zeon Corporation) to prevent interaction with the atmosphere at the back channel of the semiconductor layer. The TFTs were evaluated in the dark, at 25^{o}C using an electrical measurement system comprising a probe station and a semiconductor analyzer (Keithley 4200-SCS). The saturation mobility (μ) was calculated as

$$\mu = \frac{2L}{WC_i}\left(\frac{\partial\sqrt{I_d}}{\partial V_g}\right)^2,$$

where W is the channel width, L is the channel length, V_g is the source-gate voltage, Id is the saturation current, and C_i is the capacitance of the gate dielectric per unit area.

The fabricated films were characterized using secondary ion mass spectrometry (SIMS; PHI Corporation ADEP11010), thermal desorption spectroscopy (TDS; ESCO EMD-WA1000S), and X-ray photoelectron spectroscopy (XPS; ULVAC-PHI PHI Quantera II).

5.3 Aqueous fluorine doped IGZO precursor

To produce a high-performance solution-processed metal-oxide semiconductor at low temperature, forming dense metal–oxygen–metal bonds within the metal oxide is crucial. For solution processing, another key factor is eliminating residual species from the precursor solution like metal ligands and the solvent, highlighting the importance reagents selection. Figure 5.1 illustrates that the aqueous precursor is compositionally ideal because it is carbon-free. Furthermore, this nitrate-based aqueous precursor can form a metal aqua complex ($[M(H_2O)_n]$) by the neighboring water molecules because nitrate ion exhibits low bonding strength of coordination complexes in aqueous solution[5, 6]. This unique aqua complex results in low-temperature decomposition.

$M(NO_3)_n + nH_2O \rightarrow [M(H_2O)_n] + n(NO_3)$

As a fluorine additive, hydrogen fluoride acted as the dopant, to ensure a simple composition without organic impurities. Thus, the precursor system in this study is totally carbon-free. Considering the differences of bonding strength of coordination complexes in aqueous solution[7], suppression of residual species of nitrate ions owing to the stronger bonding energy for the fluorine additive is suggested.

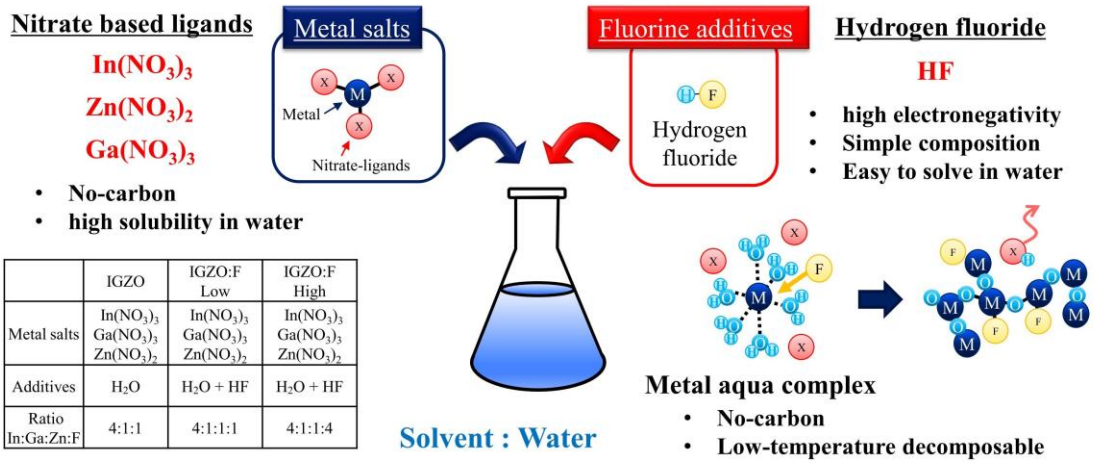

	IGZO	IGZO:F Low	IGZO:F High
Metal salts	$In(NO_3)_3$ $Ga(NO_3)_3$ $Zn(NO_3)_2$	$In(NO_3)_3$ $Ga(NO_3)_3$ $Zn(NO_3)_2$	$In(NO_3)_3$ $Ga(NO_3)_3$ $Zn(NO_3)_2$
Additives	H_2O	H_2O + HF	H_2O + HF
Ratio In:Ga:Zn:F	4:1:1	4:1:1:1	4:1:1:4

Figure 5.1. Schematic structure of the formation of hexaaqua metal complexes for the aqueous IGZO precursor; the conversion model to the metal oxide from precursor. Fluorine substitutes for ligands owing to the strong metal-fluorine bond energy. The inserted Table shows the precursors.

5.4 Chemical and structural analysis for fluorine-doped IGZO

Firstly, the depth profiles of the fluorine-doped IGZO film were measured by SIMS to confirm the presence of fluorine in the films. Figure 5.2(a) shows a depth profile in IGZO:F film on the SiO_2/Si substrate, showing that the F ion count remains uniform in the IGZO:F film. Figure 5.2(b) shows the thermal desorption spectroscopy (TDS) results for the IGZO film with and without the fluorine additive, which were annealed at 250°C in air for 1 h. The desorption of nitrogen compounds was assessed by tracking the mass fragments at m/z values of 30, corresponding to NO from the precursor compounds. Interestingly, the fluorine-doped film contains lower impurities than the film without fluorine additives, considering the amount of NO.

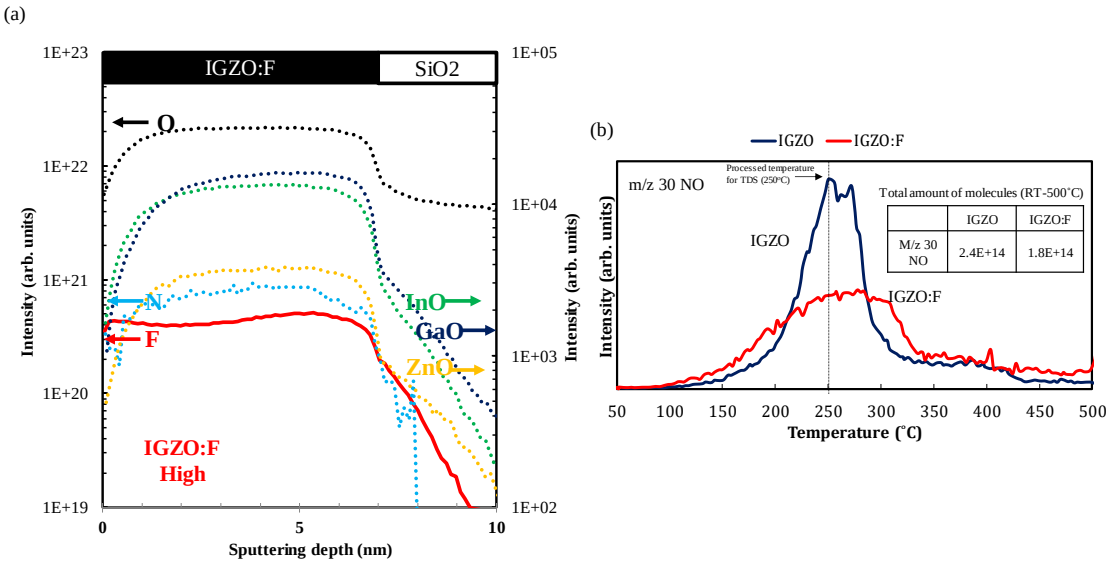

Figure 5.2. (a) SIMS spectra showing the depth profile of the IGZO film with fluorine additive fabricated at 300° C. (b) TDS spectra for NO (m/z of 30) obtained from IGZO films fabricated at a low temperature with and without the fluorine additive. The number of desorbed molecules associated with the NO is presented in the inserted Table.

The chemical states of IGZO films with and without fluorine additives were examined using X-ray photoelectron spectroscopy (XPS), and Figure 5.3 summarizes the N1s, F1s, and O1s results. The surfaces of films were cleaned through Ar^+ sputtering prior to the analysis. F1s peak at 683 eV can be associated with chemical bonding of M–F by substitution of oxygen site. N1s peak at 405 eV can be associated with the remained nitrate peaks. As Figure 5.3(a) shows the M–F signal is confirmed with the IGZO:F film. With respect to the N1s spectra, there was a minor reduction in the nitrate peak using fluorine additives. Therefore, these results are consistent with the SIMS and TDS results. To analyze the chemical state of metal–oxygen, the O1s peaks were analyzed by curve fitting the O_M (lattice oxygen), O_V (oxygen vacancy) and O_{OH} (hydroxyl) peaks at 530.4,

531.4, and 532.2 eV, respectively[8]. The XPS data indicate that the IGZO films with fluorine additives exhibit the smaller oxygen vacancy peak from the IGZO film without fluorine.

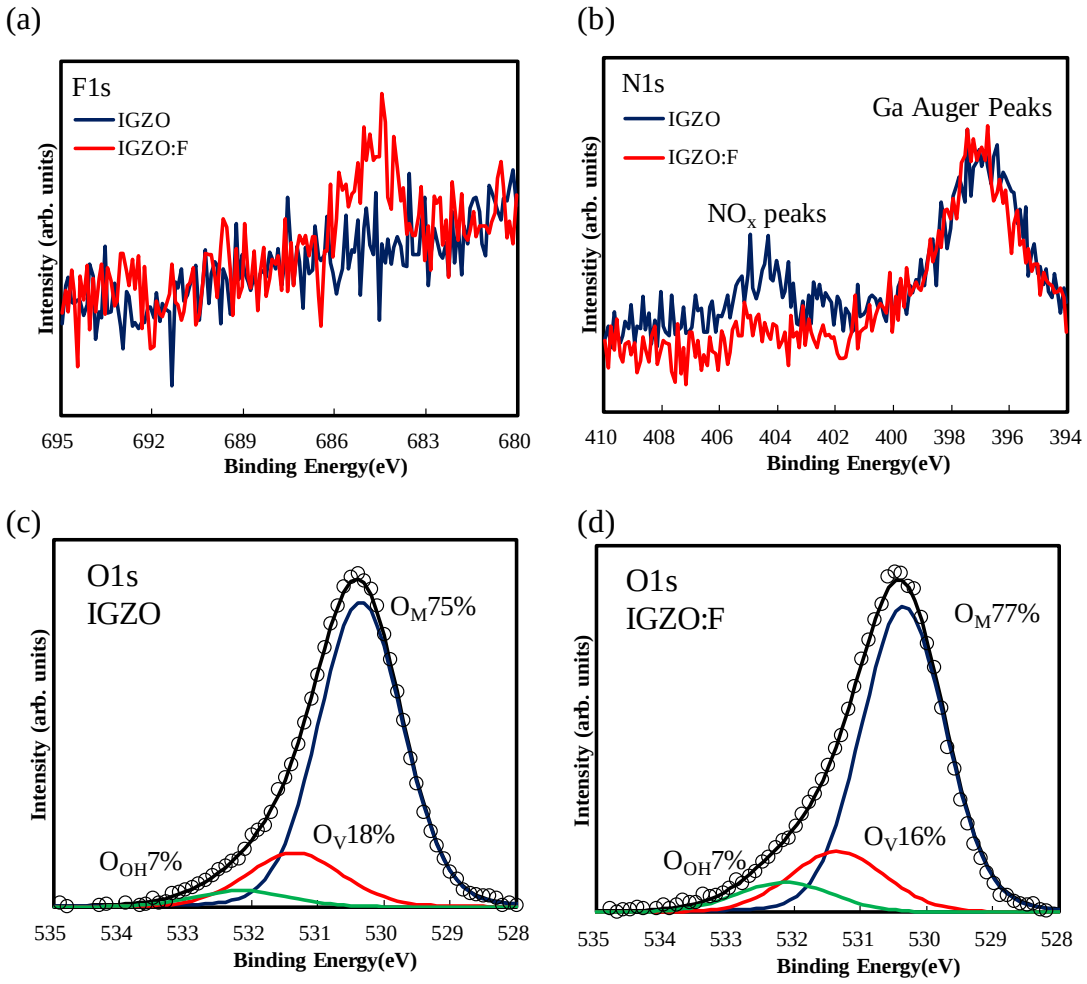

Figure 5.3. XPS spectra for (a) F1s (b) N1s obtained from IGZO films fabricated at a low temperature with and without the fluorine additive and O1s spectra of (c) IGZO film and (d) IGZO:F. The spectra were analyzed by curve fitting the O_M(lattice oxygen), O_V(oxygen vacancy), and O_{OH}(hydroxyl).

5.5 TFT characteristics for fluorine-doped IGZO

Figure 5.4 shows the transfer characteristics of the IGZO TFTs with and without the fluorine additive assessed at applied gate voltages ranging from −30 to 30 V and drain voltage of 30 V. The calculated electrical properties including mobility (μ), maximum on-current/minimum off-current ratio (I_{on}/I_{off}), subthreshold swing (S.S.), switch-on voltage (V_{on}) @ Ids = 10^{-9} A, and hysteresis of V_{on} (V_{hyst}) are presented in Table 5.1, with the conventional IGZO showing a low mobility of 1.9 cm^2/Vs. This low value indicates insufficient formation of metal-oxide–metal bonds and residual species based on nitrate-based metal salts. Nevertheless, considerable performance improvement was obtained for TFTs containing the fluorine additive, with mobilities of 4.7 and 5.1 cm^2/Vs for the IGZO low and IGZO high, respectively. Furthermore, the improvement of the I_{on}/I_{off} ratio and the subthreshold voltage swing (S.S.) were confirmed for the IGZO TFT with fluorine additives. Higher concentration of fluorine additive exhibited better switching characteristics. Figure 5.5 (a) and (b) show the transfer characteristics of the IGZO TFTs with and without fluorine additives under a positive gate bias stress (PBS). This evaluation of the electrical stability of the TFTs from −15 to 15 V, with an applied drain voltage of 10 V, stress voltage for PBS of 20 V, and maximum stress time of 1 h. The switch-on voltage shift (ΔVon) for PBS for the TFT without fluorine additive was 3.1 V with 3,600 s, whereas the PBS for the TFT with fluorine was only 0.6 V. It indicated much improvement in the PBS stability.

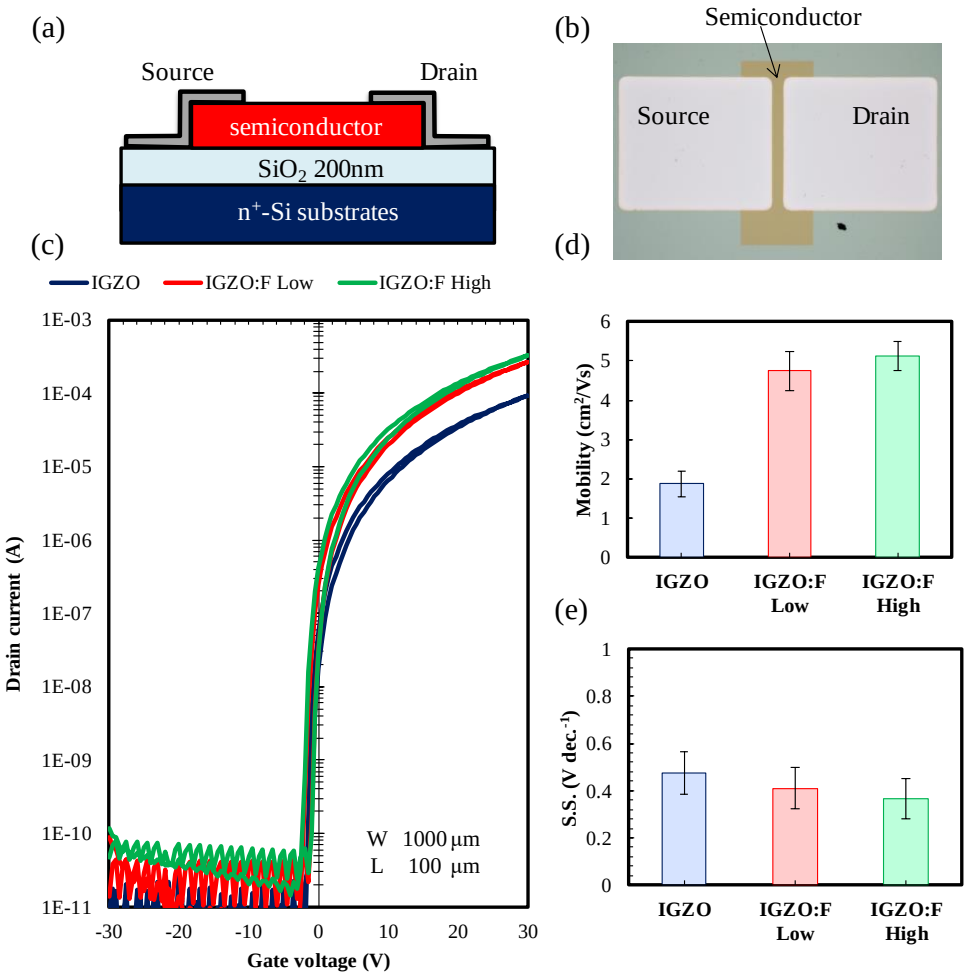

Figure 5.4. (a) Schematic diagram of a bottom-gate, top-contact TFT, and (b) a photographic image of a fabricated TFT and (c) transfer characteristics of IGZO TFTs with W/L = 1000 µm/100 µm, fabricated with and without the fluorine additives. Comparison of (d) mobility and (e) S.S. for six TFTs.

Table 5.1. Electrical characteristics of IGZO TFTs without and with the fluorine additive.

	Mobility(cm^2/Vs)	I_{on}/I_{off} ratio	S.S. (V/decade)	V_{on} (V)	V_{hyst} (V)
IGZO	1.9 ± 0.33	-10^6	0.48 ± 0.09	−1.3 ± 0.4	0.7 ± 0.4
IGZO:F Low	4.7 ± 0.51	-10^7	0.41 ± 0.09	−0.8 ± 0.2	1.0 ± 0.4
IGZO:F High	5.1 ± 0.37	-10^7	0.37 ± 0.09	−0.7 ± 0.7	0.5 ± 0.4

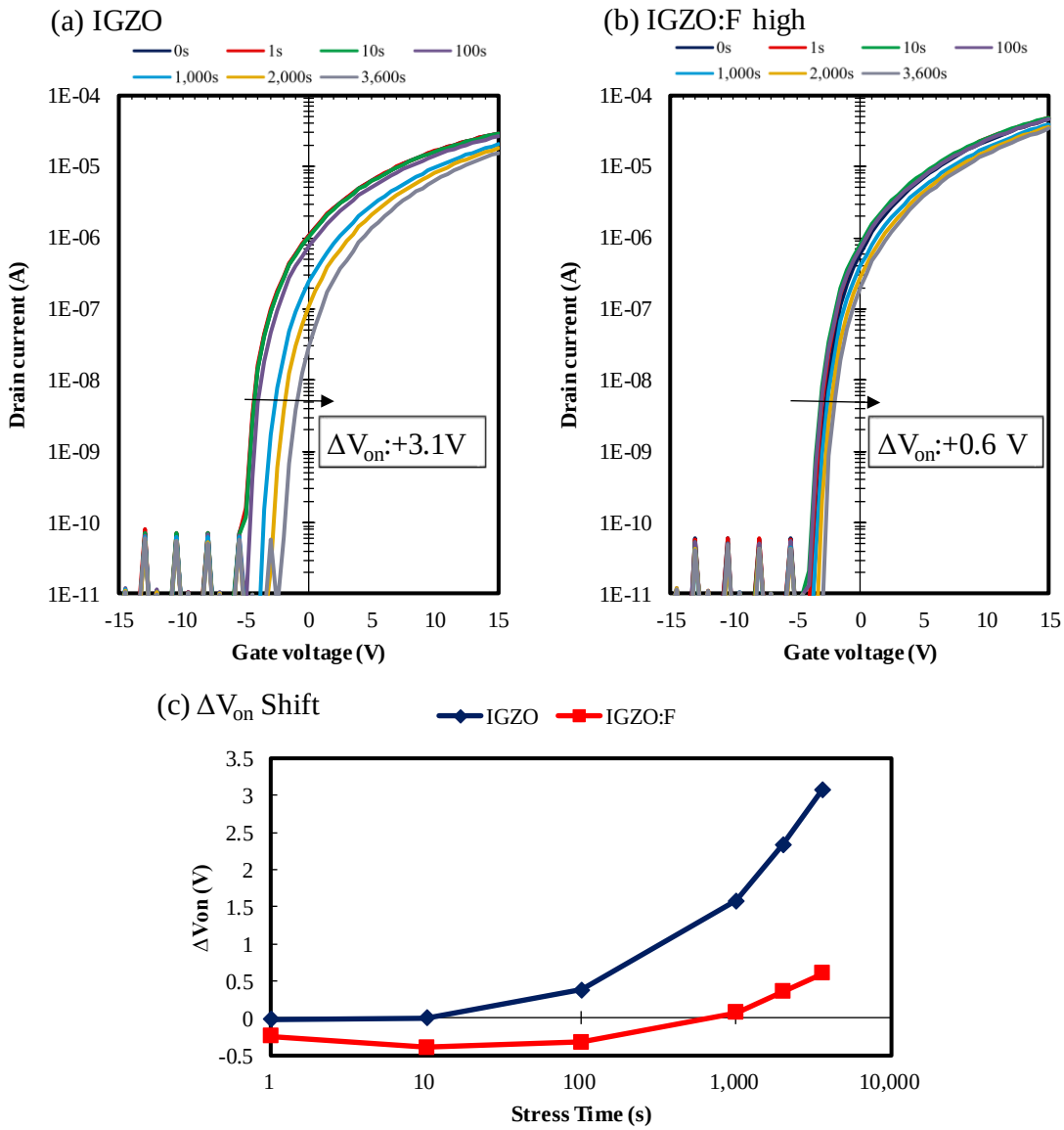

Figure 5.5. (a) and (b) Transfer characteristics of IGZO TFTs with and without the fluorine additive processed at 300°C under a positive bias stress at a drain voltage of 20 V. (c) Changes in the switch-on voltage for TFTs against the cumulative stress.

In this study, the improvement in the TFT characteristics were observed due to fluorine doping. As indicated by the TDS and XPS results, the pristine low-temperature solution-processed metal-oxide film contains impurities originated from nitrate ligands, even from the efficient aqueous route. Therefore, the impurities reduction through by adding the fluorine additive is one of the mechanisms for the enhancement of the TFT performance. Based on the bonding strength of coordination complexes in aqueous solution, stability constant (Log K1) of In–NO_3 and In–F are 0.18 and 3.75, respectively [5, 7]. When fluorine is mixed in an aqueous solution, the In–F bonding is expected to form prior to the In–NO_3 owing to the differences in the bonding strength. It is suggested that the formation of $[M(H_2O)_nF_m]$ complexes can suppress the nitrate impurities. Moreover, considering the bond-dissociation energies, the metal–fluorine bond is known to be much stronger than the metal–oxygen bond. The M–O bond energies for In–O, Ga–O, and Zn–O are 346, 374, and 284 kJ/mol, respectively, whereas the energies for the M–F bonds In–F, Ga–F, and Zn–F are 516, 584, and 364 kJ/mol, respectively[9]. This strong metal–fluorine bond energy of F ions is expected to selectively bond with metals through the substitution of oxygen or oxygen vacancy site.

Figure 5.6 shows proposed models for the fluorine-doped metal oxide. Along with the improvement of the TFT switching characteristics, the stability characteristics are also enhanced. These properties are related to electron trapping such as electrically charged ions, oxygen vacancy, or electron migration at the semiconductor–insulator interface[10]. The negatively charged residual species like NO_3^- and oxygen vacancy critically influence the major shifts for the IGZO TFTs. Although the reduction of impurities is one of rational mechanism for obtaining better TFT characteristics, the advantages of fluorine

introduction to the metal oxide was also contributed to enhance the overall performance of metal oxides. The introduction of fluorine into the sites of oxygen and oxygen vacancy is reported to increase the carrier concentration by generating free carriers[2, 11] and reduces the electron trap sites[12]. Moreover, the formation of M-F bonds at the semiconductor–insulator interface can block oxygen vacancy diffusion[13]. These advantages of the introducing fluorine could also be attributed to the improvement of the TFT performance such as mobility, S.S., hysteresis, and stability. This simple technique involving fluorine addition to an efficient aqueous precursor is a promising method for obtaining stable, high-performance TFTs at a low processing temperature.

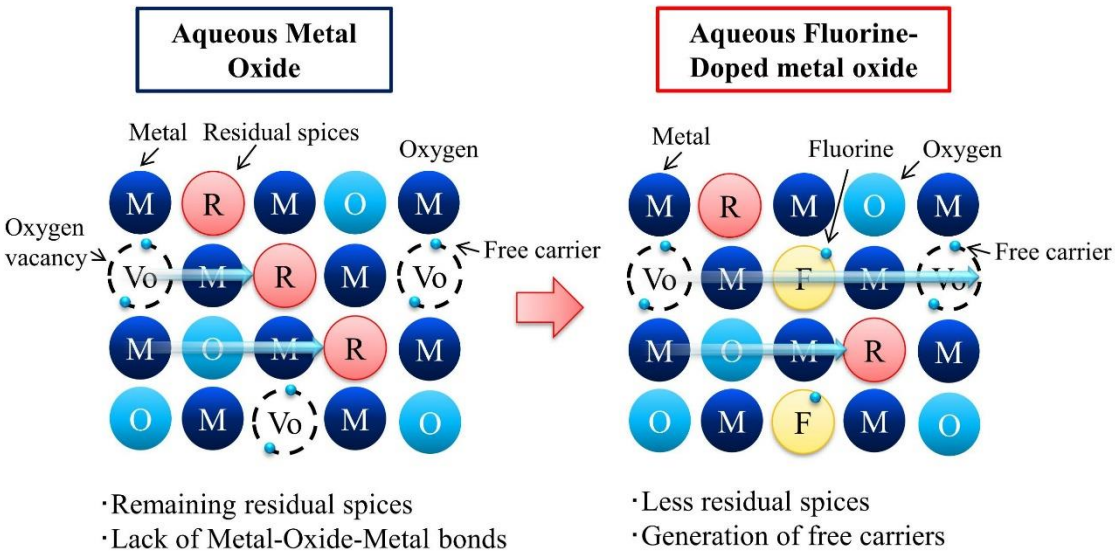

Figure 5.6. Proposed models for the aqueous fluorine-doped metal oxide at a low temperature, with impurities retained in the IGZO film. The fluorine additive reduces the impurities and generates the free carrier. The fluorine doping and efficient decrease of residual species enhances the characteristics of a metal oxide TFT.

Finally, the HIO process was performed on the fluorine-doped TFTs to improve better switching characteristics. Figure 5.7 (a)–(b) show the transfer characteristics and performance of the HIO treated IGZO TFTs with and without the fluorine additive. Along with the HIO process, the TFTs with fluorine additive display mobilities up to 7.3 cm^2/Vs for IGZO:F high at the 300°C. These TFTs performance indicate high I_{on}/I_{off} with almost no hysteresis performance. The PBS for the IGZO:F treated by HIO also exhibits better characteristics. It was suggested that the HIO treatment aided in decreasing the remaining impurities and the formation of dense metal–oxygen–metal bonds. Thus, it was confirmed that HIO is general method to improve the film quality to enhance the overall TFT characteristics.

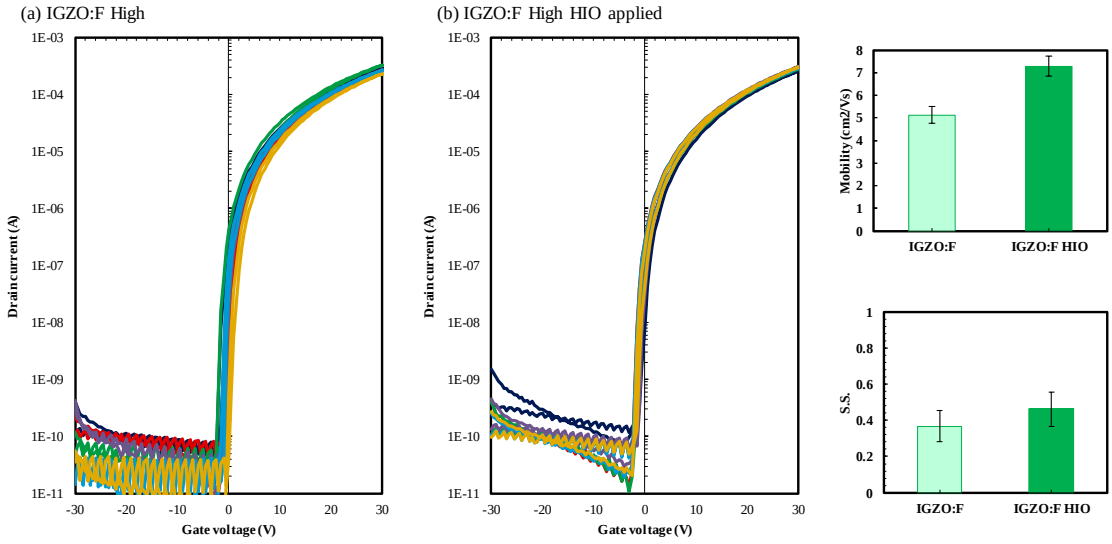

Figure 5.7. Transfer characteristics of 6 IGZO:F TFTs with and without HIO at 300°C

Table 5.2. Electrical characteristics of IGZO:F TFTs without and with HIO

	Mobility(cm^2/Vs)	I_{on}/I_{off} ratio	S.S. (V/decade)	V_{on} (V)	V_{hyst} (V)
IGZO:F High	5.1 ± 0.37	-10^7	0.37 ± 0.09	−0.7 ± 0.7	0.5 ± 0.4
IGZO:F High HIO	7.3 ± 0.46	-10^7	0.46 ± 0.10	−1.6 ± 0.3	0.0 ± 0.1

5.6 Conclusion

In summary, efficient aqueous fluorine-doped IGZO precursors were synthesized to fabricate high-performance metal-oxide TFTs at a low processing temperature of 300˚C. The fluorine doping suppressed the total impurities from metal ligands and form M–F bonding at the sites of oxygen or oxygen vacancy. The fabricated metal-oxide TFTs with IGZO:F exhibited higher mobilities, better switching characteristics, and enhancing the overall TFT performance. This was achieved by suppressing bonds with residual components and the introducing the fluorine dopant. Along with HIO method, the total performance can be enhanced. This simple approach with fluorine doping is expected to gain wide application for fabricating metal-oxide TFTs.

5.7 References

1. B. caLiu, M. Gu, X. Liu, S. Huang, and C. Ni, *First-principles study of fluorine-doped zinc oxide.* Applied Physics Letters, 2010. **97**(12).
2. H.Y. Xu, et al., *F-doping effects on electrical and optical properties of ZnO nanocrystalline films.* Applied Physics Letters, 2005. **86**(12).
3. J.W. Park, et al., *Optical and Structural Properties of Ion-implanted InGaZnO Thin Films Studied with Spectroscopic Ellipsometry and Transmission Electron Microscopy.* Japanese Journal of Applied Physics, 2009. **48**(11).
4. Z. Ye and M. Wong, *Characteristics of Thin-Film Transistors Fabricated on Fluorinated Zinc Oxide.* IEEE Electron Device Letters, 2012. **33**(4): p. 549-551.
5. Y.S. Rim, H. Chen, T.-B. Song, S.-H. Bae, and Y. Yang, *Hexaaqua Metal Complexes for Low-Temperature Formation of Fully Metal Oxide Thin-Film Transistors.* Chemistry of Materials, 2015. **27**(16): p. 5808-5812.
6. Y. Hwan Hwang, et al., *An 'aqueous route' for the fabrication of low-temperature-processable oxide flexible transparent thin-film transistors on plastic substrates.* NPG Asia Materials, 2013. **5**(4).
7. A.E. Martell and R.M. Smith, *Critical stability constants*. Vol. 1. 1974: Springer.
8. S. Jeong, Y.G. Ha, J. Moon, A. Facchetti, and T.J. Marks, *Role of gallium doping in dramatically lowering amorphous-oxide processing temperatures for solution-derived indium zinc oxide thin-film transistors.* Adv Mater, 2010. **22**(12): p. 1346-50.
9. J.A. Dean, *Lange's handbook of chemistry.* Material and manufacturing process, 1990. **5**(4): p. 687-688.
10. L.-C. Liu, J.-S. Chen, and J.-S. Jeng, *Role of oxygen vacancies on the bias illumination stress stability of solution-processed zinc tin oxide thin film transistors.* Applied Physics Letters, 2014. **105**(2).
11. J. Jiang, T. Toda, M.P. Hung, D. Wang, and M. Furuta, *Highly stable fluorine-passivated In–Ga–Zn–O thin-film transistors under positive gate bias and temperature stress.* Applied Physics Express, 2014. **7**(11).
12. J.-H. Jeon, Y.H. Hwang, J. Jin, and B.-S. Bae, *Low-temperature aqueous solution processed fluorine-doped zinc tin oxide thin-film transistors.* MRS Communications, 2012. **2**(01): p. 17-22.
13. J.-H. Jeon, Y.H. Hwang, and B.-S. Bae, *Bias-Temperature-Illumination Stability of Aqueous Solution Processed Fluorine Doped Zinc Tin Oxide (ZTO:F) Transistor.* Electrochemical and Solid-State Letters, 2012. **15**(4).

14. M. Miyakawa, M. Nakata, H. Tsuji, Y. Fujisaki, and T. Yamamoto, *Application of hydrogen injection and oxidation to low temperature solution-processed oxide semiconductors.* AIP Advances, 2016. **6**(8).
15. M. Miyakawa, M. Nakata, H. Tsuji, and Y. Fujisaki, *Highly stable low-temperature aqueous solution-processed oxide thin-film transistors by the hydrogen injection and oxidation method.* Flexible and Printed Electronics, 2018. **3**(2).

Chapter 6: Simple and reliable direct patterning method for carbon-free solution-processed metal oxide TFTs

6.1 Introduction

In this chapter, a simple and reliable direct patterning method for the carbon-free metal oxide thin films was demonstrated using a simple aqueous metal oxide precursor for process improvements.

The precursor was prepared by only a pure aqueous precursor without any carbon-related species. In the proposed method, the water molecules underwent photochemical reaction directly in aqueous precursor based on free-radical reactions induced by UV irradiation. A safe etching processes based on a dilute non-toxic organic acid (citric acid) was also developed. The entire process does not require any organic solvents. The fabricated TFT by the direct patterning of carbon-free, aqueous solution-processed oxide TFTs showed good device performance, which is comparable to the TFTs fabricated by conventional photolithography process.

6.2 Experimental

Precursor synthesis

A 0.3 M IGZO precursor solution was prepared by dissolving indium nitrate hydrate [$In(NO_3)_3 \cdot xH_2O$], gallium nitrate hydrate [$Ga(NO_3)_3 \cdot xH_2O$], and zinc nitrate hydrate [$Zn(NO_3)_2 \cdot xH_2O$] in pure water (Millipore system, resistivity: ~18 MΩ·cm, 25°C). The molar concentration of 0.3 M was achieved by setting the molar ratio of In:Ga:Zn to 4:1:1. Prior to the spin-coating process, the precursor was stirred vigorously to completely dissolve the precursors in solution. All reagents were obtained from Aldrich and used as received without further purification.

TFT fabrication and characterization

Solution-processed IGZO thin films were fabricated by spin-coating onto 100 nm thick, thermally oxidized SiO_2/n^+-Si substrates. The n^+-Si substrate was used as the gate electrode, while the SiO_2 layer was used as the dielectric. The substrate was treated with oxygen plasma for 30 s before spin-coating to enhance hydrophilicity. The precursor solution was passed through a 0.22 μm polytetrafluoroethylene filter. Spin-coating was performed at 4000 rpm for 30 s. Then, soft annealing was performed to retain H_2O inside the films at 60 °C for 10 s. The photoreaction was then carried out using deep-UV irradiation system (UV-300, Samco Inc.) with the primary emission line of UV of 185 nm (10%) and 254 nm (90%) provided by a low-pressure mercury lamp for 10 min. The intensity of UV lamp was 0.8 mW/cm^2 (250 nm detector, ORC MANUFACTURING CO., LTD.) with 2 cm of sample-to lamp distance. The substrate temperature after 10 min UV irradiation was about 38 °C. N_2 atmosphere was set to prevent the generation of ozone gas. Fine metal masks were used to pattern the desired island shapes. Etching was

performed using dilute citric acid (1 wt%) for 30 s. After patterning, the films were annealed at 350 °C for 1 h in air. The thickness of the resulting film was approximately 10 nm. Finally, patterned molybdenum source/drain electrodes (50 nm) were formed using a shadow mask to obtain bottom-gate, top-contact IGZO TFTs with 1000 μm channel widths and 100 μm channel lengths. To evaluate bias stability, the TFTs were encapsulated with a coating-type insulation layer (ZEOCOAT, cycloolefin resin, Zeon Corporation) to prevent interaction with the atmosphere at the back channel of the semiconductor layer. TFTs by conventional photolithography process were also fabricated. Spin-coating was performed at 4000 rpm for 30s, followed by pre-annealed at 150 °C for 10 min and subsequent annealing at 350 °C for 1h in air. After fabrication of IGZO films, the photolithography was conducted using dilute hydrochloric acid (0.01 wt%) for wet etching. After removing photoresist, drying process was then carried out at 150 °C for 30 min.

The IGZO TFTs on a flexible polyimide substrate were fabricated using polyimide varnish. A polyimide film was spin-coated on a glass substrate and a barrier layer was formed. After formation of the gate electrode of molybdenum (50nm), 200 nm thick SiO_2 film as a gate insulator was deposited by sputtering deposition. Then, the substrate was treated with oxygen plasma for 30 s to enhance hydrophilicity. The spin-coating for the IGZO film was performed. The direct-patterning process was performed by same method as mentioned above. After patterning, the films were annealed at 350 °C for 1 h in air. Source and drain (S/D) electrodes were then formed. Shadow masks were used to pattern all layers of the TFTs. After fabrication of the TFTs, the polyimide film was mechanically peeled from the glass substrate.

The TFTs were evaluated in the dark and at room temperature using an electrical measurement system with a probe station and a semiconductor analyzer (Keithley HP4156C). The mobility was calculated as

$$\mu = \frac{2L}{WC_i}\left(\frac{\partial\sqrt{I_d}}{\partial V_g}\right)^2,$$

where C_i is the capacitance of the gate dielectric per unit area, W is the channel width, and L is the channel length. The fabricated IGZO films were characterized by XPS (ULVAC-PHI PHI Quantera II), TDS (TDS; ESCO EMDWA1000S), and Fourier transform infrared spectroscopy (FT-IR; Bruker VERTEX 70v). The film thicknesses were analyzed with a surface profilometer (Bruker, Dektak stylus profiler system). The etching rate was calculated from the etched depths after the remove of the photoresist masked on the films.

6.3 Direct patterning method for aqueous precursor

The conventional photolithography requires multiple steps, from the coating process to the photoresist removal process, and involves a time-consuming baking and drying process. Besides, a lot of waste including toxic volatile organic compounds(VOCs) is produced and emitted with waste gases from those processes[1]. In contrast, the direct patterning method is markedly simpler and has advantages in terms of processing time and equipment cost, reduction of chemicals. Aqueous precursor can reduce the total amount of VOCs as well. The direct patterning process by aqueous precursor has a lot of environmental benefits.

Figure 6.1 shows a schematic of the proposed direct patterning method. The proposed direct patterning process is based on the photochemical reaction of water molecules. Aqueous precursors have been reported to form aqua complexes such as $[M(H_2O)_m]X_n$ during solvation as ligands are replaced by water molecules[2, 3]. During photoreactive patterning, the water molecules in aqua complexes react directly under UV irradiation. To effectively generate the photoreaction, the pre-irradiation annealing process was carefully adjusted so that the water molecules remained inside the films in a half-annealed condition. Upon irradiation of these complexes with short-wavelength (185 and 254 nm) UV light, the free-radical reactions of the H_2O moieties are induced by photodissociation, forming hydroxyl radical pecies[4, 5]. Along with photoreaction of H_2O, the photo-reaction of nitrate ligands of NO_3 are initiated as well [6]. The photochemical reaction is written as follows:

$$H_2O + h\nu \rightarrow H\cdot + \cdot OH$$

$$NO_3^- + h\nu \rightarrow NO_2\cdot + \cdot OH$$

The generated hydroxyl radical species are known to be strong oxidizing agents for accerating oxidation reactions[7]. The generated hydroxy radicals assist the M-OH activation, which leads to M-O-M condensation efficiently[6]. The condensation reaction for M-O-M bonds is written as follows:

$$M\text{-}OH + M\text{-}OH \rightarrow M\text{-}O\text{-}M + H_2O$$

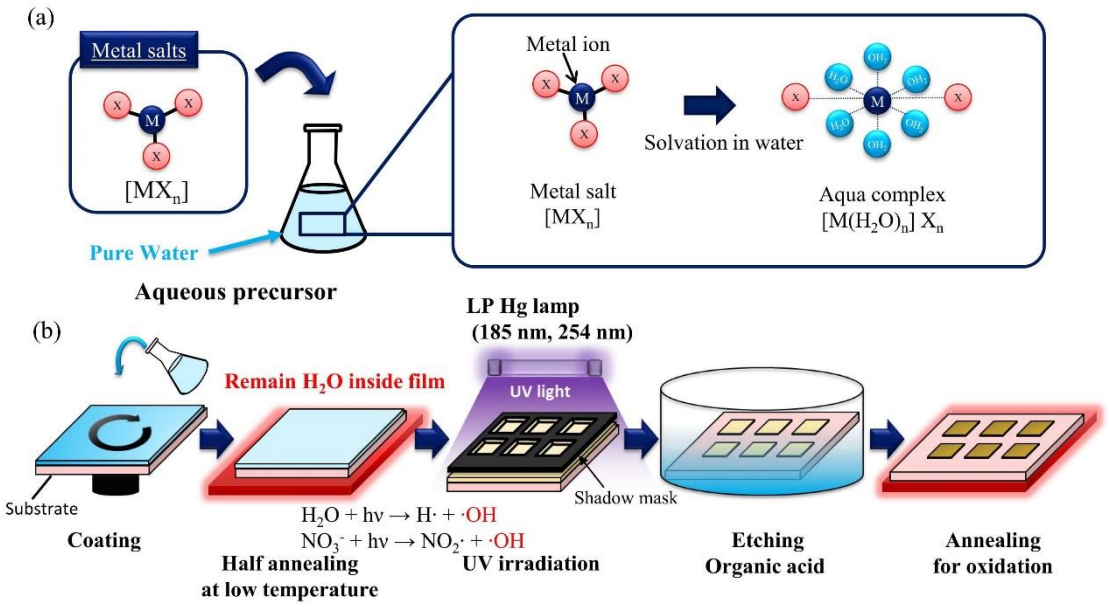

Figure 6.1. (a) Aqua complexes $[M(H_2O)_m]X_n$ formed by solvation with water molecules in the aqueous precursor. (b) Schematic illustration of the direct photoreactive patterning method.

In the proposed patterning method, these photoreactions are utilized directly for patterning. Therefore, the direct patterning was successfully achieved as an alternative to the use of organic photosensitive additives. Selective exposure to UV light was achieved by setting a metal mask on the films during UV irradiation. Thus, the direct-patterning method can be applied to simple aqueous precursors that do not contain carbon-based photosensitive additives. The oxidation of the films during UV irradiation alters the solubility of the UV-exposed films, while the regions not exposed to UV light were easily solved. Because, the aqueous precursor was synthesized only from metal-nitrate salts and pure water, the resulting solution-processed oxide film is expected to be free from carbon impurities, except those introduced by accidental contamination during the fabrication processes. Besides, the easy decomposition of nitrate based precursor in aquesous systems leads to the fewer impurities and efficient M-O-M bonds[8]. Thus, a dense oxide film is expected to result from the easy decomposition of the precursor.

Figure 6.2 shows optical microscopy images of the IGZO films fabricated using the direct photoreactive patterning method after different etching times. The direct patterning process produced stable patterning while maintaining the shape of the IGZO film. We observed high solubility during the etching process at the regions not exposed to UV irradiation, which were solved within about 10 s. In contrast, the regions exposed to UV irradiation exhibited high stability toward the etchant. Large differences in film solubility were observed. These considerable differences (a factor of approximately 40) in etching rate were sufficient to obtain uniform patterning, and the photoreactive process applied to the aqueous precursor effectively achieved stable, direct patterning.

(a)

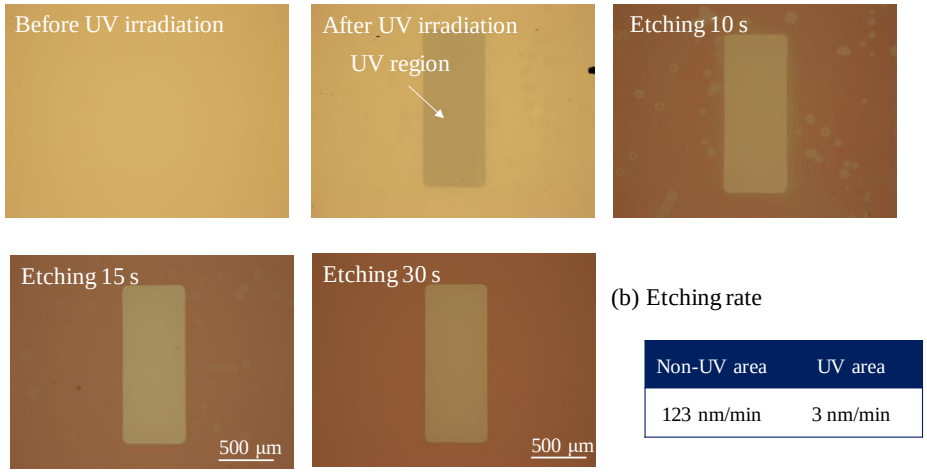

(b) Etching rate

Non-UV area	UV area
123 nm/min	3 nm/min

(c)

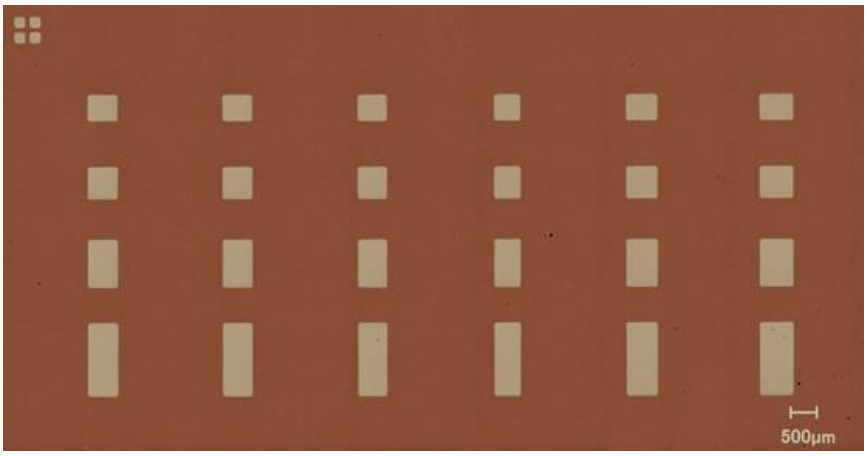

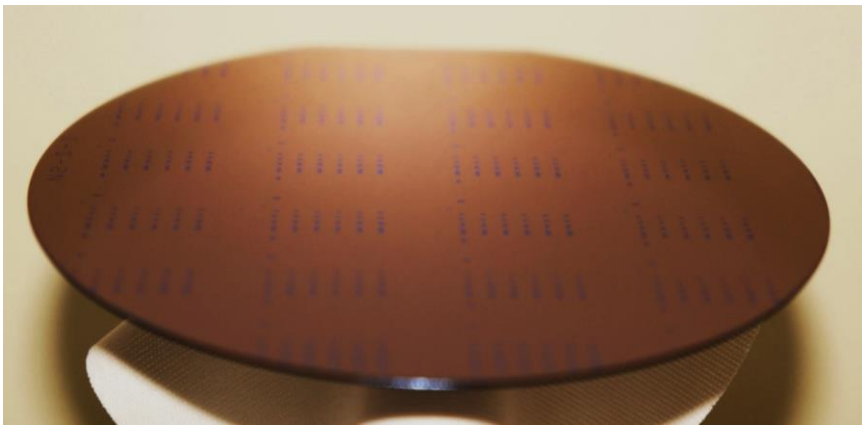

Figure 6.2. (a) Optical microscopy images acquired at different times during the direct photoreactive patterning of island-shaped IGZO films. (b) Etching rates of the IGZO films in UV-irradiated and non-irradiated areas. (c) Photograph of differently sized patterns and IGZO film on a 4-in Si wafer.

6.4 Chemical analysis for direct-patterning process

To analyze the photoreaction during the direct-patterning process, the fabricated IGZO films were evaluated by X-ray photoelectron spectroscopy [XPS; Figure 6.3(a)–(d)]. Since the residual species were limited to nitrate ligands, the changes in the N1s nitrate peaks were analyzed. The O1s peaks were also analyzed by curve-fitting the M─O (lattice oxygen), Vo (oxygen vacancy), and M─OH (hydroxyl) peaks at 530.2, 531.7, and 533.0 eV, respectively[9]. As shown in Figure 6.3 (a), UV irradiation resulted in a decrease in nitrate peaks related to NO_3, indicating that UV irradiation effectively decomposed the nitrate ligands. The XPS spectra also show that the M─O bonds were enhanced by UV irradiation. To analyze more clearly, thermal desorption spectroscopy (TDS) analysis was conducted for the IGZO films. The desorption of nitrogen compounds was assessed by tracking the mass fragments at m/z values of 28 and 30, which correspond to N2 and NO from the precursor compounds. Figure 6.4 shows the TDS spectra related to m/z of 28 (N2) and 30 (NO). A large amount of desorption signals with peak at around 300 °C was observed for the IGZO film before UV irradiation. These desorption signals were relating to the nitrate ligands because the annealing temperature of 60 °C was very low. However, considerable decreases in desorption was confirmed for the IGZO films after UV irradiation. The UV irradiation was effective to decomposed the nitrate ligands and oxidize the precursors. According to the previous reports, UV irradiation is effectively to cause oxidation reaction and decomposition of ligands only by the photoreaction of the nitrate lignads[6]. In proposed aqueous nitrate based precursor, the photochemical reactions based on water and nitrated ligands are induced to generate the oxidizing agents. Therefore, considering from XPS and TDS results, the

decomposition of nitrate ligands and enhanced M─O bonding formation contributed to the changes in film solubility, which are important for the subsequent etching process.

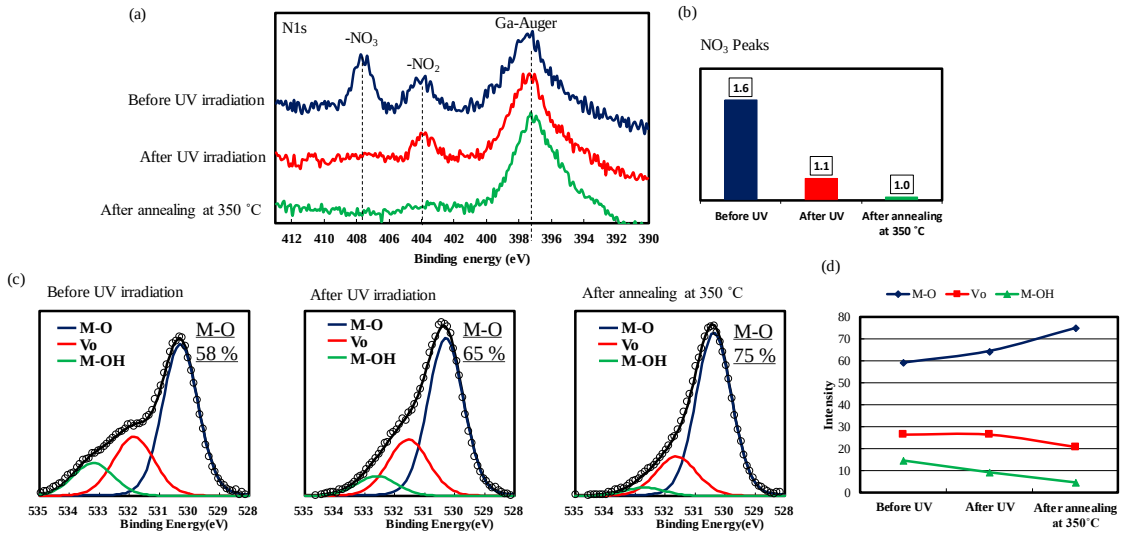

Figure 6.3. (a) XPS N1s spectra of the IGZO films fabricated by the direct-patterning process at the indicated conditions. (b) Intensity of NO_3 peaks in the corresponding IGZO films. (c) XPS O1s spectra of the IGZO films at the indicated conditions. The O1s peaks were analyzed by curve-fitting the M─O (lattice oxygen), Vo (oxygen vacancy), and M─OH (hydroxyl) peaks. (d) Intensity of the O1s peaks for M─O, Vo, and M─OH.

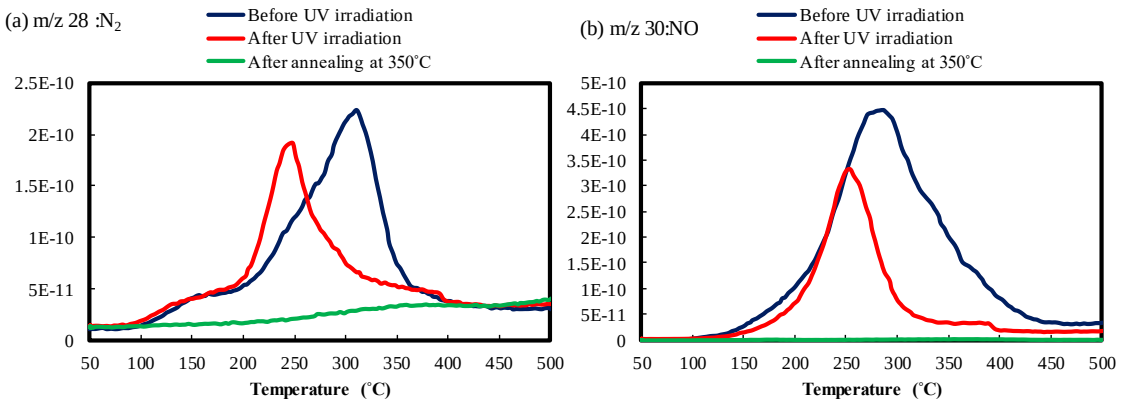

Figure 6.4. TDS spectra related to m/z of (a) 28 (N_2) and (b) 30 (NO) for IGZO films by the direct-patterning process at the indicated conditions.

Figure 6.5 shows a schematic model of the photoreaction based on the photodissociation of water molecules in the aqueous precursor followed by oxidation via thermal annealing. As indicated above, the photodissociation of water molecules and nitrate ligands under UV irradiation generated hydroxyl radicals, which acted as an strong oxidant to form M─O bonds. Compared to the films annealed at 350 °C for 1 h, the formation of the M—O bonds after the UV irradiation is insufficient in points of low intensity of the M─O bonds. However, the difference in partial oxidation between the irradiated and un-irradiated films was sufficient to achieve patterning using the etching process. Although the IGZO films after UV irradiation is not completely oxidized, the following thermal annealing enhance the formation of metal-oxide-metal bonds and decomposing the impurities of metal ligands.

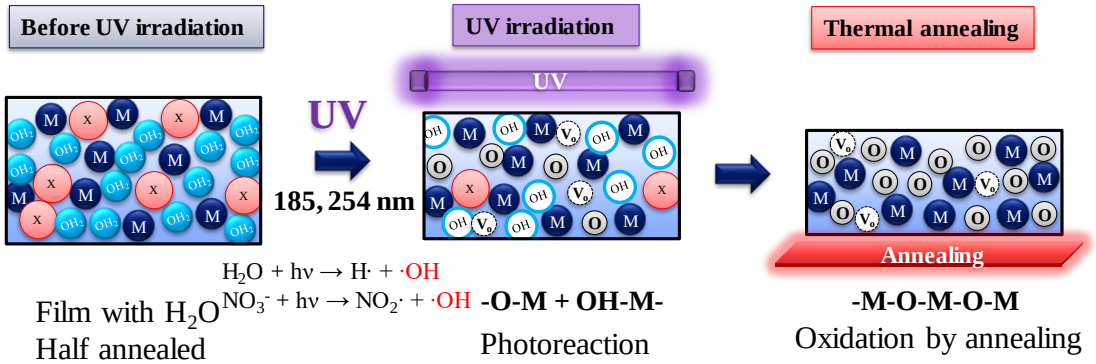

Figure 6.5. Schematic model of the oxidation reaction of metal complexes using the direct photoreactive patterning method.

6.5 TFT characteristics for direct patterned IGZO TFTs

Figure 6.6 (a)–(f) shows the transfer characteristics of the 18 IGZO TFTs fabricated using the direct patterning method in this study and the conventional photolithography process at gate voltages (V_g) ranging from −30 to 30 V and a fixed drain voltage (V_d) of 30 V. Table 1 summarizes the calculated electrical properties, including mobility (μ), ratio of maximum on-current to minimum off-current (I_{on}/I_{off}), subthreshold swing (S.S), switch-on voltage (V_{on}) @ $I_{ds} = 10^{-9}$ A, and hysteresis of V_{on}. The calculated average μ of the TFTs fabricated by direct patterning was 4.2 $cm^2/V{\cdot}s$, and only small deviation in μ was observed. Hysteresis in the switching behavior was also negligible. These results indicate that stable, uniform performance in conjunction with a high I_{on}/I_{off} and minimal hysteresis. The carbon-free aqueous precursor containing no organic additives is thought to have contributed to the stable electrical characteristics because of its ease of decomposition and lack of impurities. Comparing the TFTs fabricated by the direct patterning method with those prepared by conventional photolithography indicates that direct patterning did not produce any film-degradation effects. The almost same mobility performances were obtained for the TFTs fabricated by more simple processes based on direct patterning.

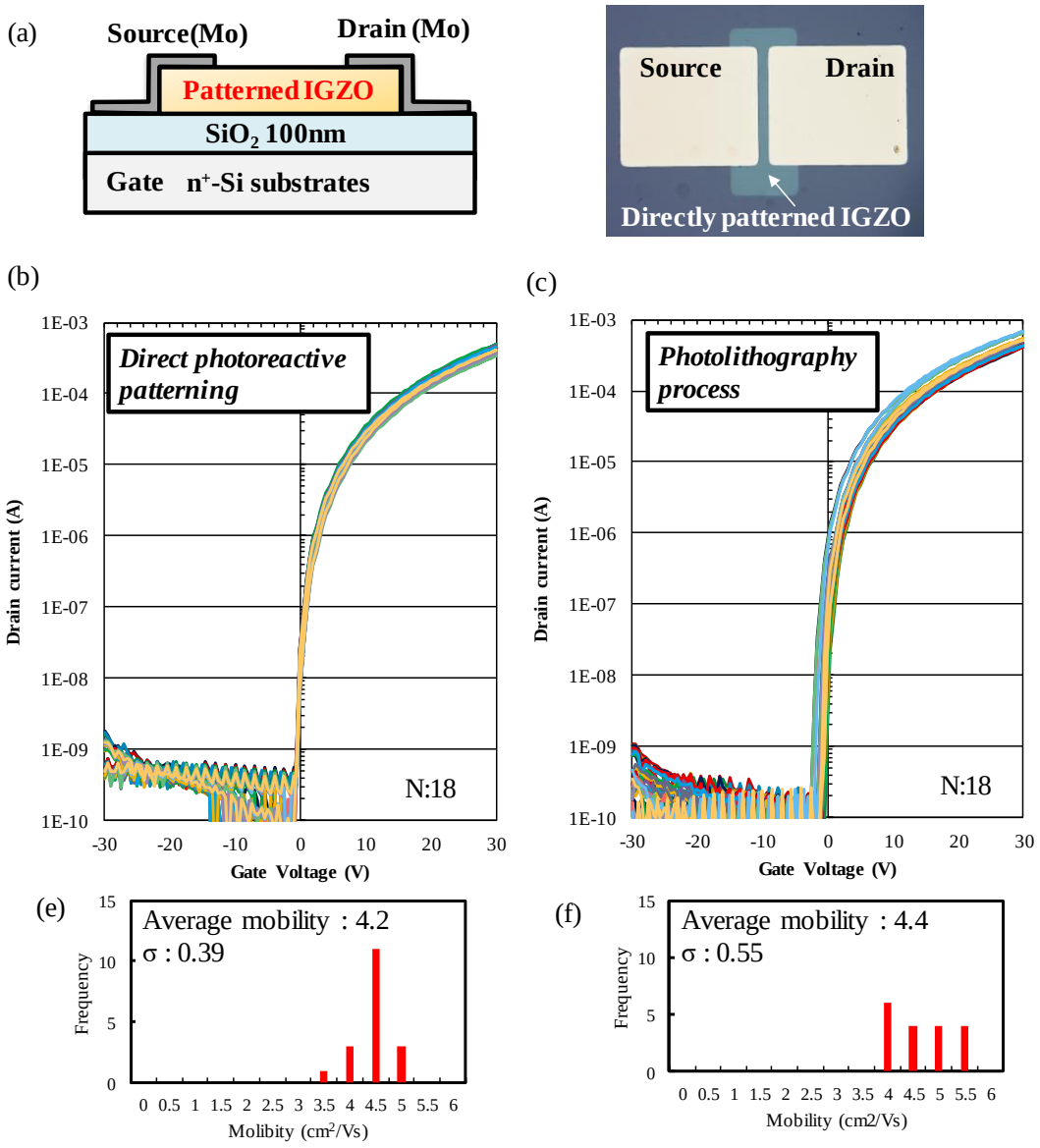

Figure 6.6. (a) Schematic diagram of a bottom-gate, top-contact TFTs and photographic image of a fabricated TFT. Transfer characteristics for 18 IGZO TFTs fabricated by (b) the direct photoreactive patterning process and (c) conventional photolithography. Mobility histograms of the TFTs fabricated by (e) direct patterning and (f) photolithography.

Table 6.1. Calculated electrical parameters of solution processed IGZO TFTs fabricated by the direct photoreactive patterning process and by conventional photolithography.

	Mobility ($cm^2/V \cdot s$)	Ion/Ioff ratio	S.S. (V/decade)	Von (V)	Hysteresis (V)
Direct photoreactive patterning	4.2 σ: 0.4	-10^6	0.4 σ: 0.03	−0.4 σ: 0.07	0.1 σ: 0.04
Conventional photolithography	4.4 σ: 0.6	-10^6	0.4 σ: 0.04	−1.3 σ: 0.48	0.7 σ: 0.20

Interestingly, the direct-patterned TFTs showed smaller deviations in electrical performance (based on μ, V_{on}, and hysteresis) compared to the conventional films. The surface state for the back channel of oxide TFT is known as very sensitive and important layer to improve the performance of oxide TFTs [10, 11].

To investigate the differences of chemical states of fabricated films between the processes, FT-IR spectroscopy were conducted. As showed in Figure 6.7(b), the increases of OH groups at the semiconductor layer was examined for the films by photolithography process compared to that by direct patterning. Besides, as showed in Figure 6.7(c), the unique residual peaks relating to silazanes ($Si\text{-}CH_3$), which is one of residues consisting of photoresist materials, were detected. It is suggested that one of possible reasons for the larger deviation is owing to the negative effect of the residual on back channel during photolithography. Residues on the back channel can lead to undesirable effects (e.g., back channel effects and additional passivation processes)[12]. The direct patterning does not

need any chemicals which were consisted of various organic compounds such as a photoresist, remover. In addition, considering from the process flows, direct pattening process apply the high temperature thermal annealing process of 350 °C to the IGZO films after finishing patterning process. Whereas the conventional photolithography apply annealing is before patterning process. The difference of process flows is considered as another reason to cause the larger deviation of TFT performance. Thus, the chemical state at the surface of TFT by direct patterning is considered to be cleaner and more stable. The proposed direct patterning method is considered as a reliable patterning method for a production of electrical devices.

Finally, to evaluate the electrical stability of the IGZO TFTs by direct patterning method, both positive gate bias stress (PBS) and negative bias stress (NBS) were assessed. Figure 6.8 shows the transfer characteristics of the direct-patterned IGZO TFTs under PBS and NBS. To suppress the interaction between the air atmosphere and back channels of the TFTs, the back channels were passivated with a coating-type insulation layer, and the transfer characteristics of the TFTs at V_g ranging from −15 to 15 V were assessed at an applied drain voltage of 10 V. The stress conditions for PBS and NBS were ±1 MV/cm, and the maximum stress time was 3,600 s at room temperature. The direct-patterned TFTs exhibited reliable switch-on voltage with ΔV_{on} less than 1.0 V under both PBS and NBS. It is found that the aqueous solution processed TFTs fabricated via simple direct photoreactive patterning method exhibit stable reliability. It is likely that the simple carbon-free aqueous precursor with the simple patterning process, which involves few steps without organic solvents, allows achieving good stability under bias stress condition. Since reliability of TFTs is very important characteristic for practical device applications,

this direct patterning method is promising technology to easy device integration in terms of practical future applications.

To confirm the process compatibility of fabrication for the flexible electronics, flexible IGZO TFTs were fabricated using direct patterning method. As shown in Figure 6.9, a bottom-gate, top-contact IGZO TFT onto flexible polyimide substrate was fabricated. The calculated μ of the TFT fabricated on flexible substrate was 4.8 $cm^2/V \cdot s$. The proposed direct patterning method was demonstrated for fabrication of flexible electronics.

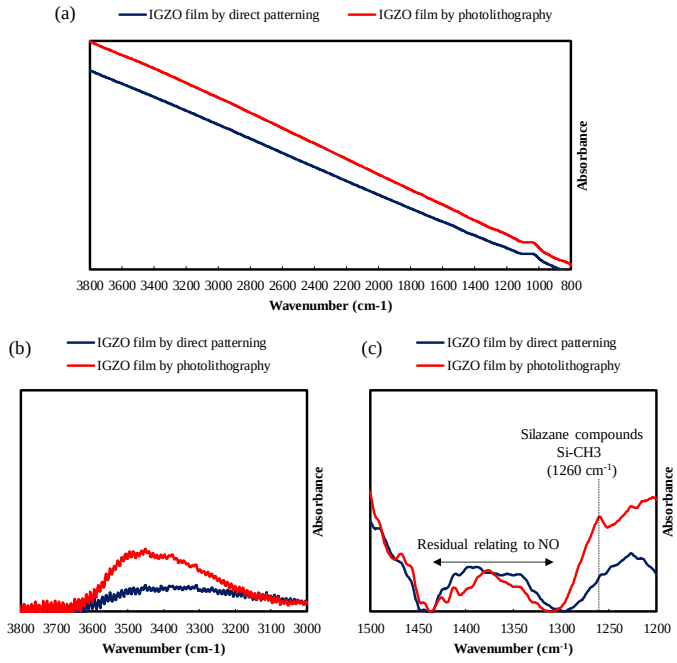

Figure 6.7. FT-IR spectra for the IGZO films by the direct photoreactive patterning process and conventional photolithography.

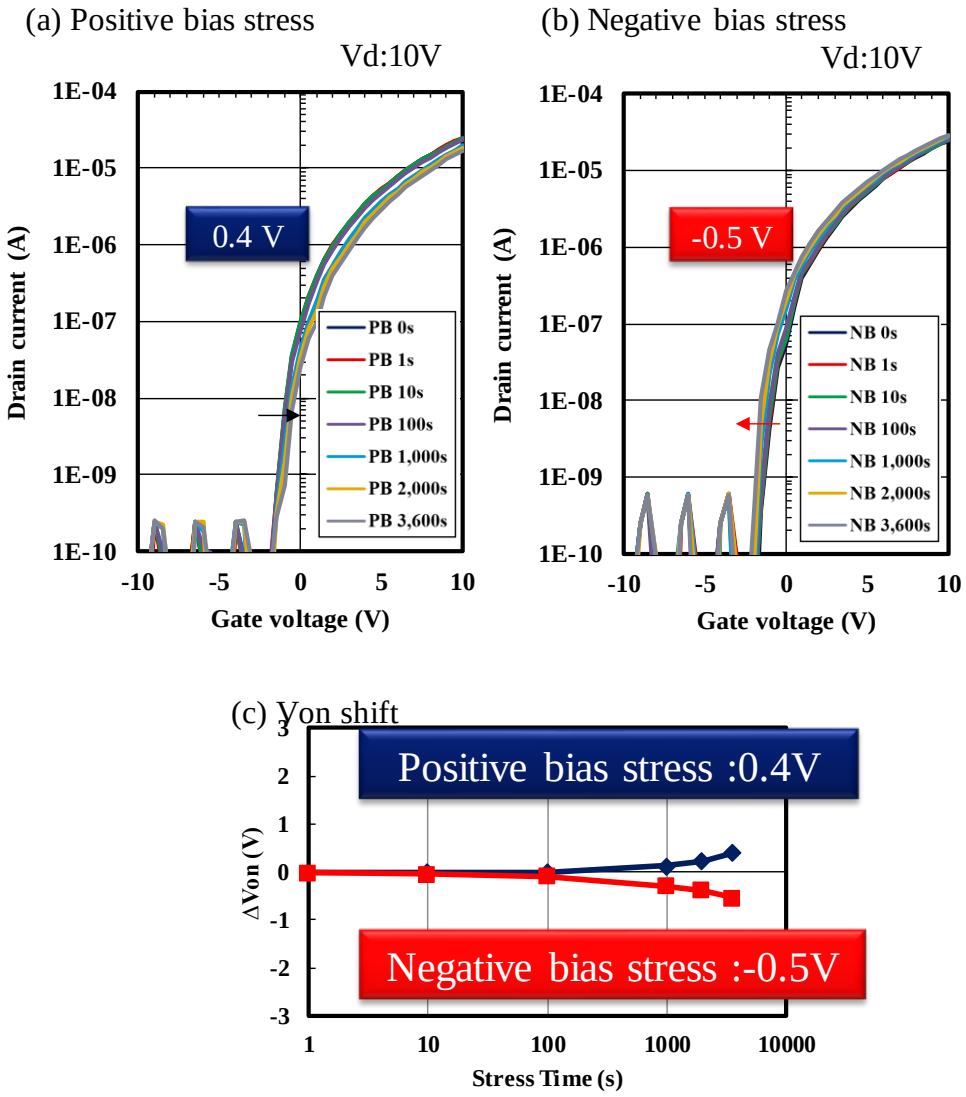

Figure 6.8. Transfer characteristics of a direct-patterned IGZO TFT under (a) positive bias stress and (b) negative bias stress at an applied drain voltage of 10 V. (c) Changes in switch-on voltage as a function of cumulative stress time for positive and negative bias stresses.

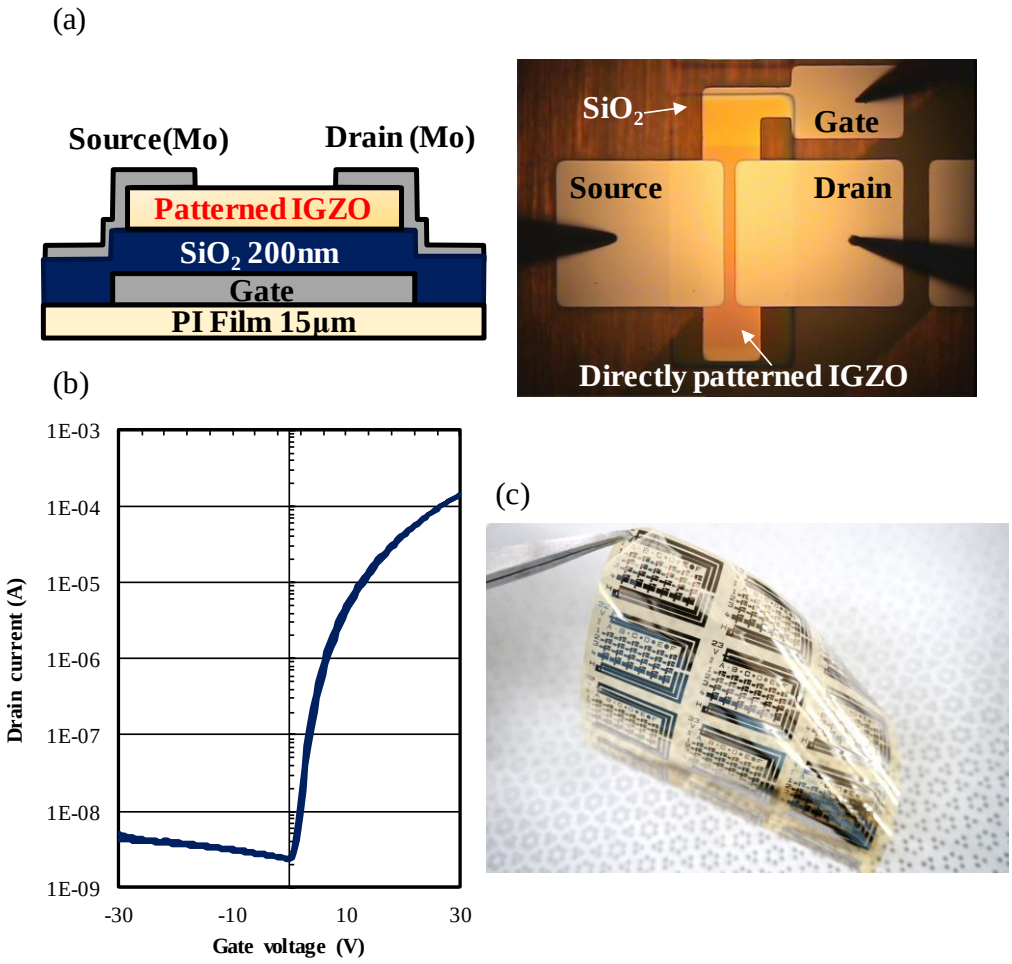

Figure 6.9. (a) Schematic diagram of a bottom-gate, top-contact TFTs and photographic image of a fabricated TFT on flexible polyimide substrate. (b) Transfer characteristics for IGZO TFT fabricated by the direct photoreactive patterning process. (c) Photograph of IGZO TFTs on the flexible polyimide substrate.

6.6 Conclusion

In summary, a simple and easy photoreactive direct-patterning method is develop a simple and reliable direct patterning method for carbon-free aqueous solution-processed IGZO TFTs. The patterning method is achieved by the photooxidation of water molecules and nitrate ligands. XPS and TDS analysis indicated that UV irradiation leads to the dissociation of nitrate ligands and oxide formation, altering the film solubility for the subsequent etching process. The fabricated TFTs annealed at 350 °C exhibited good electrical performance and uniformity. The mobilities of the fabricated TFTs were uniformed, with an average value of 4.3 $cm^2/V \cdot s$ and small deviations. Since the proposed photoreactive patterning method is simple in its mechanism, namely the photooxidation of water molecules and nitrate ligands, it expects the method to be applicable to various types of aqueous metal oxide precursors, including semiconductors, dielectric oxide materials, and other conductive materials. In addition, given the environmental benefits of this method, the method can be used in various electrical device applications.

6.7 References

1. H. Chein and T.M. Chen, *Emission Characteristics of Volatile Organic Compounds from Semiconductor Manufacturing.* Journal of the Air & Waste Management Association, 2012. **53**(8): p. 1029-1036.
2. Y.S. Rim, H. Chen, T.-B. Song, S.-H. Bae, and Y. Yang, *Hexaaqua Metal Complexes for Low-Temperature Formation of Fully Metal Oxide Thin-Film Transistors.* Chemistry of Materials, 2015. **27**(16): p. 5808-5812.
3. K.H. Lee, et al., *Modulation of aqueous precursor solution temperature for the fabrication of high-performance metal oxide thin-film transistors.* Applied Physics Express, 2015. **8**(8).
4. K. Zoschke, H. Bornick, and E. Worch, *Vacuum-UV radiation at 185 nm in water treatment--a review.* Water Res, 2014. **52**: p. 131-45.
5. R.E. Van de Leest, *UV photo-annealing of thin sol-gel films.* Applied Surface Science, 1995. **86**(1-4): p. 278-285.
6. S. Park, et al., *In-Depth Studies on Rapid Photochemical Activation of Various Sol-Gel Metal Oxide Films for Flexible Transparent Electronics.* Advanced Functional Materials, 2015. **25**(19): p. 2807-2815.
7. J. Leppäniemi, et al., *Rapid low-temperature processing of metal-oxide thin film transistors with combined far ultraviolet and thermal annealing.* Applied Physics Letters, 2014. **105**(11).
8. H. Jae-Sang, et al., *Photochemically Activated Flexible Metal-Oxide Transistors and Circuits Using Low Impurity Aqueous System.* IEEE Electron Device Letters, 2015. **36**(2): p. 162-164.
9. Y. Hwan Hwang, et al., *An 'aqueous route' for the fabrication of low-temperature-processable oxide flexible transparent thin-film transistors on plastic substrates.* NPG Asia Materials, 2013. **5**(4).
10. P. Xiao, et al., *InGaZnO thin-film transistors with back channel modification by organic self-assembled monolayers.* Applied Physics Letters, 2014. **104**(5).
11. P. Xiao, et al., *Effects of Solvent Treatment on the Characteristics of InGaZnO Thin-Film Transistors.* ECS Journal of Solid State Science and Technology, 2014. **3**(9): p. Q3081-Q3084.
12. W.-T. Park and Y.-Y. Noh, *A self-aligned high resolution patterning process for large area printed electronics.* Journal of Materials Chemistry C, 2017. **5**(26): p. 6467-6470.

Chapter 7: Conclusions and outlook

In this thesis, the technology for achieving high-performance low-temperature solution-processed oxides for various flexible electronics were thoroughly investigated and find its potential for various applications. The investigations by the processing and materials approaches show the great potential of the solution-processed metal oxide TFT even at low-temperature processing for the flexible electronics.

In chapter 3, the work demonstrated a general method employing the HIO process for the fabrication of low temperature solution-processed oxide semiconductors using ZTO with organic precursor. The HIO method was demonstrate efficiently elimination a large amount of residual species as well as to promote film densification upon sequential oxidation. Moreover, improvements in the TFT characteristics were seen upon applying the HIO process to ZTO TFTs.

In chapter 4, the high stability of low-temperature solution-processed IGZO TFTs was demonstrated by application of the HIO method. Improvement in the TFT characteristics was confirmed in terms of the mobility and electrical stability. To achieve low-temperature solution-processed oxide materials, the decomposition of residual species is of primary importance. The effectiveness of HIO method was demonstrated by aqueous precursor based on IGZO for realizing solution-processed oxide semiconductors for device applications.

In chapter 5, efficient aqueous fluorine-doped IGZO precursors were synthesized to fabricate high-performance metal-oxide TFTs at a low processing temperature of 300˚C. The fluorine doping suppressed the total impurities from metal ligands and form M–F bonding at the sites of oxygen or oxygen vacancy. The fabricated metal-oxide TFTs with IGZO:F exhibited higher mobilities, better switching characteristics, and enhancing the overall TFT performance. This was achieved by suppressing bonds with residual components and the introducing the fluorine dopant. Along with HIO method, the total performance can be enhanced. This simple approach with fluorine doping is expected to gain wide application for fabricating metal-oxide TFTs.

In chapter 6, a simple and easy photoreactive direct-patterning method is develop a simple and reliable direct patterning method for carbon-free aqueous solution-processed IGZO TFTs. The patterning method is achieved by the photooxidation of water molecules and nitrate ligands. The fabricated TFTs exhibited good electrical performance and uniformity. Since the proposed photoreactive patterning method is simple in its mechanism, namely the photooxidation of water molecules and nitrate ligands, it expects the method to be applicable to various types of aqueous metal oxide precursors, including semiconductors, dielectric oxide materials, and other conductive materials. In addition, given the environmental benefits of this method, the method can be used in various electrical device applications.

During the processing approaches, hydrogen injection and oxidation methods were investigated for the conventional organic precursor of ZTO and aqueous precursor of IGZO. Regardless of the precursor systems, the effectiveness of the method was revealed by detailed chemical analysis using SIMS, TDS, XPS, and FT-IR. Furthermore, the

overall TFT performances including mobility, On-Off ratio, S.S, and reliability were demonstrated by adopting HIO methods. Thus, these results indicate its generality for the solution-processed oxide at low-temperature. It can be applicable for various precursor to improve its TFT performance owing to decomposing the residuals and improving the film qualities. Besides, it was clarified that the key requirement is to eliminate impurities and to produce dense films, such as those that are obtained from physical vapor deposition processing in the production of high-performance solution-processed oxide TFTs at low temperatures.

Associated with precursor engineering, fluorine doped precursors were investigated to improve the TFT performances. The fluorine doping was effective to reduce the total impurities from metal ligands and form M–F bonding at the sites of oxygen or oxygen vacancy. Furthermore, the fabricated metal-oxide TFTs with IGZO:F improved mobilities, switching characteristics. Along with the HIO method, mobility over 7 cm^2/Vs was achieved for the IGZO:F by low-temperature solution processing.

The facile fabrication technology using direct patterning was investigated for process improvement. Simple and reliable direct patterning process for carbon-free aqueous precursor was successfully demonstrated with good electrical performance and uniformity by using the photooxidation of water molecules and nitrate ligands. The method is expected to be applicable to various types of aqueous metal oxide precursors.

Solution processing for oxide materials is a promising technology for widen the possibility of its application. However, low-temperature processing of oxide TFTs still need to improve its performance compared to the oxides by vacuum processing on flexible substrates. Therefore, further researches are required for practical application of

the next generation flexible electronics. Considering from the improvement using HIO and fluorine doped precursor, the use of multiple improvement technology could be essential to boost the performance of metal oxide. Those results reveal that the further improvement of its performances is still possible to meet the requirement of practical applications by combining the technology from process and material engineering. Further investigation develops the better solutions for obtaining facie and better performance of solution-processed oxide.

This thesis focused mainly on the oxide material as a semiconductor, however, the solution-processing technology can be applicable widely including dielectric oxide materials, conductive materials, coating layer, optical layer with high-refractive index etc. Therefore, more wider application area is expected using current solution-processing technology of metal oxides.

In general, system integrations require more detail circuit structure using n-type and p-type. Therefore, another challenges for solution-processing oxide is investigations of p-type materials because complementary logic circuits enable more efficient driving with simple structure. Therefore, solution-processed p-type oxide as well as solution-processible p-type organic semiconductors are considered as p-type candidates for realizing CMOS structure. Further researches must expand its application using solution-processing.

As mentioned, the application area of TFTs are not limited to display applications. Current momentum towards IoT in society 5.0 needs more ubiquitous electronics. To meet its demands, facile fabrication process without costly vacuum processing must be a promising. Besides, given the environmental benefits of this method, the advantages

without costly vacuum processing is significantly important. Complete alternation of existing technology is not realistic, however, hybrid electronic using solution-processed and vacuum-processed electronics must be possible. The solution to maximize the advantages of facile processing of solution-processing and the superior performance of existing device technology is next step to expand the solution-processing of oxides. Accelerating of the practical application for solution-processing oxides are expected by this knowledge of the solution-processed oxides for future various flexible electronics.

LIST OF PUBLICATIONS

[1] **M. Miyakawa**, M. Nakata, H. Tsuji, H. Iino, and Y. Fujisaki, Impact of fluorine doping on solution-processed In–Ga–Zn–O thin-film transistors using an efficient aqueous route. AIP Advances, 2020. 10(6).

[2] **M. Miyakawa**, M. Nakata, H. Tsuji, and Y. Fujisaki, (Invited) Fabrication Technique for Low-Temperature Aqueous Solution-Processed Oxide Thin-Film Transistors. ECS Transactions, 2018. 86(11): p. 105-109.

[3] **M. Miyakawa,** M. Nakata, H. Tsuji, and Y. Fujisaki, Simple and reliable direct patterning method for carbon-free solution-processed metal oxide TFTs. Scientific Reports, 2018. 8(1).

[4] **M. Miyakawa**, M. Nakata, H. Tsuji, and Y. Fujisaki, Highly stable low-temperature aqueous solution-processed oxide thin-film transistors by the hydrogen injection and oxidation method. Flexible and Printed Electronics, 2018. 3(2).

[5] **M. Miyakawa**, M. Nakata, H. Tsuji, Y. Fujisaki, and T. Yamamoto, Improvement of TFT Characteristics for Low-Temperature Solution-Processed Oxide Semiconductors with Hydrogen Injection and Oxidation Process. ECS Transactions, 2016. 75(10): p. 133-138.

[6] **M. Miyakawa**, M. Nakata, H. Tsuji, Y. Fujisaki, and T. Yamamoto, Application of hydrogen injection and oxidation to low temperature solution-processed oxide semiconductors. AIP Advances, 2016. 6(8).

AWARD

M. Miyakawa, M. Nakata, H. Tsuji, Y. Fujisaki, High-Performance Solution-Processed Thin-Film Transistors Using Fluorine-Doped Aqueous Metal Oxides, AM-FPD '18 Best PAPER AWARD

International conference presentations

[1] **M. Miyakawa** et. al., B29-2 High-performance reliable solution processed metal oxide TFTs for large area and flexible electronics, IMID 2019, kyonju, Aug., 2019 **(Invited)**

[2] **M. Miyakawa** et. al., H03-1217: Fabrication Technique for Low-Temperature Aqueous Solution-Processed Oxide Thin-Film Transistors, AiMES 2018, Cancun, Oct., 2018 **(Invited)**

[3] **M. Miyakawa** et. al., 3-2 High-performance solution-processed thin-film transistors using fluorine-doped aqueous metal oxides, AM-FPD 2018, Kyoto, Sep., 2018

[4] **M. Miyakawa** et. al., European Materials Research Society (E-MRS) Fall Meeting 2017, Warsaw, Sep, 2017, Effect of fluorine additive on low-temperature solution processed IGZO TFT

[5] **M. Miyakawa**, M. Nakata, H. Tsuji, Y. Fujisaki, and T. Yamamoto, PRiME 2016, Hawaii, Oct. 2016, Improvement of TFT Characteristics for Solution-processed Oxide Thin-film Transistor with Hydrogen Injection and Oxidation Process

ACKNOWLEDGMENTS

First of all, I would like to extend my sincere gratitude to Prof. Hiroaki Iino, Tokyo institute of technology, for advising my doctoral research on accomplishing this thesis. I would also like to thank to Prof. Junichi Hanna, Tokyo institute of technology; and to Prof. Akira Oono, Tokyo institute of technology for insightful discussions.

I would like to express my deepest gratitude to my dissertation committee members, Prof. Toshio Kamiya, Tokyo institute of technology; Prof. Takaaki Manaka, Tokyo institute of technology; Prof. Shunichiro Ohmi, Tokyo institute of technology; and Prof. Satoshi Sugahara, Tokyo institute of technology for their constructive comments on my research.

Most studies in this thesis had been done from 2016 to 2020 in NHK science and technology research laboratories. I sincerely thank Dr. Kohji Mitani, Director of NHK Science & Technology Research Laboratories; and Dr. Toru Kuroda, former Director of NHK Science & Technology Research Laboratories to support my research. I am grateful to Dr. Hiroshi Shimamoto, Head of Advanced Functional Devices Research Division; Dr. Keiji Ishii, Head of Planning & Coordination Division; Dr. Naoto Hayashi, former Head of Advanced Functional Devices Research Division for assisting me explore my research interests.

I would like to acknowledge all members of the Display group members in Advanced Functional Devices Research Division. In particular, I thank Dr. Toshihiro Yamamoto, former senior researcher; Dr. Yoshihide Fujisaki, senior researcher; Dr. Takahisa Shimizu, senior researcher; Dr. Yoshiki Nakajima, senior researcher for their valuable comments. In addition, I would like to thank all TFT team members, Dr. Mitsuru

Nakata; Dr. Hiroshi Tsuji, Mr. Tatsuya Takei for their sharing knowledge and being encouraging.

Finally, I want to give special thanks to my family for daily supports and helping my inspiration.